AARHUS UNIVERSITY

On the contributions of retinal direction selectivity to cortical motion processing in mice

PhD dissertation
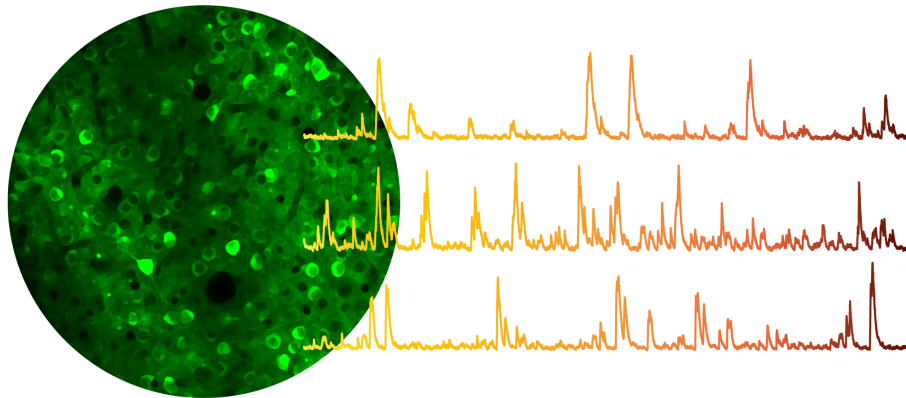
Rune Nguyen Rasmussen

Health
Aarhus University
December 2020

On the contributions of retinal direction selectivity to cortical motion processing in mice

PhD dissertation

Rune Nguyen Rasmussen

Supervisor:

Keisuke Yonehara, Associate Professor and Group Leader, DVM PhD
Department of Biomedicine, Aarhus University, Denmark

Co-supervisor:

Duda Kvitsiani, Associate Professor and Group Leader, PhD
Department of Molecular Biology and Genetics, Aarhus University, Denmark

Graduate programme:

Biomedicine

Submitted on:

31st December 2020

Assessment committee:

Mai Marie Holm, Associate Professor, PhD (Chair of the committee)
Department of Biomedicine, Aarhus University, Denmark

Sonja Hofer, Professor, PhD
Sainsbury Wellcome Centre for Neural Circuits and Behaviour, University College London, United Kingdom

Hajime Hirase, Professor, PhD
Center for Translational Neuromedicine, University of Copenhagen, Denmark

Contents

Preface

Roughly four years ago, in the summer of 2016, I approached Associate Professor Keisuke Yonehara from the Department of Biomedicine regarding the possibility of pursuing a PhD in his laboratory at Aarhus University. Quite fortunately for me, he looked positively upon this, and in 2017 I began my three-year PhD studies in the Yonehara laboratory. This dissertation serves as the final scientific outcome of my research conducted during these three years.

The overall goal of my studies has been to provide answers to questions pertaining to how the sensory periphery of the visual system, the retina, contributes to visual motion processing by the cortex in mice. My pursuit of this goal has taken me on a truly wonderful journey. In addition to the countless hours in front of a two-photon microscope, I have been privileged to visit a number of inspiring scientific environments around the world. I can genuinely say that I have relished these three years, I have learned an exceptional amount — knowledge both theoretical and practical — I have made new friends and collaborators from around the world, and I am certain that this experience has prepared me well for a future within the realm of neuroscience research.

This dissertation is structured as a collection of papers related to my PhD project. Chapters 1 and 2 provide a general introduction and background to the research area, and outline the aim and main scientific objectives that the work presented in this dissertation seeks to answer. Chapter 3 presents work published in the journal *Nature Communications*, in which we demonstrate a segregated cortical stream for direction selectivity computed in the retina (Rasmussen et al., 2020a). Chapter 4 provides a bridge between experimental studies, offers an updated synthesis on the roles of retinal direction selectivity for visual processing in central brain areas, and formulates specific testable hypotheses, which we published as a review in the journal *Current Biology* (Rasmussen and Yonehara, 2020). Chapter 5 presents unpublished work testing one of these hypotheses, in which we demonstrate that optic flow processing in the visual cortex is influenced by retinal direction selectivity (Rasmussen et al., 2020b). Finally, Chapter 6 draws conclusions and ends on considerations and future directions.

Rune N. Rasmussen
December 2020

Acknowledgements

First and foremost, I would like to express my sincere gratitude to Keisuke Yonehara for being a remarkable supervisor. Thank you for taking me on as a PhD student, for being so immersed in my project, for always helping me out when I need it, and finally, thank you for (almost) always being available on Slack! A special thanks to my office colleague, my scientific partner-in-crime, and my friend, Akihiro Matsumoto. You have taught and helped me immensely, and it has been such a joy working together. I will truly miss our weekend-coffee expeditions[a].

I would also like to thank a number of people from outside Aarhus University. Eric P. Nicholas, who supported me in pursuing this PhD. Eva M. Carlsen, for many great discussions and scientific collaborations. Ubadah Sabbagh, for valuable discussions and for always reminding me (by example) that my scientific writing is mediocre at best. Zoltan Raics, for always being available for technical assistance. Ashley Juavinett, Kachi Odoemene, and Daniel E. Wilson, for crucial assistance on how to set up *in vivo* imaging. Finally, a big thanks to Mathias L. Heltberg and Mogens H. Jensen for providing me office space at the Niels Bohr Institute while writing this dissertation. Furthermore, I would like to extend my appreciation to the principal investigators who allowed me to visit their laboratory during my studies: Botond Roska, Georg Keller, Carl C.H. Petersen, and Ole Kiehn.

Science is not possible without funding, and I would like to thank the Lundbeck Foundation, the Niels Bohr Foundation, the Augustinus Foundation, the Biochemical Association at Aarhus University, and the Howard Hughes Medical Institute for generous financial support.

And finally, thank you to my family. Thank you to my parents, Kai and Lone, for their unwavering support during all these years; no one was prouder than them when I published my first paper. Thank you to my sister, Lykke, for paving the way and for showing that with hard work you can achieve what you set out for. In closing, I would like to sincerely thank my wife, An. You hung-on with me in spite of my leaving for Aarhus, only months after we first met in Copenhagen. You always believe in me, no matter whether my papers are rejected, or experiments are troubling me. Finally, thank you An, for your extraordinary patience when I am (almost) always available on Slack.

---

[a] The best coffee in Aarhus is without any doubt served at Stiller's Coffee.

Abstract

Vision is an essential sensory modality, and motion is arguably one of the most salient features that the visual system needs to detect. Cells preferentially responding to visual motion in a particular direction are said to be direction-selective (DS), and these were first identified in the primary visual cortex (V1). Since then, DS responses have been observed in the retina of a number of species, including mice, indicating motion analysis has begun even at the earliest stage of the visual hierarchy. These retinal DS cells send projections to the visual cortex via the visual thalamus. Yet little is known about how direction selectivity computed in the retina contributes to motion processing in primary and higher-order areas of the visual cortex. The aim of this PhD project was to provide answers to this question.

The first study of this dissertation examined whether retinal direction selectivity contributes to the refinement of specialized neuronal representations in higher visual cortical areas. We used two complementary genetic approaches to disrupt direction selectivity in the retina and mapped cellular responses to visual motion in anaesthetized and awake mice. We found that a subset of DS cells in the rostrolateral (RL) cortical area were reduced when retinal direction selectivity was disrupted. These cells were characterized by responding more vigorously, and developing a prominent preference for posterior motion, when a stimulus moved at higher temporal frequencies. In stark contrast, DS cells in the posteromedial (PM) cortical area were not affected by the retinal manipulations. Notably, the response properties of DS cells in V1 projecting to area RL, but not those projecting to area PM, were also affected by disruption of retinal direction selectivity. This indicates that the specific connectivity of cortico-cortical projections carries signaling originating from retinal DS cells preferentially to area RL. This work thus identified a cortical processing stream for direction selectivity computed in the retina.

The second study investigated whether retinal direction selectivity contributes to optic flow processing in the visual cortex. We employed a visual stimulus that tests the full horizontal motion repertoire, combined with genetic disruption of retinal horizontal direction selectivity and mapping of cellular responses in the cortex of awake mice. We found that all cortical areas imaged — V1, RL, PM, anterior (A), and anteromedial (AM) — contained cells exhibiting response selectivity to translational or rotational optic flow, but areas RL and A were preferentially enriched with these cells. Notably, the proportions of translation-selective cells in V1 and translation- and rotation-selective cells in areas RL and A, but not in areas AM and PM, were decreased in mice with disrupted retinal direction selectivity. Furthermore, in wild-type mice, visual cortical areas were

clearly functionally segregated based on their proportions of optic flow-sensitive cells, while in mice with disrupted retinal direction selectivity this segregation was blurred. Thus, this work revealed that retinal direction selectivity causally influences area-specific optic flow representations in the visual cortex.

Altogether, this PhD dissertation presents a novel account of how the brain processes motion from the visual world. Our work demonstrates that direction selectivity computed at the level of the retina — a stage of the visual hierarchy previously held to provide considerably more mundane contributions to higher-order levels — serves to establish specialized motion responses in distinct areas of the mouse visual cortex. Thus, the findings gathered from these lines of investigation should compel us to revisit our notions of how the brain builds complex visual representations, and underscores the importance of the processing performed in the periphery of sensory systems.

Resumé

Synet er en fundamental sans, og sansningen af bevægelse er velsagtens en af de vigtigste opgaver for synsapparatet. Til dette formål findes der celler, som særligt reagerer på objekter, der bevæger sig i en bestemt retning og derfor siges at være retnings-selektive (RS). Siden denne type celler først blev opdaget i den primære visuelle hjernebark (V1), har man fundet RS-celler i nethinden hos en række dyrearter inklusiv mus, hvilket indikerer, at sansningen af bevægelser starter allerede her, i det første trin af synsbearbejdningen. Disse RS-celler sender forbindelser til den visuelle hjernebark via den visuelle del af thalamus, men man ved ganske lidt om, hvordan nethindens RS-celler bidrager til sansningen af visuel bevægelse i den visuelle hjernebark. Denne PhD afhandling sigter mod at belyse netop dette spørgsmål.

Det første studie i afhandlingen undersøgte, hvordan specialiseret neuronal aktivitet i højerestående områder af den visuelle hjernebark afhænger af nethindens RS-celler. For at undersøge dette anvendte vi to genetiske strategier med det formål at forstyrre nethindens retningsselektivitet, samtidig med at vi målte den cellulære aktivitet, der opstod, når synet blev stimuleret. For at udelukke uønskede effekter af generel anæstesi udførte vi målingerne i både bedøvede og vågne mus. Vi fandt, at en særlig gruppe af RS-celler i det rostrolaterale (RL) område af den visuelle hjernebark var reducerede, når nethindens retningsselektivitet var forstyrret. Denne type celler var karakteriseret ved at udvikle en iøjefaldende præference for bagudrettet bevægelse og ved at reagere kraftigere, når stimulus bevægede sig med høje hastigheder. I kontrast til dette var RS-celler i det posteromediale (PM) område upåvirkede af ændrede forhold i nethinden. Særligt interessant var det, at aktiviteten af RS-cellerne i V1 med forbindelse til RL, men ikke RS-cellerne med forbindelse til PM, også var påvirket, når nethindens retningsselektivitet var forstyrret. Dette studie kortlagde dermed et neuronalt netværk, som sikrer, at information fra nethindens RS-celler bliver dirigeret fortrinsvist til området RL via højt-specialiserede neuronale forbindelser.

Det andet studie undersøgte, hvorvidt nethindens RS-celler bidrager til sansningen af optisk flow i den visuelle hjernebark. Til dette anvendte vi en type synsstimuli, som tester hele repertoiret for horisontal bevægelse i kombination med, at vi ved hjælp af genetiske redskaber forstyrrede nethindens retningsselektivitet og efterfølgende målte den cellulære aktivitet i hjernebarken på vågne mus. I alle målte områder — V1, RL, PM, samt det anteromediale (AM) og anteriore (A) område — fandt vi celler som udviste selektivitet for enten translationel eller rotationel optisk flow. Dog fandtes disse celler især hyppigt i områderne RL og A. Særligt interessant var det, at antallet af de translations-selektive celler i V1 og af de translations-selektive og rotations-selektive

celler i RL og A var reducerede i mus, hvor nethindens retningsselektivitet var forstyrret, mens antallet af denne type celler i PM og AM var uændret. Herudover fandt vi at de visuelle hjernebarksområder i vildtype mus funktionelt kunne opdeles baseret på deres komposition af optisk flow-sensitive celler, mens denne opdeling var mindre klar i mus med forstyrret retningsselektivitet i nethinden. Dette studie påviste dermed, at nethindens RS-celler bidrager til område-specifik sansning af optisk flow i den visuelle hjernebark.

Alt i alt præsenterer denne PhD afhandling en ny fortælling om hvordan hjernen bearbejder visuel bevægelse i omgivelserne. Vores resultater viser hvordan specialiseret neuronal aktivitet i særlige områder af den visuelle hjernebark på mus afhænger af sansningen af visuel bevægelse i øjets nethinde — en del af synsapparatet som man tidligere mente bidrog langt mere beskedent til aktiviteten i højerestående områder. Således bør fundne fra disse studier få os til at revidere vores forestillinger om, hvordan hjernen skaber komplekse visuelle repræsentationer, og de understreger vigtigheden af sansebearbejdning i den perifere del af sensoriske systemer.

Papers

The PhD dissertation is based on the following three papers:

- <u>Rasmussen, R.N.</u>*, Matsumoto, A.*, Arvin, S., and Yonehara, K. (2020). Binocular integration of retinal motion information underlies optic flow processing by the cortex. bioRxiv 2020.10.16.342402.
  Doi: https://doi.org/10.1101/2020.10.16.342402 (*Accepted by Current Biology*)

- <u>Rasmussen, R.</u> and Yonehara, K. (2020). Contributions of Retinal Direction Selectivity to Central Visual Processing. Curr. Biol. *30*, R897–R903.
  Doi: https://doi.org/10.1016/j.cub.2020.06.002 (*Published*)

- <u>Rasmussen, R.</u>*, Matsumoto, A.*, Dahlstrup Sietam, M., and Yonehara, K. (2020). A segregated cortical stream for retinal direction selectivity. Nat. Commun. *11*, 831.
  Doi: https://doi.org/10.1038/s41467-020-14643-z (*Published*)

  Authors contributed equally.

In addition, the following papers were published or submitted during the PhD enrollment period but are not considered part of the PhD dissertation:

- Arvin, S., <u>Rasmussen, R.N.</u>, and Yonehara, K. (2020). EyeLoop: An open-source, high-speed eye-tracker designed for dynamic experiments. bioRxiv 2020.07.03.186387.
  Doi: https://doi.org/10.1101/2020.07.03.186387 (*In preparation*)

- Heltberg, M.L., Awada, H.N., Lucchetti, A., Jensen, M.H., Dreyer, J.K., and <u>Rasmussen, R.N.</u> (2020). Theoretical analysis predicts an optimal therapeutic strategy in distinct parkinsonian landscapes of the striatum. bioRxiv 2020.07.19.210690.
  Doi: https://doi.org/10.1101/2020.07.19.210690 (*Revised and resubmitted*)

- <u>Rasmussen, R.</u> and Sabbagh, U. (2020). Neural Polyamory: One Cell Forms Meaningful Connections with Hundreds of Partners. Cell Syst. *10*, 381–383.
  Doi: https://doi.org/10.1016/j.cels.2020.04.009 (*Published*)

- Rasmussen, R.*, O'Donnell, J.*, Ding, F., and Nedergaard, M. (2020). Interstitial ions: A key regulator of state-dependent neural activity? Prog. Neurobiol. *193*, 101802.
  Doi: https://doi.org/10.1016/j.pneurobio.2020.101802 (*Published*)

- Rasmussen, R., Nicholas, E., Petersen, N.C., Dietz, A.G., Xu, Q., Sun, Q., and Nedergaard, M. (2019). Cortex-wide Changes in Extracellular Potassium Ions Parallel Brain State Transitions in Awake Behaving Mice. Cell Rep. *28*, 1182–1194.
  Doi: https://doi.org/10.1016/j.celrep.2019.06.082 (*Published*)

- Rasmussen, R., Jensen, M.H., and Heltberg, M.L. (2017). Chaotic Dynamics Mediate Brain State Transitions, Driven by Changes in Extracellular Ion Concentrations. Cell Syst. *5*, 591–603.
  Doi: https://doi.org/10.1016/j.cels.2017.11.011 (*Published*)

- Rasmussen, R. and Yonehara, K. (2017). Circuit Mechanisms Governing Local vs. Global Motion Processing in Mouse Visual Cortex. Front. Neural Circuits *11*.
  Doi: https://doi.org/10.3389/fncir.2017.00109 (*Published*)

- Kjaerby, C.*, Rasmussen, R.*, Andersen, M., and Nedergaard, M. (2017). Does Global Astrocytic Calcium Signaling Participate in Awake Brain State Transitions and Neuronal Circuit Function? Neurochem. Res. *42*, 1810–1822.
  Doi: https://doi.org/10.1007/s11064-017-2195-y (*Published*)

- Rasmussen, R. and Samson, A.J. (2017). Astrocytes: Tailored to Support the Demand of Neural Circuits? Cell Syst. *5*, 165–167.
  Doi: https://doi.org/10.1016/j.cels.2017.09.008 (*Published*)

- Carlsen, E.M. and Rasmussen, R. (2017). Protein Networks in Alzheimer's Disease. Cell Syst. *4*, 153–155.
  Doi: https://doi.org/10.1016/j.cels.2017.02.006 (*Published*)

Abbreviations

Abbreviation	Full description
A	Anterior visual area
AL	Anterolateral visual area
AM	Anteromedial visual area
ChAT	Choline acetyltransferase
dLGN	Dorsal lateral geniculate nucleus
DS	Direction-selective
$Frmd7^{tm}$	$Frmd7$ mutant mouse
HVA	Higher visual area
LI	Laterointermediate visual area
LM	Lateromedial visual area
LP	Lateral posterior nucleus
OS	Orientation-selective
P	Posterior visual area
PM	Posteromedial visual area
POR	Postrhinal visual area
PPC	Posterior parietal cortex
RGC	Retinal ganglion cell
RL	Rostrolateral visual area
SAC	Starburst amacrine cell
SC	Superior colliculus
V1	Primary visual cortex

1 Introduction

Sensations and perceptions from the surrounding world are delivered to us by our various sensory systems and are fundamental to our everyday behavior. Many animals, including humans, rely on vision as their primary sense for navigating the world and for making decisions. Hence, deciphering the mechanisms giving rise to the experience of sight is a major goal of neuroscience. This is a profound challenge because the visual system is faced with the non-trivial task of transforming vast amounts of scene information from the outside world into useful neural representations within the brain. The most salient feature that the visual system detects and processes is arguably motion, and we still do not fully understand how it accomplishes this.

A central function of the visual motion system is to provide sensory information for the control of self-motion during periods of dynamic movement like locomotion (Gibson, 1950; Lappe et al., 1999). In humans, this is easily experienced firsthand, simply imagine the difficulty of walking or running toward a goal with eyes closed. The global patterns of visual motion generated by, and experienced during locomotion are called optic flow. The precise pattern of optic flow depends on the specific movements made, such as whether moving forward or making a turn, and therefore provides a powerful source of visual information about self-motion. Thus, optic flow information is used to regulate walking speed (Prokop et al., 1997), estimate distance travelled (Frenz and Lappe, 2005; Srinivasan et al., 2000), and importantly, to control the direction of self-motion (Gibson, 1950; Schubert et al., 2003; Warren et al., 1988); all tasks relevant to navigation and course control. Another important function of the visual motion system is the ability to detect and represent the speed and direction of moving objects. Such information advises animals as to which direction prey or a predator may be moving, allowing it to decide whether it should flee, freeze, or attack.

Neurons which are deemed visually responsive react to certain visual stimulus features presented within their receptive field — the volume of visual space that can elicit responses from a particular neuron when a stimulus is presented. The foundation for our present understanding of how the brain represents visual motion builds upon the discovery of explicit neural representations of motion, namely in the form of neurons which exhibit response selectivity depending on the direction in which an image feature moves across its receptive field. Neurons exhibiting this property are classified as direction-selective (DS), and were first observed in the primary visual cortex (V1) of cats and monkeys (Hubel and Wiesel, 1959, 1968). Later, neurons of this type were found within the visual cortex of many other mammalian species, including mice (Niell and Stryker, 2008), one of the most common laboratory animals in modern times.

A common notion in the field is that the brain constructs its visual motion perceptions from information encoded by the responses of cortical DS neurons. This assumption is largely built on work in monkeys that causally linked the activity of DS neurons residing in a particular higher-order area of the visual cortex, the middle temporal area, to the ability to successfully report the direction of object motion (Salzman et al., 1990), indicating that cortical DS neurons may be the functional basis for creating motion perceptions.

The detection of complex visual features within a scene, such as motion, was historically thought to be a property unique to the visual cortex alone (Seabrook et al., 2017). Along the same vein, DS responses are typically thought to emerge *de novo* within V1 from the convergence of thalamic inputs, and such a mechanism has indeed been identified in mice (Lien and Scanziani, 2018). Yet, fascinatingly, more than 50 years ago DS responses were first recorded in the retina of rabbits (Barlow and Hill, 1963) and have later been documented in several other species including mice (Weng et al., 2005), indicating that motion analysis is not exclusive to the visual cortex, and instead begins at the level of the retina. We now know that the retina of mice contains mosaic arrangements of DS retinal ganglion cells (RGCs) that preferentially respond to motion in one of the four cardinal directions (anterior, posterior, dorsal, and ventral) (Borst and Euler, 2011; Dhande and Huberman, 2014). These cells fall into two main classes: ON and ON-OFF DS cells (Dhande and Huberman, 2014; Wei and Feller, 2011; Yonehara et al., 2009). The ON DS cells respond solely to light increments, while ON-OFF DS cells respond to both light increments and decrements. Of these two cell classes, the function of ON DS cells is best understood; these cells send projections exclusively to nuclei of the accessory optic system and are thought to be dedicated to the mediation of the optokinetic reflex, a type of involuntary eye movement used for gaze stabilization (Yonehara et al., 2016; Yoshida et al., 2001). Conversely, while we know that ON-OFF DS cells send their axons to areas of the central visual pathways (Borst and Euler, 2011; Dhande and Huberman, 2014; Seabrook et al., 2017), their behavioral role remains largely unknown. Furthermore, our causal and mechanistic understanding of how signaling from these retinal DS cells influences visual processing in V1 and higher-order visual cortical areas is very limited. Thus, the aspiration of the work presented in this PhD dissertation was to narrow the gap in our knowledge of how direction selectivity computed in the retina of mice subserves visual motion processing performed by the visual cortex.

2 Background

In this chapter, I provide background information useful for interpreting the subsequent experimental work. I cover key structures and pathways of the mouse visual system, and models for manipulating retinal direction selectivity; I present what we knew about the contribution of retinal direction selectivity to cortical processing before I began my PhD project; and finally, I outline the overall aim and research objectives to which the work presented in this dissertation seeks to provide answers.

2.1 Overview of the mouse visual system

Much of our early knowledge of how the visual system processes information stems from experiments performed in cats and non-human primates, such as monkeys. However, nowadays the mouse is a preeminent animal model for studying the neural mechanisms governing sight and the malfunctions thereof. Several advantages have prompted the use of mice for studying vision, despite the fact that the mouse visual system exhibits some notable differences to that of carnivores and primates (Baker, 2013; Huberman and Niell, 2011; Seabrook et al., 2017). These advantages include the mouse's convenient size, relatively low cost, and, most importantly, its outstanding tractability for genetic manipulations. In this species, powerful tools for *in vivo* labeling, activity monitoring, and perturbations of neural cells are now available, making it possible to test the causal involvement of specific cell types in visual processing and behavior.

The separation of visual circuits into image-forming and non-image-forming pathways is possibly the roughest functional distinction one can use to segregate the organization of the visual system (Seabrook et al., 2017). Image-forming pathways give rise to sight and are involved in perceiving visual features such as shape, color, depth, and motion. Conversely, non-image-forming pathways are involved in behaviors that occur below our conscious perception, including the regulation of pupil size and circadian rhythm. The image-forming pathways of mice can be further segregated into two pathways: the retino-geniculate and the retino-collicular pathways (Dhande et al., 2015; Huberman and Niell, 2011; Seabrook et al., 2017) (Figure 1). The retino-geniculate pathway conveys retinal information directly to the visual cortex via the dorsal lateral geniculate nucleus (dLGN) of the thalamus, whereas in the retino-collicular pathway, information reaches the cortex only after passing through the superior colliculus (SC) and then lateral posterior nucleus (LP, analogous to the primate pulvinar nucleus) of the thalamus (Figure 1). To limit the amount of information in this background chapter, this section focuses predominantly on the retino-geniculate pathway, since this is the primary pathway under experimental

investigation in the work presented in this dissertation, and historically thought to be the pathway supporting conscious visual perceptions. The section is not intended as an exhaustive review, but rather as an introduction to the visual areas, pathways, and cell types that are directly relevant to the empirical investigations that comprise the presented dissertation.
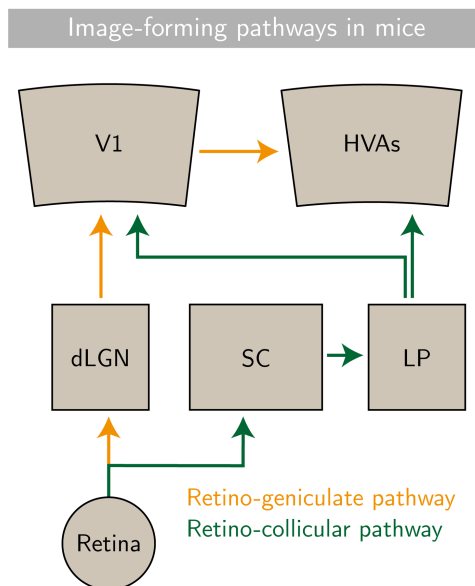

Figure 1 | Image-forming pathways of the mouse visual system. Diagram of the feedforward connections in the retino-geniculate and retino-collicular pathways. The retino-geniculate pathway conveys retina-originating information to the primary visual cortex (V1) and higher visual areas (HVA) via the dorsal lateral geniculate nucleus (dLGN) of the thalamus. In the retino-collicular pathway, retina-originating information reaches the visual cortex after passing through the superior colliculus (SC) in the midbrain and the lateral posterior nucleus (LP) of the thalamus. Note that dLGN sends information only to V1, whereas LP sends information to both V1 and HVAs. Diagram is adapted from Glickfeld and Olsen (2017).

2.1.1 Cell types and the general circuit motif of the retina

The first steps of vision occur in the retina. The retina is a thin layer of neural tissue located at the back of the eye (Figure 2), whose ultimate job is to detect and convert incoming patterns of light into electrical signals — action potentials — and to transmit them to downstream visual areas. Consistent with being part of the central nervous system, the retina contains complex neural circuits (Baden et al., 2020; Dhande et al., 2015; Masland, 2001). The retina contains five classes of neurons: photoreceptors, bipolar cells, horizontal cells, amacrine cells, and RGCs (retinal ganglion cells), which are organized into five layers: three nuclear and two synaptic layers (Figure 2). The cell
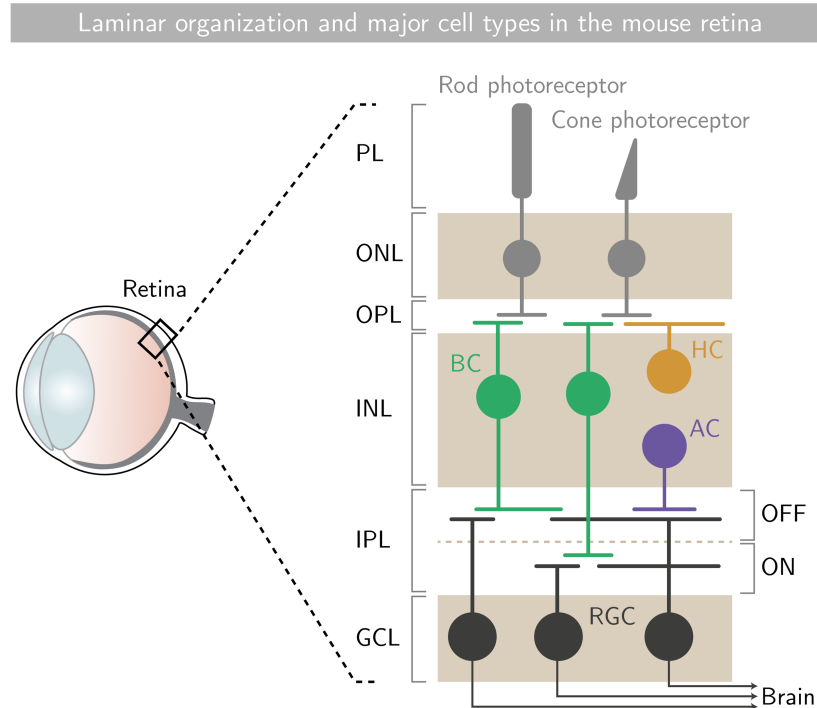
Figure 2 | General organization and major cell types in the mouse retina. Diagram of the organization of the retina, and the major classes of retinal cells (photoreceptors, bipolar cells [BC], horizontal cells [HC], amacrine cells [AC], and retinal ganglion cells [RGCs]). Photoreceptors have their outer segment within the photoreceptor layer (PL). Cell bodies reside in the nuclear layers (outer nuclear layer [ONL], inner nuclear layer [INL], and ganglion cell layer [GCL]), and their dendrites and synapses reside in the synaptic layers (outer plexiform layer [OPL] and inner plexiform layer [IPL]). The IPL contains two sublaminae: the OFF and ON sublamina. Cells with their synapses or dendrites in the OFF and ON sublamina are excited by light decrements and increments, respectively. The output information, encoded by the action potential firing pattern of RGCs, is sent to the brain via the RGC axons, forming the optic nerve. Diagram is adapted from Baden et al. (2020).

bodies reside in the outer, inner, and ganglion cell layers, and the dendrites and synapses reside in the outer plexiform and inner plexiform layers. In the first synaptic layer, the outer plexiform layer, rod and cone photoreceptors synapse onto bipolar and horizontal cells. Upon the absorption of light, rods and cones hyperpolarize and release less glutamate onto the postsynaptic dendritic processes of bipolar and horizontal cells. Bipolar cells come in two main variants: OFF and ON bipolar cells (Masland, 2001). OFF bipolar cells are excited by glutamate, and thus when glutamate release decreases during light exposure, these cells hyperpolarize, whereas they are activated when light is off. Conversely, ON bipolar cells hyperpolarize in response to glutamate, and thus when light is on, and glutamate release is low, these cells are excited. Horizontal cells connect laterally and provide modulatory feedback and feedforward signals to photoreceptors and

bipolar cells, respectively. The bipolar cells extend their axons into the second synaptic layer, the inner plexiform layer, where they form glutamatergic synapses on the dendrites of amacrine cells and RGCs. OFF bipolar cells make connections in the OFF sublamina of the inner plexiform layer, whereas ON bipolar cells make connections in the ON sublamina (Figure 2). Similar to horizontal cells, amacrine cells connect laterally, but also across the inner plexiform layer, to provide inhibitory feedback and feedforward signals to bipolar cells and RGCs, respectively. Finally, the RGCs, existing as ON, OFF, and ON-OFF variants, integrate the synaptic input from bipolar and amacrine cells and send their output as action potentials to the brain via the optic nerve (Figure 2). Hence, all the information that the brain receives about the visual world, and builds its representations from, is encoded by the patterns of action potentials in the RGCs.

The general circuit organization described here is highly conserved across species (Baden et al., 2020). Yet, the mouse is arguably the species for which we have the most detailed understanding of the anatomical, molecular, and functional properties of retinal cell types and circuits processing distinct features (Baden et al., 2020). The current estimate is that the mouse retina contains 40–50 types of RGCs (Baden et al., 2016; Masland, 2001). Of these, seven or more are directionally selective (Borst and Euler, 2011; Vaney et al., 2012). Noticeably, retinal DS cells are numerous in the mouse, where they are suggested to comprise up to 35% of the RGCs (Baden et al., 2016), indicating that these cells likely serve important functions in this species. The next subsection focuses on these retinal DS cells by introducing the different types, the computational mechanisms for creating retinal direction selectivity, and their downstream projection patterns. Parts of this text are represented in the review article presented in Chapter 4 but have been paraphrased for this subsection.

2.1.2 Direction-selective cells of the retina

The first experimental evidence of DS cells in the mammalian retina emerged in the 1960s in a series of foundational experiments by Barlow, Levick, and colleagues, wherein they demonstrated DS responses in the retina of rabbits (Barlow and Hill, 1963; Barlow and Levick, 1965; Barlow et al., 1964). Since then, retinal DS cells have been identified in a range of species, including mice (Weng et al., 2005), and the circuitry creating retinal DS responses is likely one of the most investigated and best understood neural circuitries of the mammalian brain (Borst and Euler, 2011).

2.1.2.1 Retinal DS cell types

The retina contains several types of DS cells which fall into two main classes: ON-OFF and ON DS cells (Borst and Euler, 2011; Mauss et al., 2017; Vaney et al., 2012). ON-

OFF DS cells fire action potentials both at the leading and the trailing edge of a bright stimulus when moving along the preferred direction through the receptive field on a dark background, that is, they respond to both light increments and decrements (Barlow and Levick, 1965). Conversely, ON DS cells respond only to the leading edge of a bright stimuli moving on a dark background through the receptive field, meaning they only respond to light increments. Thus, ON-OFF DS cells are bistratified and ramify their dendrites within both the ON and OFF sublamina of the inner plexiform layer, whereas ON DS cells only ramify within the ON sublamina (Borst and Euler, 2011; Vaney et al., 2012). Another distinction between ON-OFF and ON DS cells is their motion speed preference; ON-OFF DS cells respond to a broad range of speeds up to at least 100 degrees per second, whereas ON DS cells are best tuned to slower motion speeds around 5 degrees per second (Weng et al., 2005; Yonehara et al., 2016).

ON-OFF and ON DS cells can be classified into several subtypes based on their preferred direction of motion (Oyster and Barlow, 1967) and, more recently, on genetic markers (Huberman et al., 2009; Kay et al., 2011; Rivlin-Etzion et al., 2011; Trenholm et al., 2011; Yonehara et al., 2008). ON-OFF DS cells include four subtypes, each of which prefers motion in one of the four cardinal directions: anterior, posterior, dorsal, or ventral motion (Figure 3A). ON DS cells can be grouped into three subtypes, preferring anterior, dorsal, or ventral motion (Figure 3A). It should be noted that a third type of retinal DS cells, named OFF DS cells, has been described (Kim et al., 2008). These cells are characterized by having their dendrites located in the OFF sublamina of the inner plexiform layer, responding to light decrements, and they have a response preference to dorsal motion. However, these OFF DS responses have not been consistently detected in other studies (Sabbah et al., 2017), and it is therefore still debated whether these cells comprise a distinct type of retinal DS cell.

2.1.2.2 Synaptic mechanisms creating retinal direction selectivity

Both ON-OFF and ON DS cells receive glutamatergic excitation from bipolar cells and GABAergic inhibition and cholinergic excitation from a type of amacrine cell called starburst amacrine cells (SACs) (Figure 3B). The SACs exist in ON and OFF variants and co-stratify with the respective dendritic trees of ON-OFF and ON DS cells. This can be visualized by staining retinal tissue for choline acetyltransferase (ChAT), a marker of SACs, revealing stratification in two distinct ChAT-positive bands, corresponding to the ON and OFF sublamina of the inner plexiform layer (Jeon et al., 1998). Importantly, the inhibition from SACs is directionally tuned: during motion in the retinal DS cell's preferred direction, SAC-mediated inhibition is minimal, while during motion in the opposite direction (also known as the null direction), inhibition is maximal (Figure 3B). This directionally tuned inhibition is necessary for establishing DS responses in ON-OFF

and ON DS cells (Yonehara et al., 2016). Two key mechanisms underlying this tuned inhibition are the spatially asymmetric inhibitory connectivity between the SAC and the RGC (Briggman et al., 2011; Wei et al., 2011; Yonehara et al., 2011), and the centrifugal direction selectivity within the dendrites of the SAC (Borst and Euler, 2011; Vaney et al., 2012). Recently it was discovered that ON DS cells have an additional circuit mechanism, consisting of glutamatergic excitation provided by two different groups of bipolar cells with distinct temporal dynamics: slow sustained and fast transient inputs (Matsumoto et al., 2019) (Figure 3B). Slow sustained and fast transient inputs are biased to the preferred and null sides of the ON DS cell's dendrites, respectively. When motion is in the preferred direction, the synaptic delays between the two types of input are offset by the preceding activation of the slow sustained input, yielding temporal summation, however, in the null direction such temporal summation is less efficient (Figure 3B).
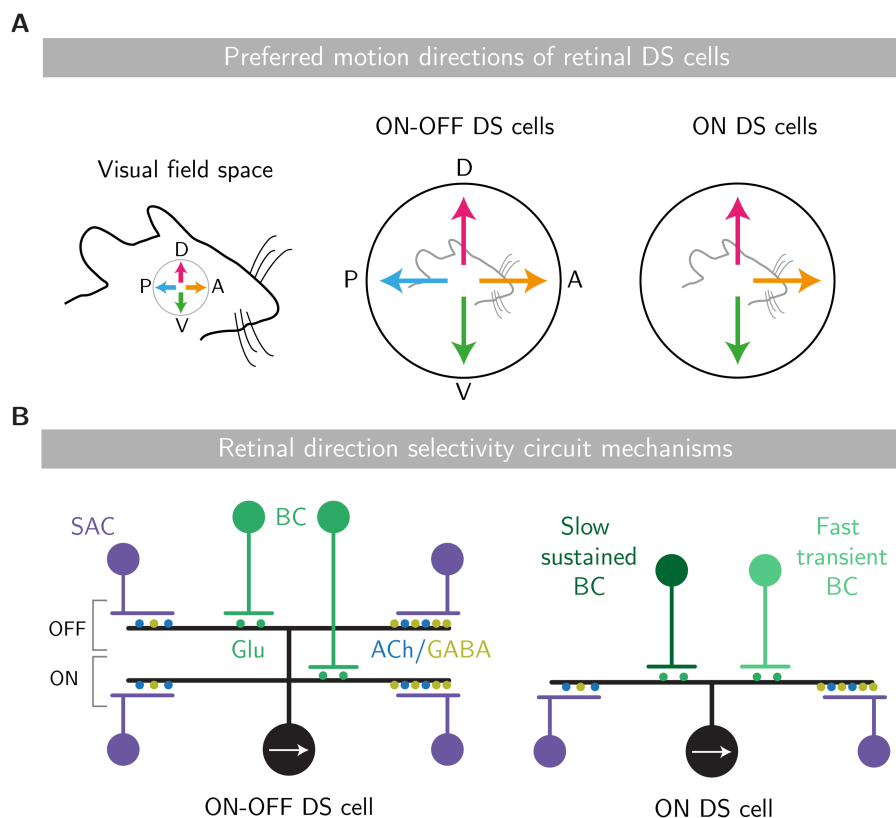
Figure 3 | Retinal direction selectivity in the mouse. (A) Diagram of the preferred motion directions of retinal direction-selective (DS) cells with respect to the visual field. ON-OFF DS cells include four subtypes, each preferring motion in one of the four cardinal directions: anterior (A), posterior (P), dorsal (D), or ventral (V). ON DS cells contain three subtypes, each preferring either anterior, dorsal, or ventral motion. (B) Diagram of the circuitry underlying direction selectivity in ON-OFF and ON DS cells. ON-OFF and ON DS cells receive glutamatergic excitation (Glu) from bipolar cells (BC) and GABAergic inhibition (GABA) and cholinergic excitation (ACh) from starburst

amacrine cells (SAC). The inhibition from SACs is directionally tuned: during motion in the preferred direction (indicated by the white arrow), SAC-mediated inhibition is small, while during motion in the null direction, inhibition is stronger. ON DS cells have an additional mechanism, mediated by two different groups of BCs: slow sustained and fast transient inputs, each biased to the preferred and null sides of the ON DS cell's dendrites, respectively. During motion in the preferred direction, excitatory inputs summate, whereas in the null direction, summations is less efficient. Panel (A) is adapted from Borst and Euler (2011); (B) is adapted from Rasmussen and Yonehara (2020).

2.1.2.3 Projection targets of retinal DS cells

Between the ON-OFF and ON DS cells, the behavioral role of ON DS cells is more well understood. Earlier work, done mainly in rabbits, implicated ON DS cells as the main RGC type involved in gaze-stabilizing eye movements (Simpson, 1984). These cells do indeed project selectively to nuclei of the accessory optic system that are involved in generating the reflexive eye movements required for gaze stabilization (Yonehara et al., 2008, 2009). More recent work tested the causal involvement of retinal DS for eye movements, and showed that interfering with direction selectivity in these cells abolishes optokinetic reflex eye movements (Sun et al., 2015; Yonehara et al., 2009, 2016; Yoshida et al., 2001). These findings provide a compelling case for ON DS cells as the main RGC type for eliciting involuntary eye movements.

Importantly, unlike ON DS cells, ON-OFF DS cells project to visual areas of the image-forming pathways and send their main axonal projections to the SC and their collaterals innervate the dLGN (Huberman et al., 2009; Kay et al., 2011; Rivlin-Etzion et al., 2011) (Figures 1 and 4A). This difference in connectivity may suggest that ON-OFF DS cells contribute to functions occurring in higher-order areas of the visual hierarchy including the visual cortex (Huberman and Niell, 2011). Yet, this question remains largely unexplored and the behavioral roles of ON-OFF DS cells are still unresolved.

2.1.3 The dorsal lateral geniculate nucleus

The dLGN of the thalamus is a main conduit for visual information from the retina to V1 and thus considered a starting point of higher-order visual processing (Dhande et al., 2015). In mice, the dLGN is located in the dorsal aspect of the diencephalon, situated between the intergeniculate leaflet and ventral lateral geniculate nucleus on the ventrolateral border, and the LP on the dorsomedial border (Kerschensteiner and Guido, 2017; Liang and Chen, 2020). The simple organization of the mouse dLGN compared to that described in cats and monkeys highlights the distinct evolutionary path of different species, recently reviewed in detail (Liang and Chen, 2020).

2.1.3.1 Retinal inputs are functionally organized in the dLGN

The dLGN receives inputs from several different types of RGCs, including DS cells (Dhande et al., 2015; Liang and Chen, 2020; Seabrook et al., 2017). In the adult mouse, most of these RGCs innervate the contralateral dLGN, but a small portion project ipsilaterally. Hence, the majority of the dLGN is innervated by the contralateral eye, with only a small volume of ipsilateral projections being located in the anteromedial aspect of this nucleus. Although eye-specific zones distinguish different regions of the dLGN, the dLGN of rodents lacks clear lamination, which is in contrast to its counterparts in carnivores and primates (Kerschensteiner and Guido, 2017; Liang and Chen, 2020; Reese, 1988). Yet, studies using retrograde tracer injections (Martin, 1986) or genetic labeling of distinct types of RGCs (Ecker et al., 2010; Huberman et al., 2008, 2009; Kay et al., 2011; Kim et al., 2008, 2010; Rivlin-Etzion et al., 2011) have revealed that the retinal innervation of the rodent dLGN is far from random. The dLGN of the mouse can be divided into two distinct regions; the core and the shell, each containing a retinotopic representation of visual space (Dhande et al., 2015; Liang and Chen, 2020; Reese, 1988). The core and the shell regions receive inputs from different types of RGCs (Figure 4A). The core gets the majority of its input from non-DS RGCs, such as alpha-like and melanopsin-expressing intrinsically photosensitive RGCs (Ecker et al., 2010; Huberman et al., 2008). Conversely, the shell is notably innervated by different types of retinal DS cells (Cruz-Martín et al., 2014; Huberman et al., 2009; Kay et al., 2011; Kim et al., 2008, 2010; Martersteck et al., 2017; Rivlin-Etzion et al., 2011). ON-OFF DS cells preferring posterior motion in the visual field exclusively innervate the superficial part of the shell region (Cruz-Martín et al., 2014; Huberman et al., 2009; Kay et al., 2011; Rivlin-Etzion et al., 2011), while ON-OFF DS cells tuned to dorsal motion innervate both the shell and the core region, with maybe a slight preference for the core (Hong et al., 2014; Kay et al., 2011; Kim et al., 2010) (Figure 4A).

2.1.3.2 Functional responses of dLGN neurons

The cellular landscape of the dLGN is populated by two types of neurons that receive direct inputs from the retina: excitatory thalamocortical relay neurons and GABAergic local interneurons, the latter represents roughly 10% of dLGN neurons and have neurites that never exit the dLGN (Kerschensteiner and Guido, 2017; Rasmussen and Sabbagh, 2020). To date, a handful of studies have characterized the response properties of neurons residing within the dLGN of the mouse. One study used *in vivo* calcium imaging (Marshel et al., 2012) and four others used single-unit electrophysiology (Piscopo et al., 2013; Román Rosón et al., 2019; Scholl et al., 2013; Zhao et al., 2013). In addition to center-surround neurons, these studies showed that mouse dLGN contains a substantial

population of neurons with more complex and selective functional properties, including direction and orientation selectivity. This is congruent with studies measuring the tuning properties of dLGN-originating axonal boutons in V1 (Cruz-Martín et al., 2014; Kondo and Ohki, 2015; Roth et al., 2015; Sun et al., 2016). Interestingly, two studies also discovered that the shell region is enriched with DS and orientation-selective (OS) neurons (Marshel et al., 2012; Piscopo et al., 2013). With this notable anatomical and functional correspondence between ON-OFF DS cell innervation and density of DS and OS neurons in the shell region of the dLGN, a pressing question is whether the convergence of ON-OFF DS cells is involved in creating DS and OS responses in the thalamocortical relay neurons. For now, this remains an unresolved question. However, the finding that at least a dozen or more RGCs converge onto a single thalamocortical relay neuron (Hammer et al., 2015; Morgan et al., 2016; Rompani et al., 2017) and that RGC inputs onto dLGN shell neurons are functionally organized (Liang et al., 2018) makes this a reasonable hypothesis to consider.
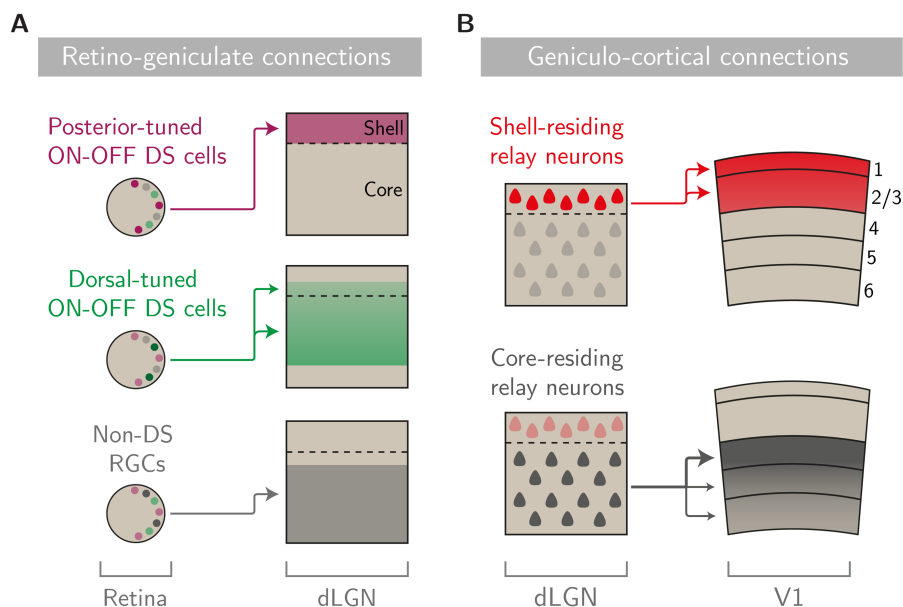

Figure 4 | Connectivity patterns within the retino-geniculate pathway in mice. (A) Diagram of the retino-geniculate projection pattern of direction-selective (DS) and non-DS retinal ganglion cells (RGCs). ON-OFF DS cells tuned to posterior motion in the visual field selectively project to the shell region of the dorsal lateral geniculate nucleus (dLGN) of the thalamus; ON-OFF DS cells tuned to dorsal motion project to both the shell and core regions; non-DS RGCs project to the core region. (B) Diagram of the geniculo-cortical projection pattern of thalamocortical relay cells. Relay cells residing in the shell region of the dLGN target the superficial layers 1 and 2/3 of the primary visual cortex (V1), whereas core-residing relay neurons target deep layers — mainly layer 4, but also layers 5 and 6. Panels (A) and (B) are adapted from Seabrook et al. (2017).

2.1.4 The primary visual cortex

In the mouse, like other mammals, the visual cortex resides in the dorsal aspect of the posterior cortex. The visual cortex is often considered to be the site where conscious motion perceptions are formed (Albright and Stoner, 1995; Andersen, 1997; Salzman et al., 1990; Tong, 2003). In the retino-geniculate pathway, visual information from the dLGN converges within V1, and is, after further processing, split into distinct parallel processing streams targeting specific higher visual areas (HVAs, or extrastriate areas) of the cortex (Nassi and Callaway, 2009). The visual cortex of the mouse, including V1, exhibits many similarities to that of other species, including its characteristic six-layered anatomy, retinotopic organization of visual space, and populations of excitatory pyramidal neurons intermixed with inhibitory interneurons.

2.1.4.1 Regions of the dLGN differentially innervate V1

Careful anatomical work has established that the specific innervation of RGC types to the core and shell dLGN regions recapitulates as segregated output circuits as well (Bickford et al., 2015; Cruz-Martín et al., 2014). Thus, a general picture of how thalamocortical relay neurons innervate V1 has emerged. Neurons residing in the shell region of the dLGN, innervated preferentially by retinal DS cells, project to layers 1 and 2/3 of V1 (Figure 4B). Interestingly, one study showed that a notable fraction of the neurons projecting from the shell to the superficial layers of V1 are indeed directionally tuned, suggesting a disynaptic circuit motif through which signaling from retinal DS cells reach V1 (Cruz-Martín et al., 2014). Conversely, neurons located in the core region of the dLGN, preferentially innervated by non-DS RGCs, send their projections mainly to layer 4 of V1 (Cruz-Martín et al., 2014), the layer receiving the densest dLGN innervation (Ji et al., 2016; Morgenstern et al., 2016; Roth et al., 2015) (Figure 4B). Collectively, these data seem to indicate parallel processing streams from the dLGN to V1 in the mouse. It should, however, be noted that one study employing *in vivo* calcium imaging found that a considerable portion of dLGN-originating axonal boutons in layer 4 of V1 are also DS (Sun et al., 2016), seeming to suggest that different subnetworks may convey motion-related information to V1 in parallel.

2.1.4.2 Functional responses of V1 neurons

Experimental investigations of the response properties of visual cortex neurons in the mouse began more than 40 years ago (Dräger, 1975). Since then, a staggering number of studies have probed the visually evoked responses of V1 neurons in mice using *in vivo* electrophysiology or calcium imaging, a few of them referenced here (Adesnik, 2017;

Adesnik et al., 2012; Dräger, 1975; Gao et al., 2010; Girman et al., 1999; Hofer et al., 2011; Van Hooser et al., 2005; Kerlin et al., 2010; Ko et al., 2011; Lien and Scanziani, 2018; Marshel et al., 2011; Métin et al., 1988; Niell and Stryker, 2008; Ohki and Reid, 2007; Ohki et al., 2005; Scholl et al., 2017). These studies have shown that V1 neurons in mice exhibit orientation selectivity, spatial and temporal frequency tuning, speed tuning, contrast-invariant tuning, contrast gain control, surround suppression, linear and nonlinear receptive field structure, and not least direction selectivity. The emerging picture is thus that mouse V1 contains all of the fundamental response properties that have been described in other mammals, such as cats or monkeys, indicating that the mouse visual cortex may be performing computations similar to those in other species, including motion processing (Hübener, 2003; Huberman and Niell, 2011). On this note, a recent study that investigated the role of V1 neurons for the ability of mice to discriminate and report different motion directions is worth highlighting (Marques et al., 2018). Inspired by previous experiments carried out in primates (Britten et al., 1992; Newsome and Paré, 1988), this work showed that a visual stimulus consisting of a random pattern of moving dots strongly drove DS responses in a subset of V1 neurons. Interestingly, when the authors inactivated V1 using a pharmacological approach, the mice were now worse at discriminating the global motion direction of the moving dots stimulus. This suggests that neuronal activity in mouse V1 is causally involved in the perception of visual motion, a plausible finding due to the motion representation encoded by cortical DS neurons. With the large experimental toolbox afforded to the mouse (O'Connor et al., 2009), this species therefore provides a tractable model system for probing the detailed circuit mechanisms of motion processing and perception.

Yet, in this endeavor, it should be kept in mind that a number of differences do exist between V1 of mice and that of carnivores and primates. One of these is that mouse V1 neurons prefer lower spatial frequencies, and their receptive fields are generally larger, compared to other mammals (Girman et al., 1999; Niell and Stryker, 2008). Another difference is the absence of a columnar architecture for feature selectivity; neighboring neurons in V1 of rodents do not show a strong functional clustering for orientation or direction preference (Van Hooser et al., 2005; Ohki and Reid, 2007; Ohki et al., 2005; Roth et al., 2012; Scholl et al., 2017) nor for ocular dominance (Mrsic-Flogel et al., 2007) or motion speed preference (Glickfeld et al., 2013). This, however, does not mean that the organization of response selectivity in mouse V1 is entirely random. Seminal studies have shown that excitatory pyramidal neurons sharing similar tuning preferences are more likely to be connected than neurons exhibiting different preferences (Cossell et al., 2015; Hofer et al., 2011; Ko et al., 2011; Lee et al., 2016; Li et al., 2012), suggesting the existence of intracortical subnetworks dedicated to processing of related visual information.

2.1.4.3 Direction selectivity computed *de novo* in layer 4 of V1

Although the work in this dissertation focused on the role of retinal direction selectivity for motion processing by the cortex, it is important to establish that a form of *de novo* direction selectivity arises in mouse V1. One impressive study leveraged *in vivo* single-unit and whole-cell electrophysiology, in combination with optogenetics, to demonstrate that DS responses in layer 4 of V1 emerge from non-DS dLGN inputs that are spatially and temporally offset (Lien and Scanziani, 2018). Mechanistically, when gratings move in a layer 4 DS neuron's preferred direction, dLGN inputs with sustained excitatory temporal kinetics are initially activated and as the stimulus phase moves across the visual field, inputs with transient excitatory kinetics are subsequently activated. Conversely, when gratings move in the opposite, null direction, excitatory inputs with transient kinetics are activated before inputs with sustained excitation. As a result, the temporal summation of the excitatory inputs reaches a greater amplitude, causing more action potentials being fired, for motion in the preferred rather than the null direction. This finding raises fascinating questions regarding why the mouse visual system creates direction selectivity *de novo* at two separate stages of the visual hierarchy, whether retinal and cortically generated direction selectivity converges or stays segregated within the cortex, and whether retinal and cortically generated direction selectivity subserve different behavioral functions.

2.1.5 Higher visual areas of the cortex

V1 sends its outputs to a series of HVAs (higher visual areas) within the cortex, which are increasingly specialized in the visual features they encode (Nassi and Callaway, 2009). In primates, an organizing principle of these HVAs is the division into multiple parallel processing streams, including the well-known ventral and dorsal streams. Simplified, the ventral stream conveys information regarding object identity, whereas the dorsal stream conveys information about object location (Maunsell and Newsome, 1987). However, the specific circuits from which these specialized neuronal responses emerge are not sufficiently understood in detail, primarily due to experimental challenges and the lack of extensive genetic manipulations in the primate.

2.1.5.1 Discrete HVAs of the mouse visual cortex

Over the last decade, anatomical and physiological studies have mapped and segmented the mouse visual cortex into a discrete set of HVAs, each containing a retinotopic representation of visual space (Andermann et al., 2011; Garrett et al., 2014; Juavinett et al., 2016; Marshel et al., 2011; Wang and Burkhalter, 2007; Wang et al., 2011, 2012;

Zhuang et al., 2017). Due to the use of different experimental techniques across studies, reaching a consensus on the exact number of HVAs has been challenging — a topic that has been comprehensively reviewed (Glickfeld and Olsen, 2017). For use in the work presented in this dissertation, I lean toward the formulation of Glickfeld and Olson (2017), which considers the following HVAs to be constituents of the mouse visual cortex: lateromedial (LM), anterolateral (AL), rostrolateral (RL), anterior (A), anteromedial (AM), posteromedial (PM), laterointermediate (LI), posterior (P), and postrhinal (POR) (Figure 5A). Akin to the primate, the HVAs in the mouse have been categorized into a dorsal and ventral stream dichotomy based on their connectivity and physiology, with areas LM and LI consistently being categorized as ventral-like, and areas AL, RL, and AM as dorsal-like (Marshel et al., 2011; Smith et al., 2017; Wang et al., 2011, 2012). However, given the vast interconnectivity between visual cortical areas in the mouse (Gămănuţ et al., 2018; Wang et al., 2012) and their weaker hierarchical organization compared to the primate, it seems reasonable to suggest that the ventral and dorsal stream division may be more blurred in the mouse than in the primate.

2.1.5.2 Functional areal specialization

An important property of HVAs in the primate is the progressive specialization of their visual feature tuning (Nassi and Callaway, 2009). Intriguingly, HVAs of the mouse visual cortex seem to exhibit a similar property by being more specialized in their visual processing than V1. Generally, the receptive field size of HVA neurons is larger than those observed in V1 (Wang and Burkhalter, 2007), likely indicative of converging inputs from neurons with differential, and spatially offset, receptive field properties. In addition, although each HVA contains a retinotopic representation of visual space, each area shows a biased representation of the visual field. For example, area PM is biased toward the upper temporal part of visual space, whereas area RL is biased toward the lower nasal part (Garrett et al., 2014). However, it is not only the receptive field size and visual field bias that suggest HVA specialization. Technical advancements in functional HVA mapping, and the ability to record the activity from hundreds to thousands of neurons with *in vivo* two-photon calcium imaging, has now begun to uncover the diversity and specialization in neuronal responses within HVAs (Andermann et al., 2011; Beltramo and Scanziani, 2019; Blot et al., 2020; Glickfeld et al., 2013; Juavinett and Callaway, 2015; Marshel et al., 2011; Roth et al., 2012; Smith et al., 2017; Tohmi et al., 2014). For example, several studies have probed the spatiotemporal preference of neurons populating different HVAs (Andermann et al., 2011; Blot et al., 2020; Glickfeld et al., 2013; Marshel et al., 2011; Roth et al., 2012; Tohmi et al., 2014). These studies have painted a picture of two polarized groups. One that prefers low spatial frequencies but high temporal frequencies, such as areas AL and RL, and another that prefers high spatial frequencies

but low temporal frequencies, such as area PM (Figure 5B). Conversely, the areas LM, AM, and LI seem to prefer high spatial and intermediate temporal frequencies. Hence, areas AL and RL prefer higher motion speeds (temporal frequency divided by spatial frequency), whereas LM, AM, and LI prefer intermediate speeds, and PM prefers lower speeds (Andermann et al., 2011; Blot et al., 2020; Glickfeld et al., 2013; Marshel et al., 2011; Tohmi et al., 2014). In addition, areal specialization for orientation and direction tuning has been investigated, although these results seem more variable across studies (Andermann et al., 2011; Juavinett and Callaway, 2015; Marshel et al., 2011; Roth et al., 2012). In one study, the areas AL, RL, AM, and PM were found to contain higher proportions of, and more selective, OS and DS neurons compared to areas V1, LM, and LI (Marshel et al., 2011). Yet, another study found no difference in the abundance nor in the selectivity of OS neurons between areas V1, AL, and PM; but did find more DS neurons in V1 compared to areas AL and PM (Andermann et al., 2011).

In addition, one study explored how local and global motion is encoded by neurons in HVAs of mice (Juavinett and Callaway, 2015) — a topic that we discussed in a previous review article (Rasmussen and Yonehara, 2017). A large body of literature in primates has shown that neurons encoding the local direction of motion of a plaid visual stimulus, termed component direction-selective, are found in both V1 and HVAs (Movshon and Newsome, 1996; Movshon et al., 1985). In contrast, neurons encoding the global direction of plaid motion, called pattern direction-selective, are predominantly found in areas of the dorsal stream, particularly in the middle temporal area (Movshon et al., 1985; Rodman and Albright, 1989; Smith et al., 2005; Solomon et al., 2011). The work performed by Juavinett and Callaway (2015) found that only the areas RL and LM contained pattern direction-selective neurons, whereas areas V1, AL, and AM did not contain such neurons, but rather only component direction-selective neurons, indicating that specific HVAs may be preferentially involved in global motion analysis.

An important open question pertains to how this response specialization in HVAs relates to specific behaviors. Studies are now emerging that test the role of specific HVAs in visually guided behaviors (Goldbach et al., 2020; Jin and Glickfeld, 2020; Odoemene et al., 2018). One recent study demonstrated that inhibiting areas LM or AL during a visual stimulus orientation discrimination task significantly hampered task performance of mice, suggesting the involvement of these areas in visual perception (Jin and Glickfeld, 2020). In contrast, inhibiting area PM during this task did not affect the orientation discrimination performance. Thus, neurons within HVAs clearly exhibit response specialization, especially for spatial and temporal visual properties, but still much work remains in order to obtain a comprehensive description of neuronal specialization within HVAs of the mouse and determining how such specialization translates to behavior.

A Visual cortical areas
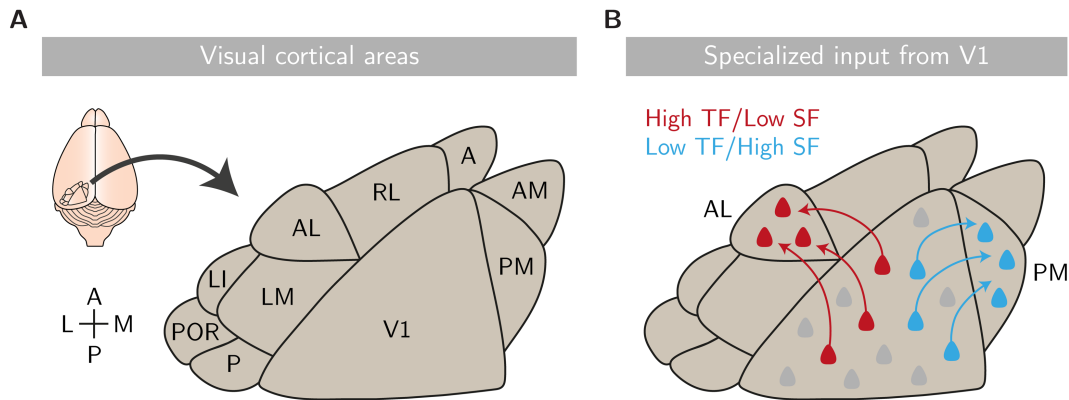
B Specialized input from V1

*Figure 5 | Organization of the mouse visual cortex and functional areal specialization.
(A) Diagram of the parcellations and anatomical organization of the mouse visual cortex. The primary
visual cortex (V1) is surrounded by at least nine higher visual areas: lateromedial (LM), anterolateral
(AL), rostrolateral (RL), anterior (A), anteromedial (AM), posteromedial (PM), laterointermediate
(LM), posterior (P), and postrhinal (POR). L, lateral; M, medial; A, anterior; P, posterior. (B)
Diagram exemplifying the functional specialization of higher visual area neurons and V1 cortico-
cortical projection neurons. Area AL neurons prefer stimuli with a high temporal frequency (TF) and
low spatial frequency (SF), whereas PM neurons prefer low TF and high SF stimuli. This functional
specialization is matched by the V1 neurons projecting to areas AL and PM. Visual cortical map in
panel (A) is adapted from Wang and Burkhalter (2007); (B) is adapted from Glickfeld et al. (2013).*

2.1.5.3 Specialized inputs from V1 to HVAs

The presence of specialized response properties in HVAs invites the question of how these
responses arise. One can imagine at least three mechanisms: 1) specialized responses
emerge locally within each HVA as a result of complex neuronal interactions; 2)
specialized responses are inherited from upstream visual areas projecting to the HVAs;
and 3) a combination of both. This question has been experimentally tackled (Blot et al.,
2020; Glickfeld et al., 2013; Kim et al., 2018; Matsui and Ohki, 2013). Foundational work
imaged V1 axonal boutons terminating in HVAs, thus probing what information is sent
from V1 to these areas (Glickfeld et al., 2013; Matsui and Ohki, 2013). One study
showed that V1 neurons projecting to areas PM, AL, or LM exhibited distinct response
properties: V1 boutons in PM preferred slower motion speeds, whereas those in LM and
AL preferred intermediate and faster speeds, respectively (Glickfeld et al., 2013) (Figure
5B). Similar trends were found in a study that imaged the activity of V1 cell bodies,
labeled in a retrograde manner from either area AL or PM (Kim et al., 2018), although,
tuning distributions overlapped considerably between AL- and PM-projecting V1
neurons. In addition, one study found that V1 boutons targeting area AL were more

selective regarding the orientation and direction of moving stimuli than to those innervating area LM (Matsui and Ohki, 2013). The stimulus preference of V1 projection neurons thus seems to match well with the preference of neurons within their target areas, indicating that the specialized responses in HVAs may, at least in part, originate from V1 inputs. However, response properties of HVA neurons are still more specialized than the V1 neurons targeting these areas (Glickfeld et al., 2013), suggesting that other mechanisms are also involved in creating HVA specialization in the mouse. These mechanisms could be local computations within the HVAs, but could also include alternative input pathways, such as the retina → SC → LP → HVA pathway (Seabrook et al., 2017) (Figure 1). Indeed, recent work has shown that the responses of projection neurons from LP targeting area AL were more similar to the responses of AL-residing neurons compared to the responses of V1 projection neurons terminating in AL (Blot et al., 2020). This suggests that HVAs may also inherit their response selectivity from the LP. Along these lines, one study demonstrated that motion-evoked responses in the cortical area POR originates from LP as opposed to from V1 (Beltramo and Scanziani, 2019). Hence, it appears that neuronal responses in HVAs of the mouse visual cortex develop via different circuits, in an area-dependent manner, but many questions and experimental avenues still remain open.

2.2 Strategies for manipulating retinal direction selectivity

A useful approach to investigate causal relationships in neural circuits is to perturb components of the circuit. As a result of our more comprehensive mechanistic knowledge, such perturbations are now possible for retinal direction selectivity. Currently, three main strategies have been employed for disturbing direction selectivity in the retina, and what they have in common is that they all target SACs (Hillier et al., 2017; Pei et al., 2015; Shi et al., 2017; Yonehara et al., 2016; Yoshida et al., 2001); the major cell type involved in creating DS responses in RGCs (Borst and Euler, 2011; Vaney et al., 2012) (Figure 3B). In this section, I briefly summarize these three models.

2.2.1 Ablating starburst amacrine cells

The first strategy is to ablate SACs. One study did this by expressing an interleukin-2 receptor under the metabotropic glutamate receptor 2 promoter, targeting the expression preferentially to SACs (Yoshida et al., 2001). Next, the authors injected an immunotoxin consisting of an interleukin-2 receptor antibody fused to a bacterial toxin into the vitreous of the eye, resulting in toxin-triggered SAC ablation. Another study employed a similar approach, but with some nuanced differences (Hillier et al., 2017). Here, the

authors selectively expressed the diphtheria toxin receptor in SACs by crossing two transgenic mouse lines: one expressing a floxed version of the diphtheria toxin receptor, and the other expressing Cre recombinase under the ChAT promoter, a specific marker of SACs. By intravitreal injection of diphtheria toxin, they could then selectively ablate SACs. Both of these strategies potently impair DS responses in retinal DS cells. The advantage of this strategy is that SAC ablation is controlled by the timing of the intravitreous injection of the toxin, and retinal direction selectivity can thus be disrupted acutely in adult mice without developmental effects or compensations. One disadvantage is that by killing cells with a toxin, immune reactions in the retina may occur. Hence, the effects observed following toxin injection might not exclusively result from the ablation of SACs per se, but immune-related alterations could also add to these effects.

2.2.2 Depleting starburst amacrine cells of GABA

Another strategy is to deplete SACs of GABA, preventing them from sending directionally tuned inhibition to the RGCs. This has been accomplished via conditional knockout of the vesicular GABA transporter gene selectively in SACs (Pei et al., 2015; Shi et al., 2017). This approach has the advantage that no toxin is injected into the eye, avoiding unwanted immune reactions. It should, however, be noted that one study employing this strategy showed that retinal direction selectivity was not completely abolished, but some DS responses persisted, potentially mediated by acetylcholine co-release from SACs (Pei et al., 2015). For this reason, this method seems imperfect when aiming to completely abolish retinal direction selectivity.

2.2.3 *Frmd7* mutant mice

The third model for disrupting retinal direction selection is the *Frmd7* mutant mouse ($Frmd7^{tm}$), in which a targeted mutation in the *Frmd7* gene is introduced (Hillier et al., 2017; Macé et al., 2018; Yonehara et al., 2016). This transgenic model was originally developed for studying the underlying molecular and circuit mechanisms causing dysfunctional eye movements in human patients with idiopathic congenital nystagmus (Yonehara et al., 2016). Specifically, the two major symptoms of this disease are oscillating eye movements along the horizontal plane, and the lack of the horizontal optokinetic reflex, resulting in impaired vision (Gottlob and Proudlock, 2014). The rationale for targeting the *Frmd7* gene was the clinical observation that in 70% of detected cases, idiopathic congenital nystagmus was associated with a mutation in this gene (Tarpey et al., 2006). Remarkably, the missing horizontal optokinetic reflex is phenocopied in mice with a mutated *Frmd7* gene (Yonehara et al., 2016). Within the
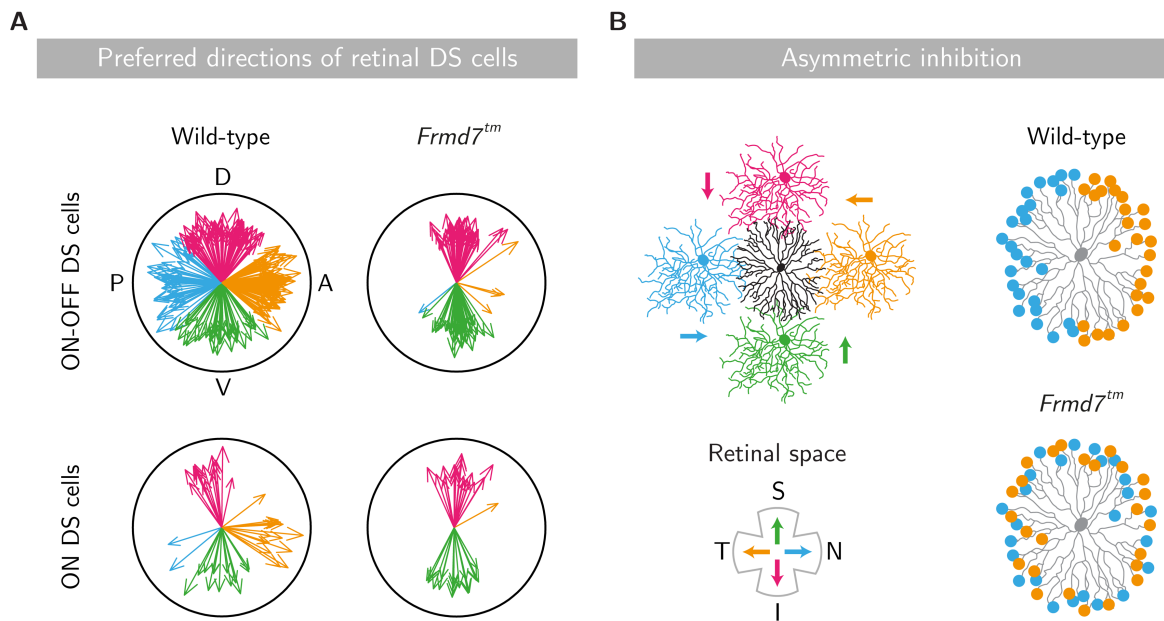
Figure 6 | Retinal direction selectivity is disrupted in Frmd7 mutant mice. *(A) Polar plots showing preferred directions of ON-OFF and ON retinal direction-selective (DS) cells with respect to the visual field from wild-type and Frmd7 mutant (Frmd7^{tm}) mice; each arrow denotes the preference of one recorded cell. A, anterior; P, posterior; D, dorsal; V, ventral. (B) Left: diagram of the spatial organization of synaptic connectivity between a starburst amacrine cell (SAC; center, black) and the four types of ON-OFF DS cells, color-coded according to their preferred direction with respect to retinal space. Right: diagrams of the proposed spatial organization of horizontal inhibitory synapses of a single SAC from a wild-type and Frmd7^{tm} adult mouse; inhibitory synapses are color-coded according to the preferred direction of the postsynaptic DS cell with respect to retinal space. Notice the lack of asymmetric inhibitory connectivity in Frmd7^{tm} mice. Data in panel (A) and diagrams in panel (B) are adapted from Yonehara et al. (2016).*

developing and adult retina of mice, *Frmd7* is selectively expressed in SACs (Yonehara et al., 2016). Importantly, *in vitro* recordings revealed that DS responses to horizontal motion, but not vertical, are lacking in both ON-OFF and ON DS cells in the *Frmd7^{tm}* mice (Hillier et al., 2017; Yonehara et al., 2016) (Figure 6A). This effect results from the absence of directionally tuned inhibition from SACs onto the RGCs, which is a consequence of the transition from asymmetric to symmetric inhibitory connections from SACs (Yonehara et al., 2016) (Figure 6B), that are critical for the establishment of direction selectivity (Briggman et al., 2011; Wei et al., 2011; Yonehara et al., 2011) (Figure 3B). Because horizontally tuned DS responses are missing in ON-OFF DS cells, *Frmd7^{tm}* mice can be used as a model to study the contribution of retinal direction selectivity to visual processing along the retino-geniculate as well as the retino-collicular pathway. The advantage of this strategy is that direction selectivity along the horizontal

axis is exclusively affected, making it more specific than the other two methods described here. In addition, SACs are not killed and abolished from the circuit, which prevents unwanted immune response-related effects. Finally, because the $Frmd7^{tm}$ mouse is a model of idiopathic congenital nystagmus, it is possible to investigate how visual processing in the cortex, or other brain areas, may be altered in this disease. The disadvantage of this model is that retinal direction selectivity is disrupted from birth, and why compensatory mechanisms due to developmental plasticity cannot be ruled out.

Taken together, as with most methodologies employed in research, the methods for disrupting retinal direction selectivity have advantages and drawbacks. Of the three strategies, depleting vesicular GABA from SACs seems least ideal because some DS responses persist in the RGCs. The SAC ablation and $Frmd7^{tm}$ mouse are not without complications either, and it therefore seems valuable to tackle research question using both methodologies to bolster the findings and conclusions.

2.3 Retinal DS cell-dependent motion processing in V1

At the outset of the work detailed in this dissertation, only one study had probed the causal influence of retinal direction selectivity on visual processing by individual neurons in the visual cortex (Hillier et al., 2017). This study disrupted retinal direction selectivity, either along all motion directions by ablating SACs, or exclusively along the horizontal axis using $Frmd7^{tm}$ mice, and showed, as expected, that both strategies significantly reduced DS responses in ON-OFF DS cells *in vitro* and *in vivo*. To monitor cortical neuronal activity, the authors performed *in vivo* two-photon calcium imaging from layer 2/3 of V1 in anaesthetized mice during monocular visual motion stimulation. In wild-type mice, they found an enrichment of V1 DS neurons preferring posterior motion, particularly at higher motion speeds, whereas in $Frmd7^{tm}$ and SAC-ablated mice this enrichment disappeared. Conversely, the authors found that the proportion of V1 DS neurons preferring dorsal motion was increased in $Frmd7^{tm}$ and SAC-ablated mice compared to wild-type mice. This work thus provided the first experimental demonstration that direction selectivity computed in the retina is causally involved in motion processing by the visual cortex. At the same time, these results inspire a stream of further questions: Does retinal direction selectivity contribute to motion processing in layers of V1 other than layer 2/3? Does retinal direction selectivity likewise influence motion processing in HVAs? Are these findings recreated in awake mice? Where along the retino-geniculate pathway does the posterior motion preference first emerge? What is the functional significance of this posterior motion bias of V1 DS neurons? Hence, the work by Hillier and co-authors serves as an excellent starting point for deciphering how retinal DS signaling contributes to visual processing in the visual cortex.

2.4 Aim and research objectives

The role of direction selectivity computed in the retina as a factor influencing visual motion processing in the cortex is not well appreciated, and has been largely overlooked in the field for the better part of a half a century. The question remains; to what extent do cortical motion representations rely on DS signaling in the retina, as opposed to direction selectivity computed *de novo* in the cortex? The aim of the work presented in this dissertation was thus to provide answers to the questions of how direction selectivity arising in the retina contributes to visual motion processing in V1 and higher-order visual cortical areas of mice.

To achieve this, the following research objectives were defined:

- Measure the influence of retinal direction selectivity on visual motion-evoked neural activity across distinct areas of the visual cortex, including V1 and HVAs.

- Investigate whether retinal direction selectivity contributes to motion processing and further functional specialization within individual neurons populating distinct HVAs.

- Examine whether a neural pathway conveying signaling from retinal DS cells to DS neurons in specific HVAs exists, or whether signaling from retinal DS cells is broadcasted evenly to all HVAs.

- Explore the functional role of direction selectivity computed in the retina; specifically, testing whether retinal DS cells causally influence optic flow responses and representations within V1 and HVAs.

This concludes the background chapter, and in the following chapters I will present the three main papers derived from my PhD studies.

3 A segregated cortical stream for retinal direction selectivity

In this chapter, I present the first research project that I carried out during my PhD studies. For this study, I needed to establish a suite of experimental techniques, new to our laboratory setting. With support from Ashley Juavinett and Kachi Odoemene (Cold Spring Harbor Laboratory, at the time), I implemented a pipeline for identifying visual cortical areas using intrinsic signal optical imaging. To visualize the activity of individual neurons, I applied *in vivo* two-photon calcium imaging. To facilitate this, I participated in an imaging course organized by the Max Planck Florida Institute for Neuroscience, and I visited the Friedrich Miescher Institute for Biomedical Research. Most critically, the inputs I received from Daniel E. Wilson (Max Planck Florida Institute for Neuroscience, at the time) were central for establishing a two-photon imaging and analysis pipeline. The results from this study were published in *Nature Communications* with myself as shared co-first author (Rasmussen et al., 2020a).

3.1 Brief introduction

In mice, the visual cortex contains multiple HVAs (Chapter 2, Figure 5A), each with a unique set of response sensitivities to visual features, resulting in areal specialization (Blot et al., 2020; Garrett et al., 2014; Jin and Glickfeld, 2020; Marshel et al., 2011; Zhuang et al., 2017). Interestingly, a degree of functional specialization is observed beforehand, in the V1 neurons projecting to the HVAs (Glickfeld et al., 2013; Kim et al., 2018; Matsui and Ohki, 2013) (Chapter 2, Figure 5B), indicating that areal specialization of HVAs may, at least in part, be inherited from V1. Yet, how signaling from specific types of RGCs contributes to the specialized neuronal activity in V1 and downstream HVAs has hitherto remained unresolved. In this work, we investigated this question in the context of visual motion processing. Specifically, we asked how signaling from retinal DS cells influences motion processing in different visual cortical areas of mice.

3.2 Brief methods

For this study we leveraged several experimental techniques, which I will here briefly summarize. For manipulating retinal direction selectivity, we used two approaches. First, we used $Frmd7^{tm}$ mice in which retinal horizontal direction selectivity is disrupted from birth (Yonehara et al., 2016) (Chapter 2, Figure 6). Second, we ablated SACs in adult mice, causing a loss of retinal direction selectivity for all motion directions (Hillier et al.,

2017; Yoshida et al., 2001). We used intrinsic signal optical imaging in anaesthetized mice to identify visual cortical areas (Juavinett et al., 2016) and to map motion-evoked areal responses. To monitor the responses of neuronal cell bodies or axonal boutons, we transfected brain areas (visual cortex, dLGN, or retina) with the genetically encoded calcium indicator GCaMP6 and measured changes in fluorescence intensity using two-photon imaging (Chen et al., 2013). With this approach, we recorded, *in vivo*, the activity of thalamic boutons in superficial layers of V1, neurons in layers 2/3 and 4 of V1, neurons in layer 2/3 of areas RL and PM, and separately recorded *in vitro* the activity of RGCs. Furthermore, by injecting an adeno-associated virus with retrograde access (Tervo et al., 2016) into either area RL or PM, we expressed GCaMP6 in RL- or PM-projecting V1 neurons, permitting us to record, in V1, the activity of layer 2/3 neurons in a projection-specific manner. These methods allowed us to investigate motion-related response differences between wild-type mice and mice with disrupted retinal direction selectivity.

3.3 Main findings

This work presents four main findings concerning how direction selectivity computed in the retina contributes to motion processing in the visual cortex of mice. First, we found that the response properties of DS neurons in layer 2/3 of area RL were notably impaired in *Frmd7^{tm}* and SAC-ablated mice with disrupted retinal direction selectivity. In contrast, the responses of DS neurons in area PM were not affected in these mice. Second, the responses of layer 2/3 cortico-cortical V1 projection neurons targeting area RL, but not those targeting area PM, were likewise impaired by disrupting retinal direction selectivity. Conversely, in layer 4 of V1, response properties of DS neurons were unaffected. Third, the responses of thalamic DS axonal boutons, originating in the dLGN and projecting to superficial layers of V1, were altered by retinal direction selectivity disruption. Finally, the major influence of retinal DS cell signaling on the response properties of thalamic and cortical DS neurons was to bias their directional preference toward posterior motion as the temporal frequency of the stimulus increased.

3.4 Reflections and significance

Our results provide new insights into how cortical areas achieve their sensory response specialization. A general notion in the field has been that specialized sensory representations in higher-order brain areas emerge from divergence and convergence of the neuronal activity originating from the peripheral sensory output channels. However, this has been difficult to establish causally. By leveraging our ability to manipulate the

activity of a single retinal output channel, namely direction selectivity, we revealed a causal relationship between the activity of retinal DS cells and motion processing in a specific HVA — area RL. From this, we put forward the idea that specialized sensory streams begin earlier than previously thought, in the periphery of the sensory system. In addition, this work provides answers to the question regarding how cortico-cortical projection neurons residing in V1 establish their response selectivity, which they propagate to HVAs. Our findings indicate that signaling from retinal DS cells is directed toward specific subsets of superficial V1 neurons, likely via the shell region of the dLGN (Cruz-Martín et al., 2014) (Chapter 2, Figure 4), and these inputs endow these cortical neurons with specialized responses. This work thus adds to our understanding of how visual feature selectivity emerges in cortical subnetworks.
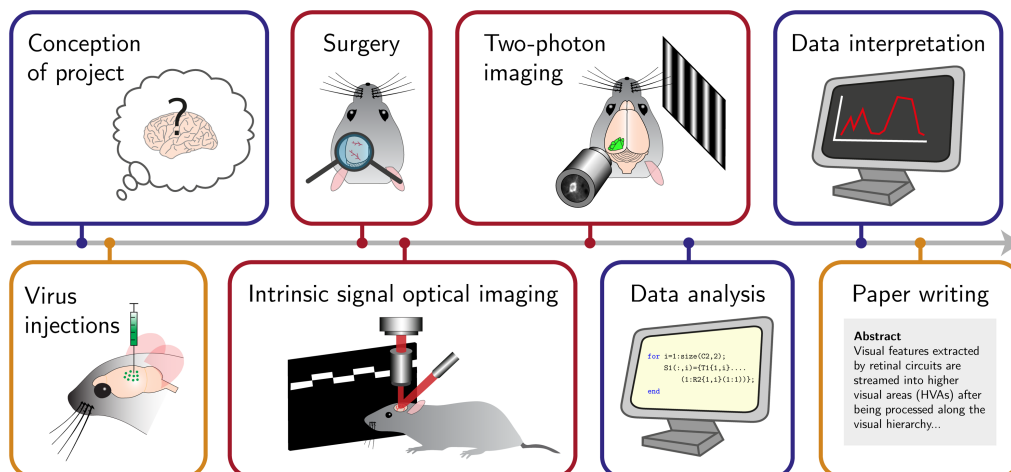
3.5 Author contributions

Figure 7 | Author contributions. *Box colors denote the relative author contribution; blue: shared the work; orange: did the majority of the work; red: did essentially all of the work.*

Supplementary material

The supplementary information accompanying the paper is in Appendix A.

ARTICLE

Check for updates

A segregated cortical stream for retinal direction selectivity

Rune Rasmussen[1,2], Akihiro Matsumoto [1,2], Monica Dahlstrup Sietam [1] & Keisuke Yonehara [1✉]

Visual features extracted by retinal circuits are streamed into higher visual areas (HVAs) after being processed along the visual hierarchy. However, how specialized neuronal representations of HVAs are built, based on retinal output channels, remained unclear. Here, we addressed this question by determining the effects of genetically disrupting retinal direction selectivity on motion-evoked responses in visual stages from the retina to HVAs in mice. Direction-selective (DS) cells in the rostrolateral (RL) area that prefer higher temporal frequencies, and that change direction tuning bias as the temporal frequency of a stimulus increases, are selectively reduced upon retinal manipulation. DS cells in the primary visual cortex projecting to area RL, but not to the posteromedial area, were similarly affected. Therefore, the specific connectivity of cortico-cortical projection neurons routes feedforward signaling originating from retinal DS cells preferentially to area RL. We thus identify a cortical processing stream for motion computed in the retina.

[1] Danish Research Institute of Translational Neuroscience—DANDRITE, Nordic-EMBL Partnership for Molecular Medicine, Department of Biomedicine, Aarhus University, 8000 Aarhus C, Denmark. [2] These authors contributed equally: Rune Rasmussen, Akihiro Matsumoto. ✉email: keisuke.yonehara@dandrite.au.dk

ARTICLE

The mammalian visual system analyzes the external world through a set of distinct spatio-temporal channels[1]. The mouse retina contains >40 distinct types of ganglion cells, each encoding a discrete set of visual features such as color, luminance, edges, and motion direction[2]. The general consensus is that central visual areas combine signaling originating from different ganglion-cell types[3], and the output from each ganglion-cell type diverges into multiple central visual areas[4], embodying a feature-combinatorial system[5].

The mouse visual cortex includes up to 16 retinotopically organized higher visual areas (HVAs), varying in preferences for temporal and spatial frequency, motion speed, color, and visual-field coverage[6–10]: these are categorized into a dorsal and ventral stream dichotomy[7,11,12]. In rodents, functionally segregated streams are already observed in the cortico-cortical projection neurons of the primary visual cortex (V1)[13,14]. However, it is not yet understood how signaling originating from individual retinal channels influences the activity of HVAs and, hence, how HVA-specific properties and distinct visual streams emerge[15,16]. One possibility is that each retinal channel influences all HVAs to a similar extent. Alternatively, in an extreme scenario, the impact of each retinal channel may be localized to a single HVA. If so, it will be critical to determine how V1 cortico-cortical projection neurons integrate inputs originating from individual retinal ganglion-cell types.

One fundamental task of the visual system is to detect the direction and speed of visual motion to analyze object motion or optic flow. The direction and speed of visual motion are first encoded by retinal direction-selective (DS) cells, preferentially responding to visual stimuli moving in a particular direction[17,18]. Retinal ON-OFF DS cells include four subtypes: each prefers one of four cardinal directions[19–21]. In mice, the shell region of the dorsal lateral geniculate nucleus (dLGN) relays signals from retinal horizontal ON-OFF DS cells to superficial layers of V1 (refs. [22–24]), and genetic knockout of retinal horizontal direction selectivity reduces a posterior motion preference in V1 layer (L) 2/3 DS cells[25]. However, how direction selectivity originating in the retina is processed beyond V1 remains unexplored. It could be broadcasted to all HVAs equally or, alternatively, it may be preferentially transmitted to specific HVAs. In addition, direction selectivity is also computed de novo at the thalamocortical synapses in L4 of V1 in mice[26], but it remains unknown whether retina-dependent and -independent direction selectivity mechanisms are combined or stay segregated in HVAs.

To probe these questions, we used *Frmd7* mutant mice (*Frmd7tm*) to disrupt horizontal direction selectivity in the retina[25,27,28], and transgenic mice expressing diphtheria toxin receptors in starburst amacrine cells (*ChAT-Cre × LSL-DTR*) to genetically ablate the cells, leading to the loss of retinal direction selectivity[25,29]. We tested the effect of these manipulations on visual motion processing in the retina, thalamic axons, V1, and HVAs in anaesthetized and awake mice. We show that the preference of the rostrolateral (RL) area for higher temporal frequencies (TFs) in the posterior direction is the major response feature affected by the alteration of retinal motion computations. We determine a functional pathway that links retinal horizontal DS cells to area RL while bypassing L4 of V1: dLGN → V1 L2/3 → RL. Importantly, V1 L2/3 neurons that project to area RL, but not the posteromedial (PM) area, were affected by the disruption of retinal horizontal direction selectivity, indicating a segregated V1 circuitry that routes retinal DS signaling preferentially to area RL. Our results indicate there is a cortical space for retinal direction selectivity and a distinct pathway that enables specialized response properties in HVAs.

Results

Mapping the sensitivity of cortical areas. We mapped the visual cortex organization in anesthetized control and *Frmd7tm* mice using intrinsic signal optical imaging (ISOI; Fig. 1a). We generated visual-field sign maps (Fig. 1a) from horizontal and vertical retinotopic maps, and reliably identified six visual areas: V1, lateromedial (LM), anterolateral (AL), RL, anteromedial (AM), and PM (Fig. 1a). It is worth noting that the RL area we identified may possibly include the anterior HVA (area A), which has been identified previously[6,7]. We found no differences in visual cortical organization or size proportions between control and *Frmd7tm* mice (Supplementary Fig. 1). To test the contribution of retinal direction selectivity to motion responses in visual areas, we measured evoked intrinsic signal activity levels[12] in response to gratings drifting in the cardinal directions at a TF of 0.3, 0.75, 1.2, or 1.8 Hz with a fixed spatial frequency of 0.03 cycles/°. In areas V1 and RL, we found significantly decreased responses to horizontal motion in *Frmd7tm* mice at multiple TFs (Fig. 1b). In control mice, these areas responded strongly to horizontal motion moving at higher TFs (Fig. 1b). In areas LM and AM, only posterior responses at 1.2 Hz were significantly decreased and increased, respectively, in *Frmd7tm* mice (Fig. 1b). These findings suggest that retinal horizontal direction selectivity contributes to motion responses in a subset of visual cortical areas. In particular, the higher-TF preference of areas V1 and RL for horizontal motion was dominantly impaired in mice with disrupted retinal horizontal DS signaling.

RL DS cells rely on retinal direction selectivity. To elucidate the cellular underpinnings of the ISOI results, we used in-vivo two-photon calcium imaging from anesthetized mice (Fig. 1c and Supplementary Fig. 2). We focused on the areas RL and PM because RL was notably affected in *Frmd7tm* mice, whereas PM was unaffected (Fig. 1b). We imaged neurons in L2/3 using the virally transduced GCaMP6f, and stimuli consisted of gratings drifting in 12 directions at TFs of 0.3, 0.75, 1.2, or 1.8 Hz with a fixed spatial frequency of 0.03 cycles/° (Fig. 1d−f). RL DS cells (direction selectivity index [DSI] > 0.3) in control mice preferred higher TFs, particularly in the posterior direction (Fig. 1g, h), whereas PM DS cells preferred low TFs at a similar level in all directions (Fig. 1g, h). In *Frmd7tm* mice, RL DS cells preferred lower TFs (Fig. 1g, h), whereas the preference of PM DS cells was unchanged (Fig. 1g, h). We found no differences in vertical motion responses in area RL or PM between control and *Frmd7tm* mice (Fig. 1h). In both control and *Frmd7tm* mice, RL DS cells developed a posterior bias in the distribution of preferred directions as the TF increased from 0.3 to 1.2 Hz ($P ≥ 0.05$ and $P < 0.01$, Rayleigh test; Fig. 1i): however, a notably smaller fraction of DS cells in RL of *Frmd7tm* mice preferred posterior motion (29.3%) compared to control mice (48.1%) at 1.2 Hz (Fig. 1j). Preferred directions of PM DS cells showed a posterior bias at 0.3 and 1.2 Hz ($P < 0.001$, Rayleigh test; Fig. 1i) in both control and *Frmd7tm* mice (Fig. 1i, j).

Anesthesia is known to influence, for example, cortical dynamics and synaptic excitation and inhibition[30,31]. Thus, to validate our findings, we repeated the experiment in awake, quietly resting mice (Supplementary Fig. 3). Overall, these experiments confirmed that the key findings in anesthetized mice (Fig. 1f−j) were preserved in awake mice. RL DS cells in awake control mice preferred motion moving along the horizontal axis at higher TFs, while PM DS cells preferred motion at low TFs equally across all directions (Supplementary Fig. 3c, d). In contrast, RL DS cells in awake *Frmd7tm* mice preferred low TFs, whereas the preference of PM DS cells was unchanged (Supplementary Fig. 3c, d). Importantly, as the
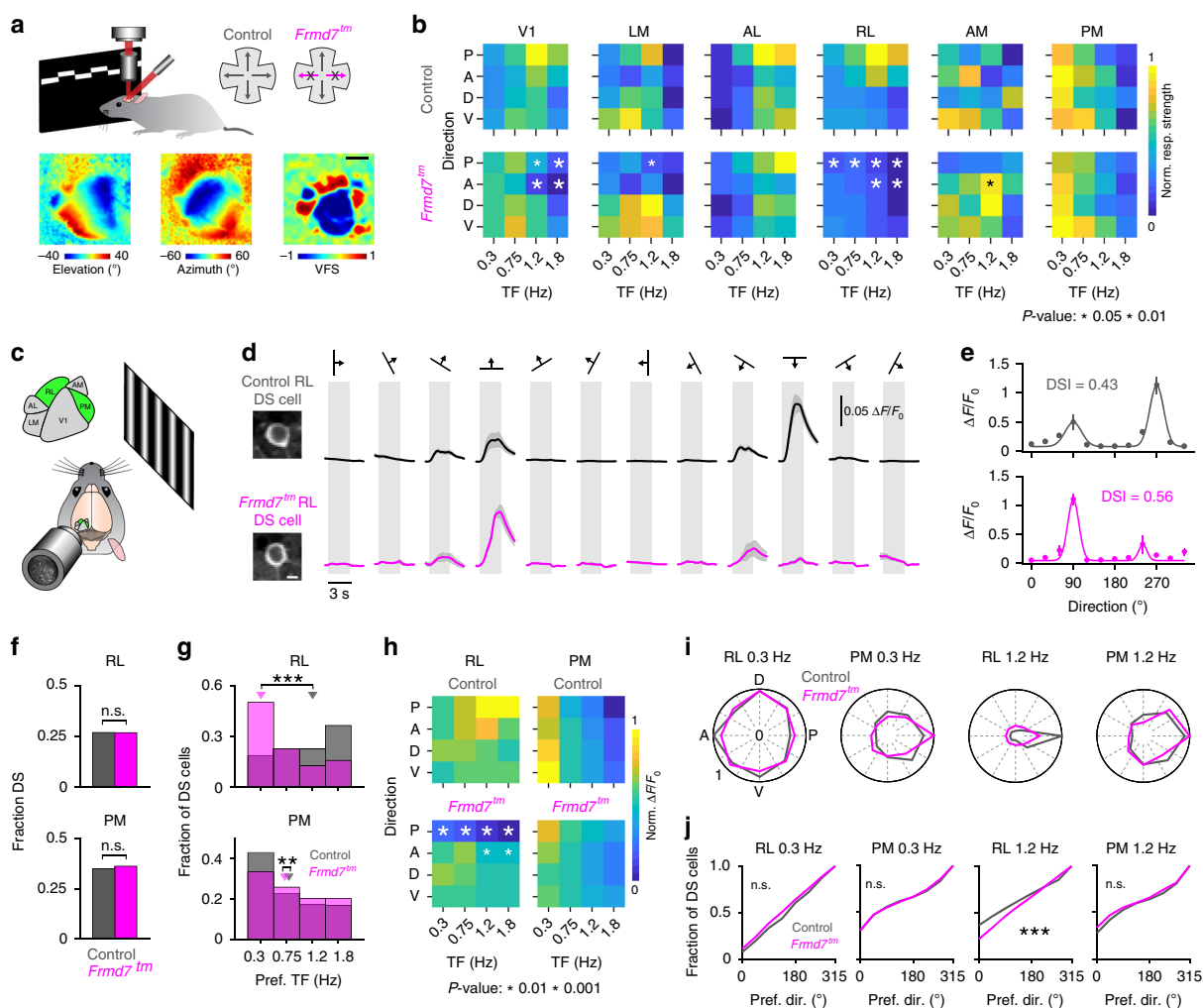
Fig. 1 Posterior motion preference of RL neurons at higher TFs depends on retinal horizontal direction selectivity. a Upper: ISOI in control and $Frmd7^{tm}$ mice. Lower: Example vertical and horizontal retinotopic maps and the computed visual-field sign map. Scale bar, 1 mm. **b** Response strength as a function of motion direction (anterior [A], posterior [P], dorsal [D], and ventral [V]) and TF (five mice per genetic group). White and black asterisks: significantly decreased and increased responses, respectively, two-sided Mann–Whitney U-test. **c** Two-photon calcium imaging from L2/3 in areas RL and PM of control (1452 and 1098 DS cells, respectively; ten mice) and $Frmd7^{tm}$ mice (1387 and 1217 DS cells, respectively; 11 mice). **d** Example control and $Frmd7^{tm}$ RL and PM neurons expressing GCaMP6f (scale bar, 5 μm) and trial-averaged fluorescence ($\Delta F/F_0$) time courses for the same neurons. Shading indicates SEM. **e** Tuning curves for neurons shown in **d**. Error bars are SEM; solid line is Gaussian fit. **f** Fraction of DS cells in RL and PM (two-sided χ^2 test with Yates correction). **g** Preferred TF for DS cells in RL (two-sided Mann–Whitney U-test) and PM (two-sided Mann–Whitney U-test). Triangles show medians. **h** Response amplitude as a function of motion direction and TF for RL and PM DS cells. White asterisks: significantly decreased response amplitude in $Frmd7^{tm}$ mice, two-sided Mann–Whitney U-test. **i** Fractional distributions of preferred motion directions for RL and PM DS cells at 0.3 and 1.2 Hz; fractions are normalized to the largest fraction across genetic groups. **j** Distributions of preferred direction at 0.3 and 1.2 Hz in RL and PM (two-sided Kolmogorov–Smirnov test). **P < 0.01, ***P < 0.001, n.s., not significant, in **f**, **g**, and **j**. Source data are provided as a Source Data file.

TF increased from 0.3 to 1.2 Hz, RL but not PM DS cells from awake control mice developed a strong bias for posterior motion, and this bias was significantly impaired in $Frmd7^{tm}$ mice (Supplementary Fig. 3e, f). These results suggest the following: First, increased response amplitude at higher TFs is correlated with a gain of bias towards posterior motion in RL DS cells. Second, these TF-dependent changes in response amplitude and directional preference in area RL depend on retinal horizontal direction selectivity. Third, the effect of disrupting retinal direction selectivity appears to be specific to certain HVAs.

RL DS cells are impaired by retinal starburst cell ablation. The effect of $Frmd7$ mutation on starburst cells is chronic from birth;

potentially triggering plasticity-related changes in the downstream visual pathways. Thus, we next genetically ablated retinal starburst amacrine cells in adult mice to acutely abolish retinal direction selectivity. For this we used $ChAT$-$Cre \times LSL$-DTR mice in which diphtheria toxin receptors are selectively expressed in starburst amacrine cells[25,29]. Intravitreal injection of diphtheria toxin into these mice led to the selective ablation of starburst amacrine cells (Supplementary Fig. 4; referred to as 'starburst-ablated mice') and a loss of optomotor responses (OMR; Supplementary Fig. 4). We imaged neurons in L2/3 of areas RL and PM in awake, quietly resting mice (Supplementary Fig. 5). We found no differences in the fraction of DS cells between control and starburst-ablated mice in area RL or PM (Supplementary Fig. 5b). In starburst-ablated mice the distribution of TF preference was shifted toward slower

TFs for RL DS cells compared to control mice, whereas we found no difference for PM DS cells (Supplementary Fig. 5c). Similar to what we observed in *Frmd7tm* mice, RL DS cells from starburst-ablated mice showed a lack of horizontal motion response preference at higher TFs, in contrast to RL DS cells from control mice (Supplementary Fig. 5d). Notably, the posterior motion bias at 1.2 Hz was significantly impaired in RL DS cells from starburst-ablated mice (19.4% of DS cells) compared to control mice (29% of DS cells), whereas we found no difference for PM DS cells (Supplementary Fig. 5e). Thus, the key findings from *Frmd7tm* mice were largely supported by results from starburst-ablated mice.
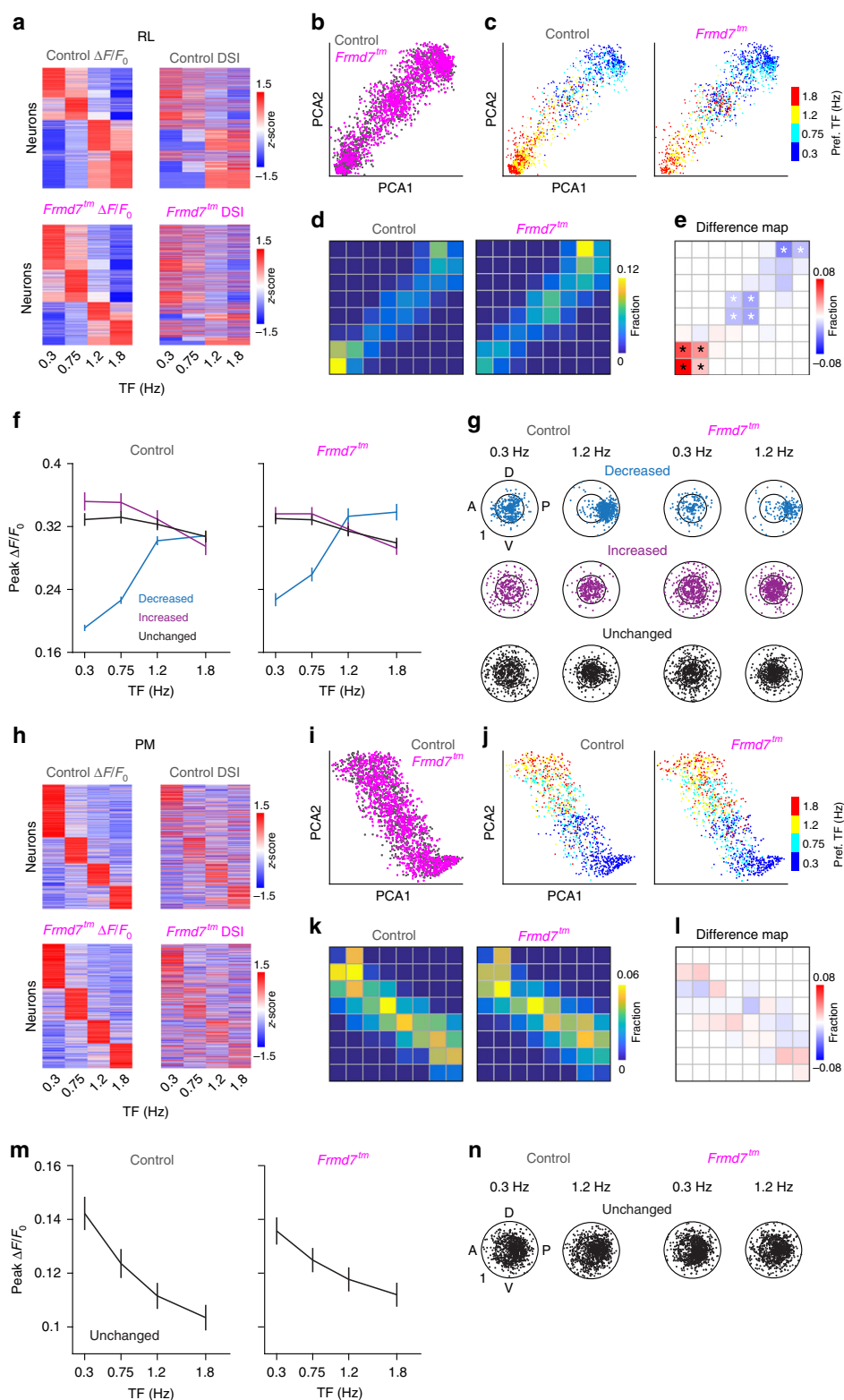
Distinct RL neurons rely on retinal motion computation. To test whether there is a trend in affected response properties in *Frmd7tm* mice, we performed decomposition and segmentation on the datasets from areas RL and PM. First, we composed a TF-dependent response matrix for RL L2/3 DS cells, pooled from control and *Frmd7tm* mice (Fig. 2a). Next, we used principal component analysis (PCA) to decompose the response matrix into two dimensions (Fig. 2b). Noticeably, the PCA distribution showed a clear distribution trend depending on the TF preference: neurons sharing the same TF preference tended to be locally clustered (Fig. 2c). We then determined the fraction of RL neurons in local regions of the PCA distribution by superimposing 8 × 8 grids (Fig. 2d and Supplementary Fig. 6). Statistical comparisons of fractions between control and *Frmd7tm* mice revealed grids where the fraction of neurons was decreased, increased, or unchanged in *Frmd7tm* mice (Fig. 2e). Next, we probed the functional characteristics of these three groups. Notably, RL neurons that were decreased in *Frmd7tm* mice showed a prominent response amplitude increase as the TF increased ($P < 0.001$ for 0.3 versus 1.2 Hz for control and *Frmd7tm* mice, Wilcoxon signed-rank; Fig. 2f). In contrast, neurons that were increased or unchanged in *Frmd7tm* mice showed a TF-dependent decrease in response ($P < 0.05$ for 0.3 versus 1.2 Hz for control and *Frmd7tm* mice, Wilcoxon signed-rank; Fig. 2f). Neurons that were decreased in *Frmd7tm* mice showed a clear shift in direction tuning: at 0.3 Hz neurons uniformly encoded all directions while at 1.2 Hz they developed a preference for posterior motion together with an increase in DSI ($P < 0.001$ for 0.3 versus 1.2 Hz for control and *Frmd7tm* mice, Wilcoxon signed-rank; Fig. 2g). In contrast, neurons that were increased or unchanged in *Frmd7tm* mice showed no obvious direction tuning bias at either low or high TFs, but did decrease their DSI at the higher TF ($P < 0.001$ for 0.3 versus 1.2 Hz for control and *Frmd7tm* mice, Wilcoxon signed-rank; Fig. 2g).

We repeated the above analysis for PM L2/3 DS cells (Fig. 2h). Similar to in area RL, neurons from area PM showed a TF-dependent PCA distribution trend (Fig. 2i, j). We found no grids where the fraction of neurons was significantly different between control and *Frmd7tm* mice (Fig. 2k, l). PM neurons decreased their response amplitude as a function of increasing TF (Fig. 2m), with no clear change in direction tuning bias or DSI ($P ≥ 0.05$ for 0.3 versus 1.2 Hz for control and *Frmd7tm* mice, Wilcoxon signed-rank; Fig. 2n). Together, these data indicate that the coupling of a high-TF motion preference and the development of posterior motion bias at high TFs is the major response feature that depends on retinal horizontal direction selectivity. Thus, the retinal contribution to motion processing in HVAs appears to be specific not only to area, but also to ensemble.

Projection-specific impairment of V1 neurons. Previous work has shown that V1 neurons provide target-specific input to

HVAs[13,14]. Here, we investigated whether the sensitivity to disruption of retinal horizontal direction selectivity is routed by V1 DS cells that project to areas RL and PM. Alternatively, such sensitivity may originate from inputs from other HVAs or higher-order thalamic areas. To probe this, we labeled RL- and PM-projecting V1 L2/3 neurons by injecting rAAV2-retro expressing GCaMP6m into either area PM or RL (Supplementary Fig. 7) and imaged these neurons and target-unspecific V1 L2/3 neurons in anaesthetized mice (Fig. 3a–c). The density of GCaMP6-labeled projection neurons did not differ significantly between genetic conditions (Supplementary Fig. 7e). Notably, the fraction of RL-projecting neurons that showed direction selectivity was reduced from 60% in control mice to 34% in *Frmd7tm* mice, whereas the fraction of DS cells among PM-projecting neurons was not altered in *Frmd7tm* mice (Fig. 3d). RL-projecting and target-unspecific DS cells from control mice preferred higher TFs, particularly in horizontal directions (Fig. 3e, f). In *Frmd7tm* mice, RL-projecting and target-unspecific DS cells preferred the lowest TF, showing lower responses than control mice to horizontal motion at higher TFs (Fig. 3e, f). PM-projecting DS cells preferred low TFs for all directions in control mice, and this was the same in *Frmd7tm* mice (Fig. 3e, f). Consistent with previous work[25], target-unspecific neurons developed a posterior bias in the distribution of preferred directions as the TF increased ($P ≥ 0.05$ and $P < 0.05$ for 0.3 and 1.2 Hz, respectively, Rayleigh test) with significantly less bias in *Frmd7tm* than in control mice at 1.2 Hz (Fig. 3g, h). PM-projecting DS cells from both control and *Frmd7tm* mice developed a posterior bias as the TF increased from 0.3 to 1.2 Hz ($P ≥ 0.05$ and $P < 0.001$, Rayleigh test; Fig. 3g, h). RL-projecting DS cells from control mice developed a posterior bias ($P ≥ 0.05$ and $P < 0.001$ for 0.3 and 1.2 Hz, respectively, Rayleigh test), but this did not occur in *Frmd7tm* mice (Fig. 3g, h). These data suggest that the distinct sensitivity of areas RL and PM to disruption of retinal horizontal direction selectivity is already found in V1 L2/3 DS cells that project to these areas.

Distinct V1 neurons rely on retinal motion computation. Next, we correlated the response properties of V1 L2/3 DS cells and the differences between control and *Frmd7tm* by first decomposing the response matrix into two dimensions using PCA (Fig. 4a, b). Similar to in areas RL and PM, V1 L2/3 neurons sharing the same TF preference were locally clustered (Fig. 4c). We found grids where the fraction of neurons was decreased, increased or unchanged in *Frmd7tm* mice (Fig. 4e). Neurons that were decreased in *Frmd7tm* mice increased their response amplitude as the TF increased ($P < 0.001$ for 0.3 versus 1.2 Hz for control and *Frmd7tm* mice, Wilcoxon signed-rank; Fig. 4f). In contrast, neurons that were increased in *Frmd7tm* mice showed a TF-dependent decrease in responses ($P < 0.001$ for 0.3 versus 1.2 Hz for control and *Frmd7tm* mice, Wilcoxon signed-rank), while neurons that were unchanged showed no TF-dependent response modulation ($P ≥ 0.05$ for 0.3 versus 1.2 Hz for control and *Frmd7tm* mice, Wilcoxon signed-rank; Fig. 4f). Analyzing preferred motion directions for individual V1 L2/3 neurons at 0.3 and 1.2 Hz revealed that neurons that were decreased in *Frmd7tm* mice exhibited a direction tuning shift: at 0.3 Hz neurons uniformly encoded all directions, while at 1.2 Hz they notably preferred posterior motion and this was paralleled with an increase in DSI ($P < 0.001$ for 0.3 versus 1.2 Hz for control and *Frmd7tm* mice, Wilcoxon signed-rank; Fig. 4g). In contrast, neurons that were increased or unchanged in *Frmd7tm* mice showed no obvious direction tuning bias at either low or high TFs, but neurons that were increased in *Frmd7tm* mice decreased their DSI ($P < 0.001$ for 0.3 versus 1.2 Hz for control and *Frmd7tm* mice, Wilcoxon signed-

rank; Fig. 4g). Finally, we investigated the relationship between the effects of altered retinal horizontal direction selectivity and the target region of V1-projecting DS cells. We analyzed the fraction of PM- and RL-projecting neurons in each of the significantly affected grids. Importantly, this showed that the grids enriched in RL- and PM-projecting DS cells tend to be decreased and increased in

Frmd7^tm mice, respectively (Fig. 4h). These results suggest that the impact of disrupted retinal horizontal direction selectivity in L2/3 of V1 is biased to a subset of neurons that prefer high-TF motion and preferentially encode posterior motion at high TFs. Furthermore, this subset of V1 neurons appeared to preferentially project to area RL.

ARTICLE

Fig. 2 Neurons with distinct functional characteristics are sensitive to disruption of retinal horizontal direction selectivity in area RL. a Response matrix composed of TF-dependent response amplitudes and DSI for RL L2/3 DS cells sorted by TF preference. **b** Two-dimensional (2D) visualization of the 1st and 2nd principal components for the response matrix shown in **a**. Each point represents one neuron. **c** TF preference of individual RL neurons. **d** Fraction of neurons in 8 × 8 grids (gray lines) calculated from the PCA plot shown in **b**. **e** Fraction difference map between control and *Frmd7^{tm}* mice. Black and white asterisks: significantly decreased and increased fractions in *Frmd7^{tm}* mice, respectively, $P < 0.05$, two-sided χ^2 test with Yates correction. **f** Peak response amplitude as a function of TF for three groups (decreased, increased, or unchanged in *Frmd7^{tm}* mice) in control (572, 304, and 575 DS cells, respectively) and *Frmd7^{tm}* mice (219, 508, and 659 DS cells, respectively). Error bars are SEM. **g** TF-dependent tuning characteristics of individual RL neurons from the three groups in control and *Frmd7^{tm}* mice. Angular coordinate: preferred direction. Radial coordinate: DSI. Inner circle: DSI of 0.5. **h** Response matrix composed of TF-dependent response amplitudes and DSI for PM L2/3 DS cells sorted by TF preference. **i** 2D visualization of the 1st and 2nd principal components for the response matrix shown in **h**. Each point represents one neuron. **j** TF preference of individual PM neurons. **k** Fraction of neurons in 8 × 8 grids (gray lines) calculated from the PCA plot in **i** for control and *Frmd7^{tm}* mice. **l** Fraction difference map between control and *Frmd7^{tm}* mice. **m** Peak response amplitude as a function of TF for the unchanged group in control (1098 DS cells) and *Frmd7^{tm}* mice (1217 DS cells). Error bars are SEM. **n** TF-dependent tuning characteristics of individual PM neurons from the unchanged group in control and *Frmd7^{tm}* mice. Angular coordinate: preferred direction. Radial coordinate: DSI. Inner circle: DSI of 0.5. Source data are provided as a Source Data file.

V1 L4 DS cells are insensitive to retinal manipulation. Signaling from the retino-geniculate pathway is conveyed to L2/3 of V1 mainly via L4 (ref. [32]), and feature-tuned V1 L2/3 neurons receive L4 inputs[33]. Here, we investigated whether retina-originating DS signaling is routed to V1 L2/3 via L4, in addition to a previously suggested dLGN to V1 L1/2 shortcut pathway[23]. We imaged GCaMP6f-labeled neurons in L4 of V1 in anaesthetized mice (Supplementary Fig. 8), and identified DS cells from control and *Frmd7^{tm}* mice (Fig. 5a). In contrast to L2/3, L4 DS cells from control and *Frmd7^{tm}* mice were quantitatively very similar, both preferring 0.75 Hz TF, and showing no significant response amplitude differences (Fig. 5b, c). In control mice, the preferred directions of L4 DS cells showed a posterior bias at 0.3 and 1.2 Hz ($P < 0.05$, Rayleigh test; Fig. 5d), and this effect was not significantly different in *Frmd7^{tm}* mice (Fig. 5d, e). The insensitivity of L4 DS cells to disruption of retinal horizontal direction selectivity at the population level was also supported by decomposition and segmentation analyses (Fig. 5f–h): none of the grids showed significantly different fractions between control and *Frmd7^{tm}* mice (Fig. 5i, g). V1 L4 neurons showed no obvious change in direction tuning bias as a function of increasing TF, but neurons in both control and *Frmd7^{tm}* mice increased their DSI ($P < 0.01$ for 0.3 versus 1.2 Hz for control and *Frmd7^{tm}* mice, Wilcoxon signed-rank; Fig. 5i). These data show that DS cells in L4 of V1 are not noticeably sensitive to disruption of retinal horizontal direction selectivity, suggesting that retina-originating DS signaling reaches L2/3 of V1 via a pathway bypassing L4.

DS thalamic axons are affected by retinal manipulation. We examined whether the coupling of a high-TF preference and the TF-dependent development of posterior motion preference, which relies on retinal horizontal direction selectivity in areas V1 and RL, is already established in dLGN neurons. For this, we transfected dLGN neurons with GCaMP6f and imaged axons in L1 and L2/3 of V1 of anaesthetized mice (Fig. 6a). During grating stimuli, fluorescence increased in individual micron-sized varicosities along the axonal arborizations (Fig. 6b, c), confirming they were putative presynaptic boutons[13,23]. The fraction of DS boutons preferring high and low TFs decreased and increased, respectively, in *Frmd7^{tm}* mice (Fig. 6e). In control mice, DS boutons preferred higher TFs in response to horizontal motion (Fig. 6f). In contrast, in *Frmd7^{tm}* mice, DS boutons preferred lower TFs in horizontal directions, showing higher responses than control mice at 0.3 Hz and markedly lower responses at 1.2 and 1.8 Hz (Fig. 6f). Responses to vertical motion were unaltered in control and *Frmd7^{tm}* mice (Fig. 6f). In control mice, the fraction of horizontally tuned DS boutons was significantly higher than vertically tuned boutons at both 0.3 and 1.2 Hz (Fig. 6g), whereas the fraction of vertically tuned DS boutons in *Frmd7^{tm}*

mice was significantly higher at 1.2 Hz than horizontally tuned boutons (Fig. 6g). Thus, in control mice, the preferred directions of DS boutons showed a TF-invariant bias for posterior motion ($P < 0.001$ for 0.3 and 1.2 Hz, Rayleigh test; Fig. 6h), whereas they were biased to ventral at 1.2 Hz in *Frmd7^{tm}* mice ($P \geq 0.05$ and $P < 0.01$ for 0.3 and 1.2 Hz, respectively; Rayleigh test; Fig. 6h, i). In control mice, 36.9% of DS boutons increased response amplitudes as the TF increased from 0.3 to 1.2 Hz, whereas only 17.1% increased in *Frmd7^{tm}* mice (Fig. 6j). Noticeably, posteriorly tuned DS boutons in control mice showed larger TF-dependent response increments than boutons preferring other directions (Fig. 6j, k). Conversely, DS boutons from *Frmd7^{tm}* mice decreased their responses as the TF increased in all preferred directions (Fig. 6k), although posteriorly tuned boutons did show a smaller response decrement than anteriorly tuned boutons (Fig. 6k). These data suggest that two response characteristics of dLGN DS axons arriving in L1 and L2/3 of V1 were impaired in *Frmd7^{tm}* mice: the preference for high-TF horizontal motion and the TF-invariant population bias for preferring posterior motion.

Altered TF-dependent responses in the retina of *Frmd7^{tm}* mice. TF-dependent responses of retinal neurons in *Frmd7^{tm}* mice have not previously been examined[25,27]. We sought to link the TF-dependent response modulation observed in thalamic axons and cortical neurons to that in retinal neurons. We performed two-photon calcium imaging from the ganglion-cell layer in isolated retinas by the virally transduced GCaMP6s (Fig. 7a–c). In control retinas, neurons preferred high-TF stimuli moving in posterior, anterior, and ventral directions (i.e., nasal, temporal, and superior on the retina, respectively), whereas we found no TF-dependent response modulation for dorsal motion (i.e., inferior on the retina; Fig. 7d). In *Frmd7^{tm}* retinas, the high-TF preference of neurons was impaired for horizontal motion: their responses to higher TFs were significantly lower than control mice (Fig. 7d). In contrast, responses to vertical motion were unaltered, as has been shown previously[27].

Next, we restricted our analyses to retinal neurons showing both ON-OFF responses and DS tuning (36.7% and 35.8% of all responsive neurons in control and *Frmd7^{tm}* retinas, respectively; Supplementary Fig. 9). As previously reported[27], *Frmd7^{tm}* retinas showed significantly decreased ON-OFF DS responses to horizontal motion (Fig. 7e). In control mice, there was a population bias for posterior motion at 1.2 Hz ($P < 0.05$, Rayleigh test; Fig. 7f), whereas DS cells from *Frmd7^{tm}* mice were biased towards vertical motion at both 0.3 and 1.2 Hz ($P < 0.001$ for 0.3 and 1.2 Hz, Rayleigh test; Fig. 7f, g). Interestingly, only posteriorly tuned ON-OFF DS cells showed larger TF-dependent response increments and a larger TF-dependent increase in DSI in control retinas ($P < 0.001$ and $P \geq 0.05$ for all comparisons in control and *Frmd7^{tm}*

mice, respectively, Mann–Whitney U-test; Fig. 7h, i). These data suggest at least two mechanisms underlying the retinal over-representation of a preference for high-TF posterior motion: First, ON–OFF DS cells that prefer posterior motion are more abundant than other populations, which becomes more evident as the DSI of these cells increases at high TFs. Second, posteriorly tuned retinal DS cells show larger response increments than DS cells preferring other directions as TF increases. Importantly, both of these posterior biases are markedly impaired in $Frmd7^{tm}$ retinas.

Discussion

Our results provide three major insights into the functional organization of murine visual pathways for processing visual

ARTICLE

Fig. 3 V1 DS cells projecting to area RL or PM respond differently to disruption of retinal direction selectivity. a Target-unspecific V1 neurons were labeled by injecting AAV2/1-GCaMP6f into the V1. PM- (PM-p) and RL-projecting (RL-p) V1 neurons were labeled by injecting rAAV2-retro-GCaMP6m into PM and RL, respectively. **b** Two-photon calcium imaging from L2/3 in V1 of control (1087 target-unspecific, 109 PM-p, and 513 RL-p DS cells; 5 mice per group) and *Frmd7^{tm}* mice (954 target-unspecific, 93 PM-p, and 235 RL-p DS cells; five mice per group). Left: example PM- and RL-projecting neurons expressing GCaMP6m (scale bar, 10 μm). Right: trial-averaged fluorescence ($\Delta F/F_0$) time courses for the same neurons. Shading: SEM. **c** Tuning curves for neurons shown in **b**. Error bars: SEM. Solid line: Gaussian fit. **d** Fraction of DS cells in target-unspecific, PM-p, and RL-p V1 neuronal populations (two-sided χ^2 test with Yates correction). **e** Preferred TF for target-unspecific (two-sided Mann–Whitney U-test), PM-p (two-sided Mann–Whitney U-test), and RL-p (two-sided Mann–Whitney U-test) V1 DS cells. Triangles: Medians. **f** Response amplitude as a function of motion direction and TF for target-unspecific, PM-p, and RL-p V1 DS cells. White asterisks: significantly decreased in *Frmd7^{tm}* mice, two-sided Mann–Whitney U-test. **g** Fractional distributions of preferred motion directions for target-unspecific, PM-p, and RL-p V1 DS cells at 0.3 and 1.2 Hz. The fractions are normalized to the largest fraction across genetic groups. **h** Distributions of preferred motion directions at 0.3 and 1.2 Hz for target-unspecific, PM-p, and RL-p V1 DS cells (two-sided Kolmogorov–Smirnov test). **$P < 0.01$, ***$P < 0.001$, n.s., not significant, in **d**, **e**, and **h**. Source data are provided as a Source Data file.
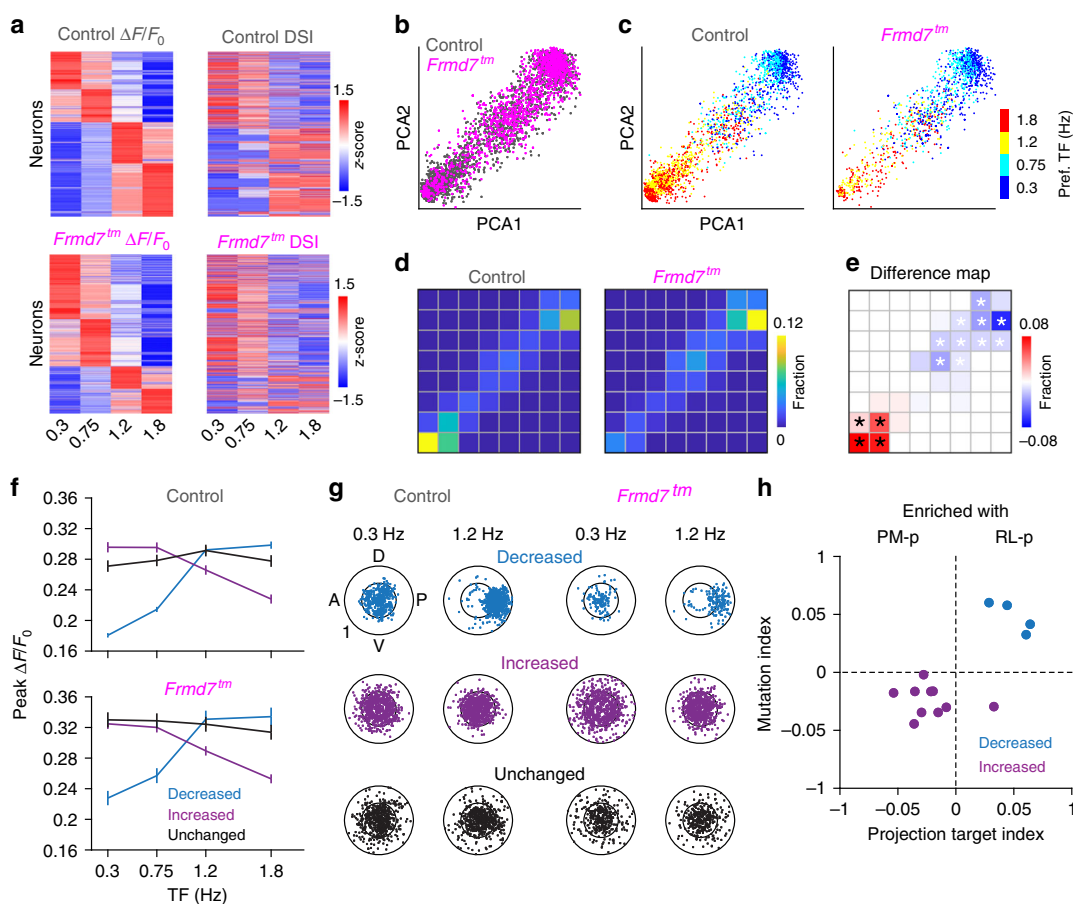

Fig. 4 V1 L2/3 neurons with distinct functional characteristics are sensitive to disruption of retinal horizontal direction selectivity. a Response matrix composed of TF-dependent response amplitudes and DSI for all pooled V1 L2/3 DS cells (target-unspecific, PM-p, and RL-p) sorted by TF preference. **b** Two-dimensional (2D) visualization of the 1st and 2nd principal components for the response matrix shown in **a**. Each point represents one neuron. **c** TF preference of individual V1 neurons. **d** Fraction of neurons in 8 × 8 grids (gray lines) calculated from the PCA plot shown in **b** for control and *Frmd7^{tm}* mice. **e** Fraction difference map between control and *Frmd7^{tm}* mice. Black and white asterisks: significantly decreased and increased fractions in *Frmd7^{tm}* mice, respectively, $P < 0.05$, two-sided χ^2 test with Yates correction. **f** Peak response amplitude as a function of TF for three groups (decreased, increased, or unchanged in *Frmd7^{tm}* mice) in control (886, 845, and 591 DS cells, respectively) and *Frmd7^{tm}* mice (169, 825, and 381 DS cells, respectively). Error bars are SEM. **g** TF-dependent tuning characteristics of individual V1 neurons from the three groups in control and *Frmd7^{tm}* mice. Angular coordinate: preferred direction. Radial coordinate: DSI. Inner circle: DSI of 0.5. **h** Relationship between effect of *Frmd7^{tm}* mutation and enrichment in PM-p or RL-p neurons. *x*-axis: Index comparing axonal projection pattern for the individual grids in **e** that were decreased and increased in *Frmd7^{tm}* mice; groups with positive and negative index values are enriched in RL- and PM-projecting neurons, respectively. *y*-axis: Index comparing sensitivity to altered retinal direction selectivity for grids; grids with a positive and negative index value are decreased and increased in *Frmd7^{tm}* mice, respectively. Source data are provided as a Source Data file.
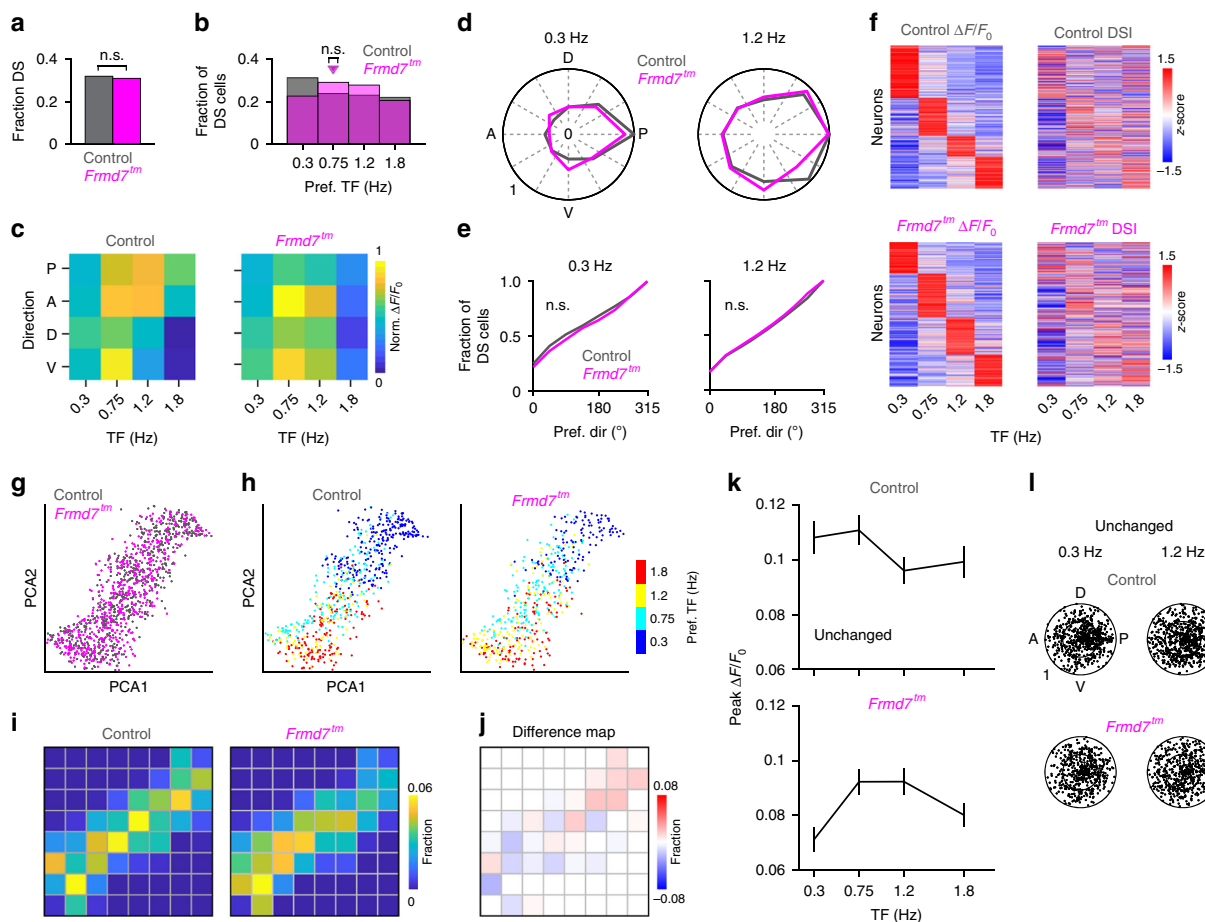
Fig. 5 Direction selectivity in V1 L4 is insensitive to disruption of retinal horizontal direction selectivity. a Fraction of DS cells in V1 L4 (678 and 536 DS cells in control and *Frmd7tm* mice, respectively; four mice per group; two-sided χ^2 test with Yates correction). **b** Preferred TF for DS cells in V1 L4 (two-sided Mann–Whitney *U*-test). Triangles: Medians. **c** Response amplitude as function of motion direction and TF for V1 L4 DS cells. **d** Fractional distributions of preferred motion directions for V1 L4 DS cells at 0.3 and 1.2 Hz, normalized to the largest fraction across genetic groups. **e** Distributions of preferred motion directions at 0.3 and 1.2 Hz for V1 L4 DS cells (two-sided Kolmogorov–Smirnov test). **f** Response matrix composed of TF-dependent response amplitudes and DSI for V1 L4 DS cells sorted by TF preference. **g** Two-dimensional (2D) visualization of the 1st and 2nd principal components for the response matrix shown in **f**. Each point represents one neuron. **h** TF preference of individual V1 L4 neurons. **i** Fraction of neurons in 8 × 8 grids (gray lines) calculated from the PCA plot shown in **g** for control and *Frmd7tm* mice. **j** Fraction difference map between control and *Frmd7tm* mice. **k** Peak response amplitude as a function of TF for the unchanged group in control (678 DS cells) and *Frmd7tm* mice (536 DS cells). Error bars are SEM. **l** TF-dependent tuning characteristics of individual V1 L4 neurons from the unchanged group in control and *Frmd7tm* mice. Angular coordinate: preferred direction. Radial coordinate: DSI. Inner circle: DSI of 0.5. n.s., not significant. Source data are provided as a Source Data file.

motion. First, we identified area RL as a higher visual cortical area, where the response properties of DS cells prominently rely on retinal motion computations. Second, we identified a connection motif in the cortico-cortical V1 L2/3 projection neurons, by which feedforward signaling, originating from retinal DS cells, is selectively routed to area RL, but not to area PM (Fig. 7j). Third, retinal DS cells influence cortical neurons by biasing their direction tuning toward posterior motion in a stimulus TF-dependent manner. Our results thus point to an unexpected causal link between a specialized response feature of HVAs and a particular form of retinal computation.

Our work provides key insights into the neural circuit mechanisms enabling functional diversity in HVAs. Examining the input-output relationship of the mouse V1 has been challenging, since distinct projection neurons do not have any known histological characteristics, unlike their counterparts in primates where V1 neurons mediating the magnocellular and parvocellular pathways can be distinguished by histological features[34,35].

Recent research has demonstrated that the connections between projection neurons in V1 that project to different targets are rare, regardless of response similarities[16]. Thus, our results suggest that each of these segregated subnetworks potentially receives a unique combination of retino-geniculate inputs, enabling specialized responses of individual HVAs to emerge. Our findings invoke the intriguing question of how such specific multi-synaptic connectivity may be established during development. One possibility is that downstream circuits of retinal DS cells are wired together based on a set of uniquely expressed molecules. Alternatively, or synergistically, mechanisms dependent on patterned spontaneous activity[36] or visual experience may guide the synaptic connections.

By analyzing the PCA distributions of the imaged neurons, we identified that the coupling of response amplitude increments and the development of a posterior motion preference as the stimulus TF increases are the key response features in RL and V1 L2/3 DS cells that rely on retinal motion computations along the
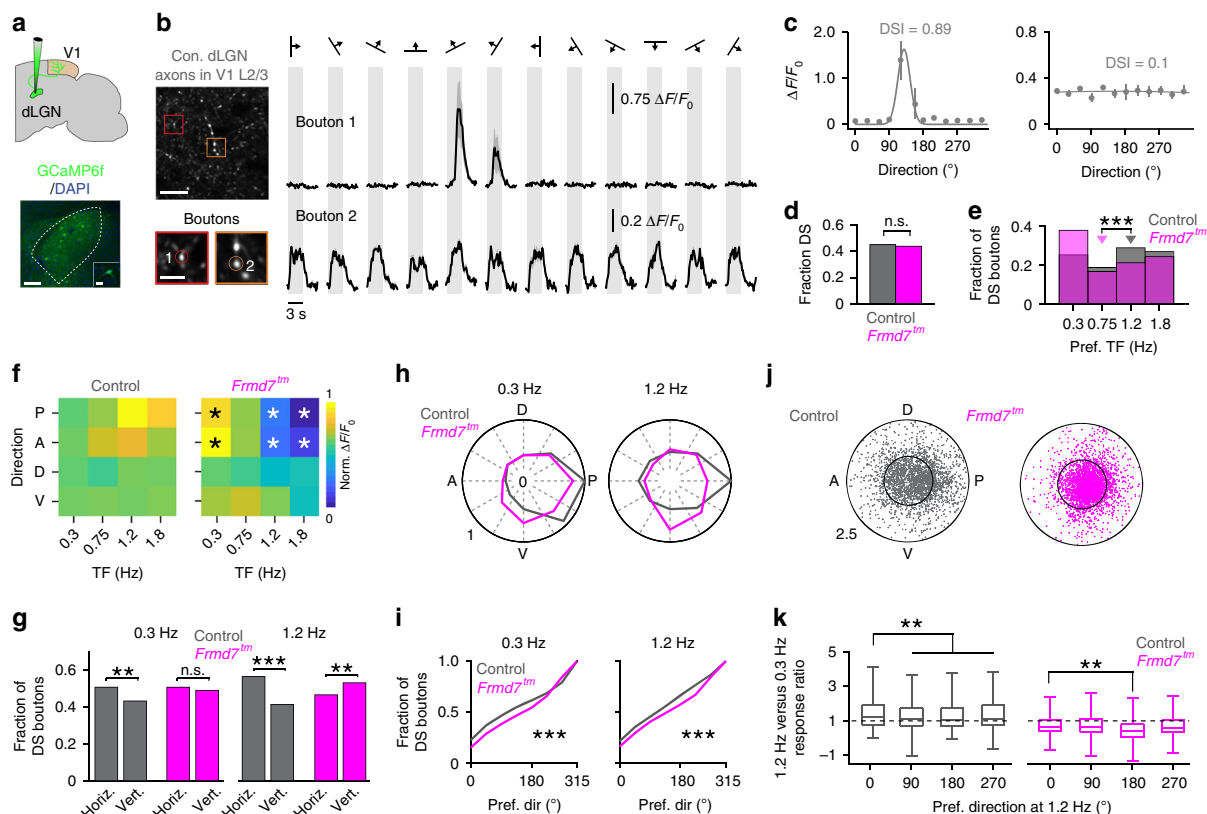
ARTICLE

Fig. 6 Directionally tuned thalamic boutons in the superficial V1 are sensitive to disruption of retinal horizontal direction selectivity. a Top: thalamocortical axons in V1 were labeled by injecting AAV2/1-GCaMP6f into the dLGN. Bottom: Example GCaMP6f-positive neurons in dLGN (scale bar, 100 µm; inset, 10 µm). **b** Left top: Example two-photon image of dLGN axons in L2/3. Left bottom: magnified axonal boutons expressing GCaMP6f (scale bar, 35 µm; inset, 10 µm). Right: trial-averaged fluorescence ($\Delta F/F_O$) time courses for the boutons indicated. Shading: SEM. **c** Tuning curves for boutons shown in **b**. Error bars: SEM. Solid line: Gaussian fit. **d** Fraction of DS boutons (5,121 and 5,525 DS boutons from control and $Frmd7^{tm}$ mice, respectively; five mice per group; two-sided χ^2 test with Yates correction). **e** Preferred TF for DS boutons (two-sided Mann–Whitney U-test). Triangles: Medians. **f** Response amplitude as a function of motion direction and TF for DS boutons. White and black asterisks: significantly decreased and increased responses, respectively, in $Frmd7^{tm}$ mice, $P < 0.05$, two-sided Mann–Whitney U-test. **g** Fraction of horizontally- and vertically-tuned DS boutons at 0.3 and 1.2 Hz (two-sided χ^2 test with Yates correction). **h** Fractional distributions of preferred motion directions for DS boutons at 0.3 and 1.2 Hz, normalized to the largest fraction across genetic groups. **i** Distribution of preferred motion directions at 0.3 and 1.2 Hz in DS boutons (two-sided Kolmogorov–Smirnov test). **j** TF-dependent characteristics of DS boutons. Angular coordinate: Directional preference at 1.2 Hz. Radial coordinate: Ratio of response amplitudes at 1.2 and 0.3 Hz. Inner circle: Response ratio of 1. **k** Ratio of response amplitudes at 1.2 and 0.3 Hz as a function of motion direction preference of DS boutons (two-sided Mann–Whitney U-test). Center line is median, box limits are 25th and 75th percentiles, and whiskers show minimum and maximum values. *$P < 0.05$, **$P < 0.01$, ***$P < 0.001$, n.s., not significant. Source data are provided as a Source Data file.

horizontal axis. How do such TF-dependent changes in responses and tuning rely on retinal motion computations? We propose that the retinal over-representation of posterior motion that develops with increasing TF, and which is conveyed via the dLGN, is amplified by the local circuitry within V1, shifting the balance of cortical DS responses to the posterior direction. The suppression of responses to non-posterior directions at higher TFs could result from cortical normalization[37]. The larger retinal population responses to posterior compared to anterior motion at higher TFs may be advantageous for distinguishing rotational and translational optic flow by enabling differences of summed output activity from left versus right retinas. The higher TF sensitivity of horizontal compared to vertical retinal DS cells may be explained by the two-dimensional nature of terrestrial navigation in mice. In contrast to RL and V1 L2/3 neurons, direction selectivity in V1 L4 and PM L2/3 neurons is most likely generated by non-retinal mechanisms[26] (Figs. 1 and 5), indicating spatially segregated processing of direction selectivity computed by retina-dependent and -independent mechanisms. Lastly, it is worth noting that we

cannot exclude the possibility that signaling from retinal DS cells is also conveyed to area RL via extrageniculate pathways[38–40], given the innervation of the superior colliculus by retinal ON-OFF DS cells[41], despite collicular outputs preferentially target the postrhinal cortex[15].

What is the possible behavioral role of area RL and retinal ON-OFF DS cells? In mice, area RL is thought to belong to a dorsal-like stream[7,11,12,38], and the anterior part of RL is considered to be part of the posterior parietal cortex[42,43], which is important for visually guided navigation[44,45]. Furthermore, area RL is strongly interconnected with other areas such as area AL, the primary somatosensory cortex, and the secondary motor cortex[46]. Notably, >50% of RL L2/3 pyramidal neurons are multisensory, integrating both tactile and visual inputs[47], and RL is also thought to be involved in visuo-motor integration[48]. Lastly, the receptive field location of RL neurons is biased to the anterior, lower visual-field[8] and the neurons respond to visual stimuli very close to the mouse[49]. Altogether, these prior findings indicate that area RL is ideally adapted to sensori-motor coordination for the lower
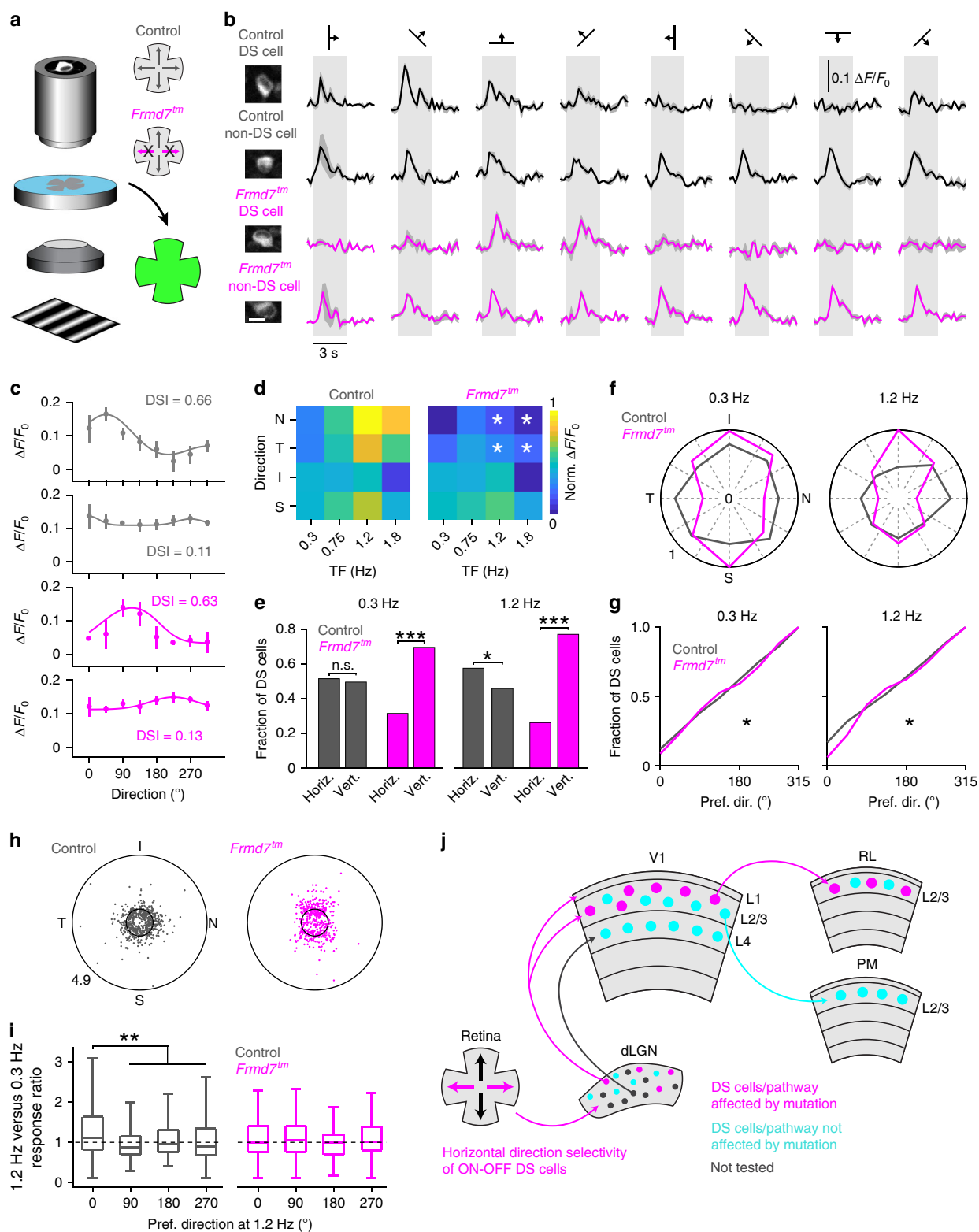
visuo-tactile space near the face of the mouse. Interestingly, the ventral intraparietal area of the human posterior parietal cortex, which is referred to as the dorsal stream of vision, also contains visual and tactile maps, and is focused on processing the face-centered sensory space[50]. In macaque monkeys, this area contains many DS cells, which prefer high speeds, and some of these cells are sensitive to the trajectory of visual stimuli moving toward the face[51]. Furthermore, this area jointly represents translation direction and rotation velocity during self-motion based on optic flow[52]. Together with a recent finding that preferred directions of

ARTICLE

Fig. 7 Preference of retinal neurons to posterior motion at higher TFs is disrupted in _Frmd7tm_ mice. a Two-photon calcium imaging was performed on retinas from control (1157 cells; four mice) and _Frmd7tm_ mice (953 cells; four mice). **b** Left: example control and _Frmd7tm_ retinal neurons expressing GCaMP6s (scale bar, 10 μm). Right: trial-averaged fluorescence ($\Delta F/F_0$) time courses for the same. Shading indicates SEM. **c** Tuning curves for neurons shown in **b**. Error bars are SEM. Solid line: Gaussian fit. **d** Response amplitude as a function of motion direction (nasal [N], temporal [T], inferior [I], and superior [S]) and TF for retinal cells. White asterisk: significantly decreased response in _Frmd7tm_ mice (two-sided Mann–Whitney U-test). **e** Fraction of horizontally- and vertically tuned retinal ON-OFF DS cells (425 and 342 ON-OFF DS cells in control and _Frmd7tm_ mice, respectively) at 0.3 and 1.2 Hz (two-sided χ^2 test with Yates correction). **f** Fractional distributions of preferred motion directions for ON-OFF DS cells at 0.3 and 1.2 Hz, normalized to the largest fraction across genetic groups. **g** Distribution of preferred motion directions at 0.3 and 1.2 Hz in ON-OFF DS cells (two-sided Kolmogorov–Smirnov test). **h** TF-dependent characteristics of ON-OFF DS cells. Angular coordinate: Directional preference at 1.2 Hz. Radial coordinate: Ratio of response amplitudes at 1.2 and 0.3 Hz. Inner circle: response ratio of 1. **i** Ratio of response amplitudes at 1.2 and 0.3 Hz as a function of motion direction preference of cells that showed ON-OFF DS responses (two-sided Mann–Whitney U-test). Center line is median, box limits are 25th and 75th percentiles, and whiskers show minimum and maximum values. **j** Schematic diagram of proposed neural pathway linking retinal ON-OFF DS cells to RL DS cells. *P < 0.05, **P < 0.01, ***P < 0.001, n.s., not significant. Source data are provided as a Source Data file.

retinal ON-OFF DS cells are aligned with translatory and rotatory optic flow fields[21], our findings raise the intriguing hypotheses that the mouse area RL may be a functional counterpart of the primate ventral intraparietal area, and visual motion analyses in the primate posterior parietal cortex may rely on signaling from such retinal DS cells. However, it is still unknown if dLGN-projecting retinal DS cells exist in primates.

Methods

Experimental animals. Wild-type control mice (C57BL/6J) were obtained from Janvier Labs. _Frmd7tm_ mice are homozygous female or hemizygous male _Frmd7tm1b(KOMP)Wtsi_ mice, which were obtained as _Frmd7tm1a(KOMP)Wtsi_ from the Knockout Mouse Project (KOMP) Repository[25,27]: Exon 4 and neo cassette flanked by loxP sequences were removed by crossing with female Cre-deleter _Edil3Tg(Sox2-cre)1Amc/J_ mice (Jackson laboratory stock 4783) as confirmed by PCR of genome DNA, and maintained in C57BL/6J background. _ChAT-Cre_ (strain: _Chattm2(cre)Lowl_/MwarJ, Jackson laboratory stock: 028861)[53] and _LSL-DTR_ (strain: _Gt(ROSA)26Sortm1(HBEGF)Awai_/J, Jackson laboratory stock: 007900)[54] were purchased from Jackson laboratory and maintained in C57BL/6J background. Experiments were performed on 34 male and female wild-type control mice, 33 male and female _Frmd7tm_ mice, and 10 female _ChAT-Cre × LSL-DTR_ mice. All mice were between two and four months old. Mice were group-housed and maintained in a 12-h/12-h light/dark cycle with ad libitum access to food and water. Experiments were performed according to standard ethical guidelines and were approved by the Danish National Animal Experiment Committee.

Head-plate and cranial window implantation. Mice were anaesthetized with an intraperitoneal injection of a fentanyl (0.05 mg/kg body weight; Hameln), midazolam (5.0 mg/kg body weight; Hameln) and medetomidine (0.5 mg/kg body weight; Domitor, Orion) mixture dissolved in saline. The depth of anesthesia was monitored by the pinch withdrawal reflex throughout the surgery. Core body temperature was monitored using a rectal probe and temperature maintained at 37−38 °C using a feedback-controlled heating pad (ATC2000, World Precision Instruments). Eyes were protected from dehydration during the surgery with eye ointment (Oculotect Augengel). The scalp overlaying the left visual cortex was removed, and a custom head-fixing imaging head-plate with a circular 8 mm diameter opening was mounted on the skull using cyanoacrylate-based glue (Super Glue Precision, Loctite) and dental cement (Jet Denture Repair Powder) to allow for subsequent head fixation during imaging. The center of the head-plate was positioned above V1, 2.5 mm lateral and 1 mm anterior of lambda[55]. To gain optical access to the cortex, a 5 mm diameter craniotomy was performed. After removing the skull flap, the cortical surface was kept moist with a cortex buffer containing 125 mM NaCl, 5 mM KCl, 10 mM glucose, 10 mM HEPES, 2 mM MgSO₄, and 2 mM CaCl₂. The dura was left intact (except in two animals in which the dura spontaneously detached with the skull flap) and any occasional bleedings were immediately stopped with Gelfoam (Pfizer). A 5 mm glass coverslip sterilized in ethanol (0.15 mm thickness, Warner Instruments) was placed onto the brain to gently compress the underlying cortex and dampen biological motion during subsequent imaging[56]. The cranial window was hermetically sealed using a cyanoacrylate-based glue (Super Glue Precision, Loctite) mixed with black dental cement (Jet Denture Repair Powder mixed with iron oxide powdered pigment) to prevent the entry of stray light from the screen through the skull and/or cement during imaging[56]. Mice were returned to their home cage after anesthesia was reversed with an intraperitoneal injection of a flumazenil (0.5 mg/kg body weight; Hameln) and atipamezole (2.5 mg/kg body weight; Antisedan, Orion Pharma) mixture dissolved in saline, and after recovering on a heating pad for one hour.

Intrinsic imaging. For ISOI mice were anesthetized with isoflurane (2−3% induction) and head-fixed in a custom holder. Chlorprothexine was administered intraperitoneally (2.5 mg/kg body weight; Sigma) as a sedative[12], and isoflurane reduced to 0.5−1% and kept constant during visual stimulation. Core body temperature was maintained at 37−38 °C using a feedback-controlled heating pad (ATC2000, World Precision Instruments). The stimulated contralateral eye was kept lubricated by hourly application of a thin layer of silicone oil (OFNA Racing, 10,000 molecular weight). The experimental setup employed for ISOI was adapted from a similar system[57] and made publicly available (https://snlc.github.io/ISI/). A 2 × air-objective (Olympus, 0.08 NA, 4 mm field of view) was mounted on our Scientifica VivoScope, which was equipped with a CMOS camera (HD1-D-D1312-160-CL-12, PhotonFocus), a large-well-depth camera that offers high signal-to-noise measurements in bright light conditions. The camera was connected to a Matrox Solios (eCL/XCL-B) frame-grabber via Camera Link. The acquisition code for the Matrox board was written in Matlab using the Image Acquisition Toolbox. From the pial surface, the microscope was defocused down 400−600 μm, where intrinsic signals were excited using a red LED (KL1600, Schott) delivered via light guides through a 610 nm long-pass filter (Chroma). Reflected light was captured through a 700 ± 50 nm (mean ± SEM) band-pass filter (Chroma) positioned right in front of the camera at a rate of 6 frames per second (512 × 512 pixels). At 700 nm there is a large change in the absorption coefficient between oxyhemoglobin and deoxyhemoglobin, contributing to the intrinsic signal measured in these experiments[12]. The 47.65 × 26.87 cm (width × height) screen was angled 30° from the mouse's midline and positioned so that the perpendicular bisector was 10 cm from the bottom of the screen, centered on the screen left to right (23.8 cm on each side), and 10 cm from the eye[57]. This resulted in a visual-field coverage from −41.98° to 60.77° (total 102.75°) in elevation and from −67.23° to 67.23° (total 134.46°) in azimuth. Thus, the stimulus covered almost the entire known visual hemi-field of the mouse, which is estimated to be at most 110° vertically and 140° horizontally. For the ISOI experiments presented in Fig. 1, each mouse was imaged on three separate days, and the data averaged to reduce the chance of day-to-day variations confounding group-level results.

Visual stimuli for ISOI. Retinotopic maps were generated by sweeping a spherically corrected (Matlab code provided by Spencer Smith: https://labrigger.com/blog/2012/03/06/mouse-visual-stim/) full-field bar across the screen in both azimuth and elevation directions[57]. The bar contained a flickering black-and-white checkerboard pattern on a black background[7,57]. The width of the bar was 12.5° and the checkerboard square size was 25°. Each square alternated between black and white at 4 Hz. In each trial, the bar was drifted 10 times in each of the four cardinal directions (0°, 90°, 180°, and 270°), moving at 8−9°/s. Usually, two to three trials were sufficient to achieve well-defined retinotopic maps. For measuring and characterizing the evoked areal activity in V1 and HVAs we presented 100% contrast black and white sinusoidal gratings drifting in each of the four cardinal directions. We presented gratings with four different TFs: 0.3, 0.75, 1.2, and 1.8 Hz (0.03 cycles/°). Each stimulus was stationary for 10 s and in motion for 10 s, comprising a stimulus period of 20 s, which was repeated 5 times in each direction. All stimuli used for ISOI were produced and presented using Matlab and the Psychophysics Toolbox[58].

Image analysis for ISOI. To generate functional visual cortex maps from the raw image data, we took the response time course for each pixel and computed the phase and magnitude of the Fourier transform at the stimulus frequencies (0.067 and 0.088 Hz, for azimuth and vertical, respectively)[59]. The bar was drifted in opposite directions in order to subtract the delay in the intrinsic signal relative to neuronal activity[59]. The resulting phase maps were then converted into retinotopic coordinates (visual degrees) from the known geometry of our setup to retrieve absolute retinotopy. We used automated, publicly available code to identify visual area borders based on their visual-field sign maps[57] (see also description below),

and superimposed those borders with the anatomical blood-vessel images to accurately localize V1 and individual HVAs.

To evaluate and quantify the spatial properties of visual areas, we first computed and identified the borders of each visual area, using a dissociation algorithm and the Image Processing Toolbox in Matlab. The identification process constituted three conventional edge-detection steps. (1) Thresholding of the obtained visual-field sign map. For this we used a definition of $\bar{I} + SD(I)$ where I equals the intensity of a pixel and $\bar{I}$ denotes the mean pixel intensity of the visual-field sign map. The thresholded image was smoothed using a median filter (filter size, 3×3 neighborhoods). (2) Isolation and segmentation of pixels. For this step we used the 8-neighbors criterion. If there were >4 non-zero pixels among the eight neighbors of one pixel, the pixel was retained and any gaps between pixels within the eight neighbors were filled with a non-zero value. If this criterion was not met, the pixel value was set to 0. The value of all non-zero pixels was set to 1. (3) Edge detection. The isolated and segmented pixels were next binarized, and each edge was computed based on a Sobel method using the edge function in Matlab. After identifying visual area borders, we computed the size of the area (first in pixels and then converted to mm2) and defined the center position of each area as a centroid. From this, we calculated two-dimensional coordinates of each HVA as coordinates relative to the V1 centroid. For ISOI experiments in which sinusoidal gratings were presented, the raw response signal was first determined as the peak power of the stimulus-evoked signal by employing Fast-Fourier transform analyses of each pixel column at the frequencies of the visual stimuli; 0.05−0.1Hz[12]. To quantify the response for each visual cortical area, the raw response signal was first normalized to the raw response signal from before the visual stimulation (averaged over a 10 s period). Next, regions of interest (ROIs) within the visual cortical areas were defined based on the visual area border map. The response strength of each area was determined as the maximum value within each ROI. For group-level quantifications, the response strength for a given area was averaged across the three experimental days before pooling data from all mice.

Local viral labeling. For local viral injections in the visual cortex or dLGN, mice were first anesthetized with an intraperitoneal injection of a fentanyl (0.05 mg/kg body weight; Hameln), midazolam (5.0 mg/kg body weight; Hameln) and medetomidine (0.5 mg/kg body weight; Domitor, Orion) mixture dissolved in saline. For injections yielding GCaMP6 expression in areas V1, RL and PM, three 0.4 mm diameter craniotomies were performed over the left visual cortex and 100 nl AAV2/1-Syn-GCaMP6f-WPRE (2.13×10^{13} vg/ml, Penn Vector Core #AV-1-PV2822) slowly injected at depths of 100−500 μm using a borosilicate glass micropipette (30 μm tip diameter) and a pressure injection system (Picospritzer III, Parker). For labeling geniculo-cortical axons projecting from the dLGN, 20−40 nl AAV2/1-Syn-GCaMP6f-WPRE (2.13×10^{13} vg/ml, Penn Vector Core #AV-1-PV2822) was slowly injected into the left dLGN using stereotaxic coordinates: 2.1 mm posterior of the Bregma; 2.2 mm lateral of the midline; 2.3 mm below the pial surface[23]. To prevent backflow during withdrawal, the micropipette was kept in the brain for a minimum of 5 min before it was slowly retracted. The skin was afterwards sutured shut. Mice were returned to their home cage after the anesthesia was reversed with an intraperitoneal injection of a flumazenil (0.5 mg/kg body weight; Hameln) and atipamezole (2.5 mg/kg body weight; Antisedan, Orion Pharma) mixture dissolved in saline, and after recovering on a heating pad for 1 h. Although the injection sites in the visual thalamus were always within the dLGN, there were sometimes spillover expressions in the neighboring ventral LGN (vLGN), intergeniculate leaflet (IGL), and the pulvinar nucleus similar to previously reported[60]. The vLGN and IGL do not project to V1 (ref. [61]); compared to the dLGN, projections from the pulvinar to V1 are much sparser and limited to the superficial L1 (ref. [62]). Hence, the majority of thalamic axons that we imaged in V1 most likely originated from the dLGN.

Retrograde viral labeling. To achieve GCaMP6 expression in V1 neurons projecting to area RL or PM we employed a slightly modified surgery protocol. First, we implanted a custom head-fixing imaging head-plate and mapped the visual cortex using ISOI through the intact skull. This allowed us to identify the precise anatomical location of areas RL and PM. Next, we performed a single, local virus injection into either area RL or PM by slowly injecting 100 nl of ssAAV-retro/2-hSyn1-mRuby2-GCaMP6m-WPRE (7×10^{12} vg/ml, VVF Zurich #v187-retro) at depths of 100−300 μm. This AAV-retro serotype permits selective retrograde labeling of projection neurons and enables sufficient expression for functional two-photon calcium imaging[63]. After slowly retracting the micropipette, the craniotomy was carefully cleaned and the exposed skull covered with a silicone sealant (Kwik-Cast, World Precision Instruments). One day later, the animal was implanted with a chronic cranial window, exposing V1 for two-photon calcium imaging targeted to V1 neurons projecting specifically to either the RL or PM area.

Diphtheria toxin injections. To abolish retinal direction selectivity acutely in adult mice, we injected diphtheria toxin intravitreously into ChAT-Cre × LSL-DTR mice[25]. Diphtheria toxin stock solution was made from diphtheria toxin (Sigma, D0564) dissolved in phosphate-buffered saline (PBS) to a concentration of 1 μg/μl and stored at −80 °C. Before injections, the stock solution was diluted in PBS to a final concentration of 0.8 ng/μl. Mice were first anesthetized with an intraperitoneal

injection of a fentanyl (0.05 mg/kg body weight; Hameln), midazolam (5.0 mg/kg body weight; Hameln) and medetomidine (0.5 mg/kg body weight; Domitor, Orion) mixture dissolved in saline. A hole was made near the border between the sclera and the cornea using a 30-gauge needle; 2 μl toxin was then injected into the vitreous of both eyes using a borosilicate glass micropipette connected to a pressure injection system (Picospritzer III, Parker). Mice were returned to their home cage after the anesthesia was reversed with an intraperitoneal injection of a flumazenil (0.5 mg/kg body weight; Hameln) and atipamezole (2.5 mg/kg body weight; Antisedan, Orion Pharma) mixture dissolved in saline. Each eye was re-injected 2 days after the initial injection. OMR recordings were performed 7−9 days after the initial injection, and in-vivo two-photon calcium imaging experiments were initiated 10−12 days after the initial injection.

Optomotor response measurement. For recording the optomotor reflex the mouse was placed on a central, raised platform and presented visual stimuli in the form of drifting sinusoidal gratings projected onto a virtual cylinder on the four surrounding computer screens[64]. The gratings were drifting horizontally at 12°/s, alternating the drift direction every 60°. One trial consisted of six 1 min repeats; after each repeat, the spatial frequency of the stimulus was sequentially changed (0.05, 0.1, 0.2, 0.25, 0.3, 0.4 cycles/°). Mouse head movements were tracked using OKR arena software[64], where the angle of the head is automatically calculated and used to quantify the OMR for each stimulus condition[64]. OMR was determined by calculating the ratio of the sum of frames where head movements occurred in the stimulus direction versus in the opposite direction[64].

Cortical two-photon calcium imaging. Imaging was performed 2−4-weeks after virus injections, when most neurons exhibited cytosolic-only GCaMP6 expression. Mice were anesthetized with 0.3–0.8% (typically 0.5%) isoflurane, and chlor-prothexine was delivered intraperitoneally (2.5 mg/kg body weight; Sigma) as a sedative[12]. The stimulated contralateral eye was kept lubricated by hourly application of a thin layer of silicone oil (OFNA Racing, 10,000 molecular weight). Core body temperature was maintained at 37−38 °C using a feedback-controlled heating pad (World Precision Instruments, ATC2000). A subset of experiments was performed in awake mice. To habituate the mice to handling and experimental conditions, each mouse was head-fixed onto the imaging stage with its body restrained in a cylindrical cover, reducing struggling and substantial body movements[60,65]. The habituation procedure was repeated for 3 days for each mouse at durations of 15, 30, and 60 min on day 1, day 2, and day 3, respectively. Mice were rewarded with chocolate paste (Nutella) at the end of each habituation/imaging session. For imaging, the mouse was placed under the microscope 10 cm from the 47.65 × 26.87 cm (width × height) screen, with the screen subtending 134.46° in azimuth and 102.75° in elevation and angled 30° from the mouse's midline. The visual area targeted for two-photon calcium imaging was localized based on superimposing the ISOI border map onto the cortical surface. Imaging was performed 50–100 μm (L1), 120–250 μm (L2/3), and 350–550 μm (L4) below the dura using a scanning microscope (VivoScope, Scientifica) with a 7.9 kHz resonant scanner running SciScan version 1.3 with dispersion-compensated 940 nm excitation provided by a mode-locked Ti:Sapphire laser (MaiTai DeepSee, Spectra-Physics) through either a Nikon 16× (0.8 NA; somata imaging) or an Olympus 25× (1.05 NA; axonal bouton imaging) objective. Clear ultrasound gel was used as an immersion medium (Aquasonic, Parker Laboratories). To prevent light leak originating from the visual stimulation, an imaging well was constructed from a black O-ring and the objective shielded with black tape. Average excitation power after the exit pupil of the objective varied from 25 to 60 mW. Typical images had 512 × 512 pixels, at 0.3−0.35 μm per pixel for axons, and 0.92 μm per pixel for somata, and were acquired at 30.9 Hz using bidirectional scanning. By correcting for any slow drifts in neuron or axon location within the field of view using a reference image[6,23], we were able to record from the same population of neurons or axons over extended periods of time (~40 min), allowing us to assess responses as a function of TF conditions. There was no evidence of GCaMP6 bleaching during experiments. Each mouse was imaged repeatedly over the course of 1–2 weeks.

Visual stimuli for cortical two-photon calcium imaging. Visual stimulation for cortical two-photon calcium imaging was generated and presented via Python-based custom-made software. To measure directional tuning, we presented 100% contrast black and white sinusoidal drifting gratings. Drifting gratings were presented in six trials for 3 s at a time, with 3 s of gray screen between presentations, and were drifted in 12 different directions (0°, 30°, 60°, 90°, 120°, 150°, 180°, 210°, 240°, 270°, 300°, and 330°) in a pseudorandomized order, with a spatial frequency of 0.03 cycles/° and TFs of 0.3, 0.75, 1.2, and 1.8 Hz.

Image analysis for cortical two-photon calcium imaging. Imaging data were excluded from analysis if motion along the z-axis was detected. Raw images from somata imaging were corrected for in-plane motion via a correlation-based approach in Matlab[55]. Raw images from axonal bouton imaging were corrected for in-plane motion using a piecewise non-rigid motion correction algorithm[66]. ROIs were drawn in ImageJ (Cell Magic Wand; https://github.com/fitzlab/CellMagicWand) and selected based on mean and maximum fluorescence images[56]: somata ROIs were polygonal; axonal bouton ROIs were circular. The same

ARTICLE

ROI set was used for all imaging stacks acquired in a given field of view. Fluorescence time courses were computed as the mean of all pixels within ROIs and were extracted using MIJ (http://bigwww.epfl.ch/sage/soft/mij/). Baseline-normalized fluorescence time courses ($\Delta F/F_0$) were computed using a 60 s 10th percentile filter and 0.01 Hz low-pass Butterworth filter to define F_0 (ref. [56]). For each of the twelve directions, the response amplitude in each trial was determined by sorting all $\Delta F/F_0$ values (down-sampled to 15.4 Hz) during the 3 s drift period, and taking the mean of the larger 50% of data points[25]. Somata and axonal boutons were defined as visually responsive if $\Delta F/F_0$ in the preferred direction of motion exceeded 0.06 (refs. [7,67]) in at least one of the four TFs. They were defined as DS if: (1) They were visually responsive; and (2) their DSI exceeded 0.3 (refs. [26,56]) in at least one of the four TFs:

$$\text{DSI} = \frac{R_{\text{pref}} - R_{\text{opp}}}{R_{\text{pref}} + R_{\text{opp}}}$$

where R_{pref} denotes the mean $\Delta F/F_0$ response to the preferred direction of motion and R_{opp} the mean $\Delta F/F_0$ response to the opposite direction. The preferred direction of motion for each cell was calculated as the angle, in polar coordinates, of the vector sum[27,68]:

$$\theta = \tan^{-1}\left(\frac{\sum_{i=1}^{12} R_i \, \sin d_i}{\sum_{i=1}^{12} R_i \, \cos d_i} \right)$$

where d_i denotes the motion direction of direction i and R_i the mean $\Delta F/F_0$ response to direction i.

OSI was computed as:

$$\text{OSI} = \frac{R_{\text{pref}} - R_{\text{orth}}}{R_{\text{pref}} + R_{\text{orth}}}$$

where R_{pref} denotes the mean $\Delta F/F_0$ response to the preferred orientation and R_{orth} the mean $\Delta F/F_0$ response to the orthogonal orientation. The preferred orientation was defined as the axis including the preferred direction and its opposite direction.

Data decomposition and segmentation. To correlate the TF-dependent response properties in individual cortical DS cells and the fractional changes of neurons between control and $Frmd7^{tm}$ mice, we performed decomposition and segmentation of datasets summarizing response features of the identified DS cells. First, we composed a response matrix for each visual area (e.g., area RL) using a total of eight parameters for each neuron: peak $\Delta F/F_0$ amplitudes and DSI values under each of the four TF conditions. The response matrix included datasets from both control and $Frmd7^{tm}$ mice. For the V1 L2/3 response matrix, we pooled the datasets from target-unspecific, PM-projecting, and RL-projecting DS cells. Next, the response matrix was decomposed into two dimensions by PCA. The resulting PCA distributions showed a distribution trend depending on the TF preference of the individual neurons, indicating that neurons sharing the same TF preference tended to be clustered in the local region of the PCA distribution. To quantify the localization of neurons, we segmented the PCA distribution by 8×8 grids. We then calculated the fraction of neurons located within each of the grids, and examined the fractional changes between control and $Frmd7^{tm}$ mice. Based on the fractional changes, we statistically classified neurons into three groups: (1) "Increased", (2) "Decreased", and (3) "Unchanged" in $Frmd7^{tm}$ mice, compared to control mice. We tested the number of grids for this segmentation, and confirmed that the results were not qualitatively changed by the size of the grids (Supplementary Fig. 6).

To investigate the relationship between the effects of altered retinal horizontal direction selectivity and the target region of V1-projecting DS cells, we analyzed the fraction of PM- and RL-projecting cells in each grid based on a projection target index (PTI):

$$\text{PTI}^i = \frac{F_{\text{RLp}}^i - F_{\text{PMp}}^i}{F_{\text{RLp}}^i + F_{\text{PMp}}^i}$$

Where F_y^x denotes the fraction of cells projecting to area y in a grid x. A positive PTI indicates that the neurons within the grid are biased towards RL-projecting neurons, while a negative PTI indicates a bias towards PM-projecting neurons.

The effects of altered retinal horizontal direction selectivity was evaluated using a mutation index (MI):

$$\text{MI}^i = \frac{F_{\text{Control}}^i - F_{\text{Frmd7tm}}^i}{F_{\text{Control}}^i + F_{\text{Frmd7tm}}^i}$$

Where F_y^x denotes the fraction of cells in population y in grid x. A positive MI indicates that the fraction of neurons originating from $Frmd7^{tm}$ mice is decreased in the grid, while a negative MI indicates that the fraction is increased.

Virus injections for retinal two-photon calcium imaging. For intravitreal viral injections, mice were anesthetized with an intraperitoneal injection of a fentanyl (0.05 mg/kg body weight; Hameln), midazolam (5.0 mg/kg body weight; Hameln), and medetomidine (0.5 mg/kg body weight; Domitor, Orion) mixture dissolved in saline. We made a small hole at the border between the sclera and the cornea with a 30-gauge needle. Next, we loaded 2 μl of AAV1-CAG-GCaMP6s-WPRE-SV40

$(1 \times 10^{13}$ vg/ml, Penn Vector Core, #AV-1-PV2833) into a pulled borosilicate glass micropipette, and the AAV was pressure-injected through the hole into the vitreous of the left eye using a Picospritzer III (Parker). Mice were returned to their home cage after anesthesia was reversed by an intraperitoneal injection of a flumazenil (0.5 mg/kg body weight; Hameln) and atipamezole (2.5 mg/kg body weight; Antisedan, Orion Pharma) mixture dissolved in saline.

Retinal two-photon calcium imaging. Retinal imaging was performed 3−4-weeks after virus injections. Mice were first dark-adapted for 1 h, and next the retina was prepared[68]. The retina was isolated from the left eye, and mounted ganglion-cell-side up on a small piece of filter paper (Millipore, MF-membrane), in which a 2×2 mm aperture window had previously been cut. During the procedure, the retina was illuminated by dim red light (KL1600 LED, Schott) filtered with a 650 nm high-pass optical filter (650/45×, Chroma) and bathed in extracellular solution (in mM): 110 NaCl, 2.5 KCl, 1 CaCl$_2$, 1.6 MgCl$_2$, 10 D-glucose, 22 NaHCO$_3$ bubbled with 5% CO$_2$, 95% O$_2$. The retina was kept at 35−36 °C and continuously superfused with oxygenated extracellular solution during recordings. For retinal two-photon calcium imaging we employed an equipment setup similar to that previously employed[68]. The isolated retina was placed under a microscope (SliceScope, Scientifica) equipped with a galvo-galvo scanning mirror system (8315 K, Cambridge Technologies), a mode-locked Ti:Sapphire laser tuned to 940 nm (MaiTai DeepSee, Spectra-Physics), and an Olympus 20× (1.0 NA) objective. The GCaMP6s signals emitted were passed through a set of optical filters (ET525/50 m, Chroma; lp GG495, Schott) and collected using a GaAsP detector (Scientifica). Images were acquired at 6−10 Hz using custom-made software developed by Zoltan Raics (SELS Software).

Visual stimuli for retinal two-photon calcium imaging. The visual stimulation was generated via custom-made software (Python and LabVIEW) developed by Zoltan Raics, projected by a DLP projector (LightCrafter Fiber E4500 MKII, EKB Technologies) coupled via a liquid light guide to an LED source (4-wavelength high-power LED Source, Thorlabs) with a 400 nm LED (LZ4-00UA00, LED Engin) through a band-pass optical filter (ET405/40×, Chroma), and focused onto the photoreceptor layer of the mounted retina through a condenser (WI-DICD, Olympus). The stimuli were exclusively presented during the fly-back period of the horizontal scanning mirror[68]. To measure directional tuning and TF preference, we presented 100% contrast black and white sinusoidal drifting gratings (mean intensity, 0.058 mW/cm^2). Light intensity was measured using a power meter (PM200, Thorlabs) and a spectrometer (USB4000-XR1, Ocean Optics). Drifting gratings were presented in 3 trials for 3 s at a time, with 3 s of gray screen between presentations, and shown in 8 different directions (0°, 45°, 90°, 135°, 180°, 225°, 270°, and 315°) in a pseudorandomized fashion, with a spatial frequency of 0.03 cycles/° and TFs of 0.3, 0.75, 1.2, and 1.8 Hz. To measure ON and OFF responses, we presented static flash spots (2 s in duration, 50, 100, 200, 400, 800 μm in diameter). To classify retinal cells into ON-OFF and non-ON-OFF populations, we used an ON-OFF index (OOI)[25] (Supplementary Fig. 9):

$$\text{OOI} = \frac{R_{\text{ON}} - R_{\text{OFF}}}{R_{\text{ON}} + R_{\text{OFF}}}$$

Where R_{ON} and R_{OFF} denote peak calcium responses during the static spot illumination phase, and the phase after the illumination, respectively. If the mean OOI for 50−800 μm spots was <0.3, the cell was defined as an ON-OFF cell. We calculated the DSI for individual cells, and defined cells with DSI > 0.3 as DS cells, similar to experiments performed in the cortex.

Image analysis for retinal two-photon calcium imaging. The raw two-photon scanning imaging data acquired was initially loaded into Matlab and converted into accessible image files. The ROIs for cell bodies of retinal cells were drawn in Matlab by fitting polygons, and selected based on mean and maximum fluorescence images. Fluorescence time courses were computed as the mean of all pixels within the ROI at each timepoint and were extracted in Matlab. The raw GCaMP6 fluorescence signals for each ROI were normalized ($\Delta F/F_0$) using the mean fluorescence (F_0) in a 2 s window before visual stimulation, and then synchronized with visual stimulus information. The $\Delta F/F_0$ signals were resampled using the *interp* function in Matlab, and smoothed by a moving average filter (width: two data points). To evaluate cell responsiveness, we determined a threshold for each cell as $\text{mean}_{\Delta F/F0} + 2\,\text{SD}_{\Delta F/F0}$, and any cell with response amplitudes higher than their threshold was defined as visually responsive and included in further analysis.

Histology and confocal imaging. To validate the injection site in the dLGN, mice were anesthetized with an intraperitoneal injection of a fentanyl (0.05 mg/kg body weight; Hameln), midazolam (5.0 mg/kg body weight; Hameln) and medetomidine (0.5 mg/kg body weight; Domitor, Orion) mixture dissolved in saline, and transcardially perfused with PBS and then with 4% paraformaldehyde (PFA). Brains were removed, fixed overnight in PFA and then transferred to PBS and stored at 4 °C. Brain slices (200 μm thick) were collected in the coronal plane using a vibratome (Leica, VT1000S). Slices were counterstained with 4′,6-diamidino-2-phenylindole (DAPI; 1:1000 dilution, ThermoFisher) before mounting with mounting medium (Fisher Scientific). Images of 1024×1024 pixels were acquired

using a confocal microscope (Zeiss LSM 780) with a 10× (0.45 NA) objective. To validate the specificity of starburst amacrine cell ablation in diphtheria toxin-injected *ChAT-Cre* × *LSL-DTR* mice and PBS-injected littermates, we performed immunohistochemical analyses of the retinas[27]. A nasal mark was applied to the eyes and fixed for 20 min at room temperature (RT) in 4% PFA before dissection. Afterwards, eyes were rinsed in PBS, dissected, mounted on flatmount paper in 4% PFA for 30 min at RT and then washed with PBS overnight at 4 °C on a shaker. The next day, retinas were incubated in 30% sucrose in PBS for at least 3 h at RT. Afterwards, retinas were transferred in the sucrose buffer to microscope slides (SUPERFROST PLUS, Thermo Scientific) and frozen and thawed three times using dry ice to enhance antibody penetration. After washing with PBS, retinas were blocked for 3 h in blocking buffer (1% bovine serum albumin (BSA), 10% normal donkey serum (NDS), 0.5% TritonX 100, 0.02% sodium azide in PBS) at RT. Primary antibodies (rabbit anti-RBPMS 1:500 [Milipore, ABN1362] and goat anti-ChAT 1:200 [Milipore, ABN1144P]) were incubated for 5 days in antibody reaction buffer (1% BSA, 3% NDS, 0.5% TritonX 100, 0.02% sodium azide in PBS) at 4 °C on a shaker. Secondary antibodies (donkey anti-rabbit IgG Alexa Fluor 568 1:200 [Invitrogen], donkey anti-goat IgG Alexa Fluor 488 1:200 [Life Technologies] together with DAPI 1:1000 [ThermoFisher]) were incubated overnight at 4 °C in antibody reaction buffer. After a final wash in PBS, retinas were embedded in Fluoromount-G (eBioscience). For cell density analysis, z-stacks containing images of 1024 × 1024 pixels (1.38 μm per pixel) were acquired at an interval of 4 μm (total thickness of 75–80 μm) with a confocal microscope (Zeiss LSM 780) using a 10× (0.45 NA) objective, and cells were counted using ImageJ. For detailed confocal z-stacks, we used a 40× (1.4 NA) objective and acquired 1024 × 1024 pixel (0.35 μm per pixel) images at an interval of 0.3 μm (total thickness of ~75 μm).

Statistical analysis. Statistical tests were performed in Matlab and we used the following statistical tests where appropriate: Mann–Whitney *U*-test, Wilcoxon signed-rank, Kolmogorov–Smirnov, and χ^2 with Yates correction. Rayleigh's test for non-uniformity of circular data was performed using the Circular Statistics Toolbox[69]. No testing was performed to check for normality or homogeneity of variance. Center and spread values are reported as mean ± SEM. We used no statistical methods to plan sample sizes, but used sample sizes similar to those frequently used in the field[6,56]. The number of animals and cells is included in the text or in figure legends. We did not use any randomization; data collection and analysis were not performed blind to the conditions of the experiments. No collected data were excluded from analysis. *P*-values <0.05 were considered to be statistically significant. When a statistical test was used, the *P*-value is noted either in the manuscript text or depicted in figures and legends as: *$P < 0.05$, **$P < 0.01$, ***$P < 0.001$, n.s., not significant, $P \geq 0.05$.

Reporting summary. Further information on research design is available in the Nature Research Reporting Summary linked to this article.

Data availability
All relevant data is provided in the Source Data file or is available from the corresponding author upon reasonable request.

Code availability
All relevant code is available from the corresponding author upon reasonable request.

References
1. Roska, B. & Werblin, F. Vertical interactions across ten parallel, stacked representations in the mammalian retina. *Nature* **410**, 583–587 (2001).
2. Baden, T. et al. The functional diversity of retinal ganglion cells in the mouse. *Nature* **529**, 345–350 (2016).
3. Liang, L. et al. A fine-scale functional logic to convergence from retina to thalamus. *Cell* **173**, 1343–1355 (2018).
4. Martersteck, E. M. et al. Diverse central projection patterns of retinal ganglion cells. *Cell Rep.* **18**, 2058–2072 (2017).
5. Robles, E., Laurell, E. & Baier, H. The retinal projectome reveals brain-area-specific visual representations generated by ganglion cell diversity. *Curr. Biol.* **24**, 2085–2096 (2014).
6. Andermann, M. L., Kerlin, A. M., Roumis, D. K., Glickfeld, L. L. & Reid, R. C. Functional specialization of mouse higher visual cortical areas. *Neuron* **72**, 1025–1039 (2011).
7. Marshel, J. H., Garrett, M. E., Nauhaus, I. & Callaway, E. M. Functional specialization of seven mouse visual cortical areas. *Neuron* **72**, 1040–1054 (2011).
8. Garrett, M. E., Nauhaus, I., Marshel, J. H. & Callaway, E. M. Topography and areal organization of mouse visual cortex. *J. Neurosci.* **34**, 12587–12600 (2014).
9. Zhuang, J. et al. An extended retinotopic map of mouse cortex. *eLife* **6**, e18372 (2017).
10. Rhim, I., Coello-Reyes, G., Ko, H. -K. & Nauhaus, I. Maps of cone opsin input to mouse V1 and higher visual areas. *J. Neurophysiol.* **117**, 1674–1682 (2017).
11. Wang, Q., Sporns, O. & Burkhalter, A. Network analysis of corticocortical connections reveals ventral and dorsal processing streams in mouse visual cortex. *J. Neurosci.* **32**, 4386–4399 (2012).
12. Smith, I. T., Townsend, L. B., Huh, R., Zhu, H. & Smith, S. L. Stream-dependent development of higher visual cortical areas. *Nat. Neurosci.* **20**, 200–208 (2017).
13. Glickfeld, L. L., Andermann, M. L., Bonin, V. & Reid, R. C. Cortico-cortical projections in mouse visual cortex are functionally target specific. *Nat. Neurosci.* **16**, 219–226 (2013).
14. Matsui, T. & Ohki, K. Target dependence of orientation and direction selectivity of corticocortical projection neurons in the mouse V1. *Front. Neural Circuits* **7**, 143 (2013).
15. Beltramo, R. & Scanziani, M. A collicular visual cortex: neocortical space for an ancient midbrain visual structure. *Science* **363**, 64–69 (2019).
16. Kim, M. -H., Znamenskiy, P., Iacaruso, M. F. & Mrsic-Flogel, T. D. Segregated subnetworks of intracortical projection neurons in primary visual cortex. *Neuron* **100**, 1313–1321.e6 (2018).
17. Mauss, A. S., Vlasits, A., Borst, A. & Feller, M. Visual circuits for direction selectivity. *Annu. Rev. Neurosci.* **40**, 211–230 (2017).
18. Briggman, K. L., Helmstaedter, M. & Denk, W. Wiring specificity in the direction-selectivity circuit of the retina. *Nature* **471**, 183–188 (2011).
19. Oyster, C. W. & Barlow, H. B. Direction-selective units in rabbit retina: distribution of preferred directions. *Science* **155**, 841–842 (1967).
20. Weng, S., Sun, W. & He, S. Identification of ON-OFF direction-selective ganglion cells in the mouse retina. *J. Physiol.* **562**, 915–923 (2005).
21. Sabbah, S. et al. A retinal code for motion along the gravitational and body axes. *Nature* **546**, 492–497 (2017).
22. Dhande, O. S. & Huberman, A. D. Retinal ganglion cell maps in the brain: implications for visual processing. *Curr. Opin. Neurobiol.* **24**, 133–142 (2014).
23. Cruz-Martín, A. et al. A dedicated circuit links direction-selective retinal ganglion cells to the primary visual cortex. *Nature* **507**, 358–361 (2014).
24. Marshel, J. H., Kaye, A. P., Nauhaus, I. & Callaway, E. M. Anterior-posterior direction opponency in the superficial mouse lateral geniculate nucleus. *Neuron* **76**, 713–720 (2012).
25. Hillier, D. et al. Causal evidence for retina-dependent and -independent visual motion computations in mouse cortex. *Nat. Neurosci.* **20**, 960–968 (2017).
26. Lien, A. D. & Scanziani, M. Cortical direction selectivity emerges at convergence of thalamic synapses. *Nature* **558**, 80–86 (2018).
27. Yonehara, K. et al. Congenital nystagmus gene FRMD7 is necessary for establishing a neuronal circuit asymmetry for direction selectivity. *Neuron* **89**, 177–193 (2016).
28. Macé, É. et al. Whole-Brain functional ultrasound imaging reveals brain modules for visuomotor integration. *Neuron* **100**, 1241–1251.e7 (2018).
29. Yoshida, K. et al. A key role of starburst amacrine cells in originating retinal directional selectivity and optokinetic eye movement. *Neuron* **30**, 771–780 (2001).
30. Durand, S. et al. A comparison of visual response properties in the lateral geniculate nucleus and primary visual cortex of awake and anesthetized mice. *J. Neurosci.* **36**, 12144–12156 (2016).
31. Niell, C. M. & Stryker, M. P. Modulation of visual responses by behavioral state in mouse visual cortex. *Neuron* **65**, 472–479 (2010).
32. Douglas, R. J. & Martin, K. A. C. Neuronal circuits of the neocortex. *Annu. Rev. Neurosci.* **27**, 419–451 (2004).
33. Wertz, A. et al. Single-cell–initiated monosynaptic tracing reveals layer-specific cortical network modules. *Science* **349**, 70–74 (2015).
34. Nassi, J. J. & Callaway, E. M. Parallel processing strategies of the primate visual system. *Nat. Rev. Neurosci.* **10**, 360–372 (2009).
35. Lachica, E. A., Beck, P. D. & Casagrande, V. A. Parallel pathways in macaque monkey striate cortex: anatomically defined columns in layer III. *Proc. Natl Acad. Sci. USA* **89**, 3566–3570 (1992).
36. Burbridge, T. J. et al. Visual circuit development requires patterned activity mediated by retinal acetylcholine receptors. *Neuron* **84**, 1049–1064 (2014).
37. Carandini, M. & Heeger, D. J. Normalization as a canonical neural computation. *Nat. Rev. Neurosci.* **13**, 51–62 (2012).
38. Bennett, C. et al. Higher-order thalamic circuits channel parallel streams of visual information in mice. *Neuron* **102**, 1–16 (2019).
39. Roth, M. M. et al. Thalamic nuclei convey diverse contextual information to layer 1 of visual cortex. *Nat. Neurosci.* **19**, 299–307 (2015).
40. Tohmi, M., Meguro, R., Tsukano, H., Hishida, R. & Shibuki, K. The extrageniculate visual pathway generates distinct response properties in the higher visual areas of mice. *Curr. Biol.* **24**, 587–597 (2014).

ARTICLE

41. Huberman, A. D. et al. Genetic identification of an on-off direction- selective retinal ganglion cell subtype reveals a layer-specific subcortical map of posterior motion. *Neuron* **62**, 327–334 (2009).

42. Hovde, K., Gianatti, M., Witter, M. P. & Whitlock, J. R. Architecture and organization of mouse posterior parietal cortex relative to extrastriate areas. *Eur. J. Neurosci.* **49**, 1313–1329 (2019).

43. Minderer, M., Brown, K. D. & Harvey, C. D. The spatial structure of neural encoding in mouse posterior cortex during navigation. *Neuron* **102**, 232–248. e11 (2019).

44. Harvey, C. D., Coen, P. & Tank, D. W. Choice-specific sequences in parietal cortex during a virtual-navigation decision task. *Nature* **484**, 62–68 (2012).

45. Krumin, M., Lee, J. J., Harris, K. D. & Carandini, M. Decision and navigation in mouse parietal cortex. *eLife* **7**, e42583 (2018).

46. Gămănuţ, R. et al. The mouse cortical connectome, characterized by an ultra-dense cortical graph, maintains specificity by distinct connectivity profiles. *Neuron* **97**, 698–715 (2018).

47. Olcese, U., Iurilli, G. & Medini, P. Cellular and synaptic architecture of multisensory integration in the mouse neocortex. *Neuron* **79**, 579–593 (2013).

48. Itokazu, T. et al. Streamlined sensory motor communication through cortical reciprocal connectivity in a visually guided eye movement task. *Nat. Commun.* **9**, 338 (2018).

49. La Chioma, A., Bonhoeffer, T. & Hübener, M. Area-specific mapping of binocular disparity across mouse visual cortex. *Curr. Biol.* **29**, 2954–2960 (2019).

50. Sereno, M. I. & Huang, R. -S. Multisensory maps in parietal cortex. *Curr. Opin. Neurobiol.* **24**, 39–46 (2014).

51. Colby, C. L., Duhamel, J. R. & Goldberg, M. E. Ventral intraparietal area of the macaque: anatomic location and visual response properties. *J. Neurophysiol.* **69**, 902–914 (1993).

52. Sunkara, A., DeAngelis, G. C. & Angelaki, D. E. Joint representation of translational and rotational components of optic flow in parietal cortex. *Proc. Natl Acad. Sci. USA* **113**, 5077–5082 (2016).

53. Ivanova, E., Hwang, G. -S. & Pan, Z. -H. Characterization of transgenic mouse lines expressing Cre recombinase in the retina. *Neuroscience* **165**, 233–243 (2010).

54. Buch, T. et al. A Cre-inducible diphtheria toxin receptor mediates cell lineage ablation after toxin administration. *Nat. Methods* **2**, 419–426 (2005).

55. Attinger, A., Wang, B. & Keller, G. B. Visuomotor coupling shapes the functional development of mouse visual cortex. *Cell* **169**, 1291–1302 (2017).

56. Wilson, D. E. et al. GABAergic neurons in ferret visual cortex participate in functionally specific networks. *Neuron* **93**, 1058–1065 (2017).

57. Juavinett, A. L., Nauhaus, I., Garrett, M. E., Zhuang, J. & Callaway, E. M. Automated identification of mouse visual areas with intrinsic signal imaging. *Nat. Protoc.* **12**, 32–43 (2016).

58. Brainard, D. H. The psychophysics toolbox. *Spat. Vis.* **10**, 433–436 (1997).

59. Kalatsky, V. A. & Stryker, M. P. New paradigm for optical imaging: temporally encoded maps of intrinsic signal. *Neuron* **38**, 529–545 (2003).

60. Sun, W., Tan, Z., Mensh, B. D. & Ji, N. Thalamus provides layer 4 of primary visual cortex with orientation- and direction-tuned inputs. *Nat. Neurosci.* **19**, 308–315 (2016).

61. Harrington, M. E. The ventral lateral geniculate nucleus and the intergeniculate leaflet: interrelated structures in the visual and circadian systems. *Neurosci. Biobehav. Rev.* **21**, 705–727 (1997).

62. Oh, S. W. et al. A mesoscale connectome of the mouse brain. *Nature* **508**, 207–214 (2014).

63. Tervo, D. G. R. et al. A designer AAV variant permits efficient retrograde access to projection neurons. *Neuron* **92**, 372–382 (2016).

64. Kretschmer, F., Sajgo, S., Kretschmer, V. & Badea, T. C. A system to measure the Optokinetic and Optomotor response in mice. *J. Neurosci. Methods* **256**, 91–105 (2015).

65. Rasmussen, R., Nedergaard, M. & Petersen, N. C. Sulforhodamine 101, a widely used astrocyte marker, can induce cortical seizure-like activity at concentrations commonly used. *Sci. Rep.* **6**, 30433 (2016).

66. Pnevmatikakis, E. A. & Giovannucci, A. NoRMCorre: An online algorithm for piecewise rigid motion correction of calcium imaging data. *J. Neurosci. Methods* **291**, 83–94 (2017).

67. Juavinett, A. L. & Callaway, E. M. Pattern and component motion responses in mouse visual cortical areas. *Curr. Biol.* **25**, 1–6 (2015).

68. Yonehara, K. et al. The first stage of cardinal direction selectivity is localized to the dendrites of retinal ganglion cells. *Neuron* **79**, 1078–1085 (2013).

69. Berens, P. CircStat: MATLAB Toolbox for Circular Statistics. *J. Stat. Softw.* https://doi.org/10.18637/jss.v031.i10 (2009).

Author contributions

R.R., A.M. and K.Y. conceived and designed the experiments and analyses. R.R. performed the intrinsic signal optical imaging experiments; R.R. and A.M. analyzed the data. R.R. performed the in-vivo calcium imaging experiments; R.R. and A.M. analyzed the data. A.M. performed the in-vitro calcium imaging experiments; R.R. and A.M. analyzed the data. M.D.S. performed the optomotor reflex experiments; M.D.S. and R.R. analyzed the data. R.R., M.D.S. and K.Y. performed the immunohistochemistry experiments; R.R., M.D.S. and K.Y. analyzed the data. R.R., A.M. and K.Y. interpreted the data and wrote the paper.

Competing interests

The authors declare no competing interests.

Additional information

Correspondence and requests for materials should be addressed to K.Y.

Peer review information *Nature Communications* thanks the anonymous reviewers for their contribution to the peer review of this work. Peer reviewer reports are available.

Reprints and permission information is available at http://www.nature.com/reprints

Publisher's note Springer Nature remains neutral with regard to jurisdictional claims in published maps and institutional affiliations.

4 Renewed view on the role of retinal direction selectivity in central visual pathways

This chapter presents a review article that I wrote together with Keisuke Yonehara, which we published in *Current Biology* (Rasmussen and Yonehara, 2020). After publishing the work presented in Chapter 3, we felt that an up-to-date resource summarizing how retinal direction selectivity contributes to visual processing in central visual pathways was missing from the existing literature — we therefore attempted to fill this gap.

4.1 Brief introduction

Direction-selective responses were first recorded in the retina of rabbits more than 50 years ago (Barlow and Hill, 1963). We now know a great deal about the mechanisms governing retinal direction selectivity (Chapter 2, Figure 3B), and the downstream projection targets of retinal DS cells, topics which have been excellently reviewed before (Dhande and Huberman, 2014; Mauss et al., 2017; Seabrook et al., 2017; Vaney et al., 2012; Wei, 2018). However, the causal role of retinal DS cells in visual processing in central brain areas of image-forming pathways has remained elusive. Facilitated by new experimental techniques, such as *in vivo* functional imaging and cell type-specific manipulations, an emerging literature has now begun to provide answers to this question, and we therefore considered the time ripe for a focused review.

4.2 Main content

Our intention with this review was that it could serve as a source of both information and inspiration to the field, and importantly, outline testable hypotheses for future investigations. In the review, we first presented fundamental properties of ON and ON-OFF DS cells. Next, we discussed the current literature on how signaling from retinal DS cells is integrated and utilized for feature-selective responses in the dLGN. From here we presented work demonstrating how signaling from retinal DS cells causally influences motion-evoked responses in V1, HVAs, SC, and other brain areas. Finally, we discussed how retinal DS cells may contribute to visually guided behaviors, and provided a clinical perspective on the functions of these cells.

4.3 Reflections and significance

From our review, several hypotheses arise. Here I would like to highlight one notion that we deem especially exciting; that ON-OFF DS cell ensembles contribute to self-motion representations in the posterior parietal cortex (PPC) by analyzing global motion experienced during locomotion, that is, optic flow. This hypothesis is founded on several discoveries. First, by demonstrating that the motion preference axes of ON-OFF DS cells are aligned with the main body axes in mice, a pioneering study proposed that these cells are ideal for encoding translational and rotational optic flows (Sabbah et al., 2017). Second, in our work, we found that area RL relied notably on signaling from retinal DS cells for establishing a posterior-motion preference at higher temporal frequencies (Rasmussen et al., 2020a) (Chapter 3). Consistently, posterior motion is the most prevalent motion direction experienced by animals with laterally positioned eyes, such as mice, during forward locomotion (Hillier et al., 2017). Interestingly, area RL is considered part of the PPC in mice (Gilissen et al., 2020; Hovde et al., 2019; Lyamzin and Benucci, 2019; Minderer et al., 2019) — a brain region containing representations of spatial and locomotor information (Mcnaughton et al., 1994; Save and Poucet, 2009). Finally, in monkeys, many PPC neurons respond to translational and rotational optic flow stimuli (Sunkara et al., 2016). Testing this hypothesis might provide clues about the behavioral roles of ON-OFF DS cells, which remain undetermined.
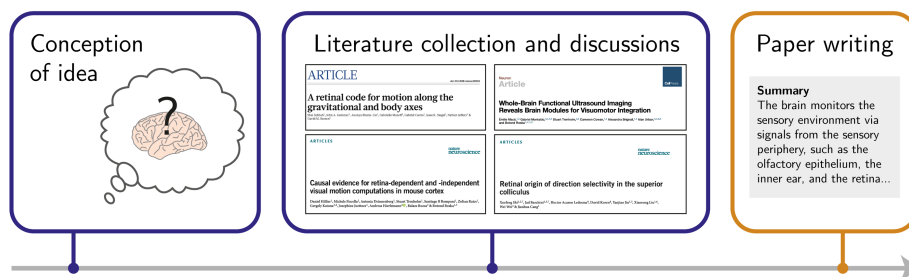
4.4 Author contributions

Figure 8 | Author contributions. *Box colors denote the relative author contribution; blue: shared the work; orange: did the majority of the work; red: did essentially all of the work.*

Current Biology

Minireview

Contributions of Retinal Direction Selectivity to Central Visual Processing

Rune Rasmussen and Keisuke Yonehara*

Danish Research Institute of Translational Neuroscience – DANDRITE, Nordic-EMBL Partnership for Molecular Medicine, Department of Biomedicine, Aarhus University, Ole Worms Allé 8, 8000 Aarhus C, Denmark

*Correspondence: keisuke.yonehara@dandrite.au.dk

https://doi.org/10.1016/j.cub.2020.06.002

The brain monitors the sensory environment via signals from the sensory periphery, such as the olfactory epithelium, the inner ear, and the retina. Understanding how sensory stimuli are processed throughout the sensory hierarchy, and how this relates to behavior, is a central outstanding question in the field of neuroscience. The processing of visual motion in mice offers unique opportunities for addressing these questions thanks to a rich literature on the anatomical and physiological properties of motion-sensitive neurons across the visual system, paired with recent developments of cutting-edge genetic and imaging approaches. A visual scene typically contains motion originating from either moving objects or optic flow caused by self-generated movements. Neurons encoding the direction of visual motion are said to be 'direction-selective'. It was historically believed the circuits responsible for creating direction selectivity *de novo* exist within the visual cortex. Yet, in mice, direction-selective responses can be found already in the retina, suggesting in this model organism visual motion analysis starts at the earliest stage of the visual hierarchy. This minireview presents emerging literature demonstrating how retinal direction-selective cells make causal contributions to central visual motion processing and visually guided behaviors in mice, and their potential clinical relevance, and outlines experiments for testing remaining questions. Research in this field will undoubtedly continue to advance our understanding of the basic principles of the visual system and how sensory neurons extract fundamental features of the world.

Introduction

Motion is one of the most common visual features we experience in everyday life. Visual motion is induced by moving objects or movement of the observer through space; as we walk down the street, the visual scene flows backward. Visual motion signals inform animals about which direction prey or a predator may be moving, allowing it to decide whether it should freeze, flee, or attack. Given the ethological importance of motion vision, it is not surprising that motion-sensitive neurons exist in many different brain regions and across the animal kingdom, from insects to humans.

Cells preferentially responding to the visual motion of a specific direction are deemed direction-selective (DS). In mammals, DS cells were first recorded in the primary visual cortex (V1) of cats [1] and later were found within the visual cortex of many mammalian species. In non-human primates, cortical DS cells have been causally linked to the ability to determine visual motion direction [2], suggesting that DS cells may be a core functional unit for creating motion perceptions. Typically, direction selectivity is thought to emerge *de novo* within the visual cortex from the convergence of geniculate thalamic inputs [3,4], and such a mechanism has been identified in mice [5]. More than 50 years ago, however, DS responses were discovered in the retina of rabbits [6], and later in several other species, including mice [7], suggesting that direction selectivity could arise earlier in the visual hierarchy. From *ex vivo* experiments, we have learned a great deal about the properties of retinal DS cells, and the synaptic mechanisms giving rise to directionally tuned responses [8–10]. The retina contains several types of DS cells that fall into two main categories: On and On-Off DS cells [11] (Figure 1A). The On cells respond to light increments, while On-Off cells respond to both increments and decrements. Between these, the role of On DS cells is best understood; these cells selectively send projections to nuclei of the accessory optic system and are dedicated to generating the optokinetic reflex, a type of eye movement used for gaze stabilization [10,12,13]. On-Off DS cells send their axons to the dorsal lateral geniculate nucleus (dLGN) and the superior colliculus (SC) [14–16]. It should be noted that Off DS cells have been described [17,18], but Off DS responses have not been consistently detected in other studies [19]. Fueled by the development of cutting-edge approaches, a growing literature is now uncovering how retinal DS cells make unexpected and important contributions to visual motion computations in central brain areas of mice.

Excellent review articles have discussed the mechanisms and properties of retinal direction selectivity [8,9,20], but an up-to-date source, describing the contributions of retinal direction selectivity to motion processing in downstream brain areas has been lacking. In the current minireview, we present how retinal DS signaling is processed in several central visual brain areas, and discuss the role of retinal DS cells in visually guided behaviors as well as their clinical relevance.

Fundamental Properties of Retinal DS Cells

In this minireview, we mainly focus our attention on the role of On-Off DS cells. Unlike On DS cells, On-Off DS cells prominently project to image-forming visual areas such as the dLGN and SC, and
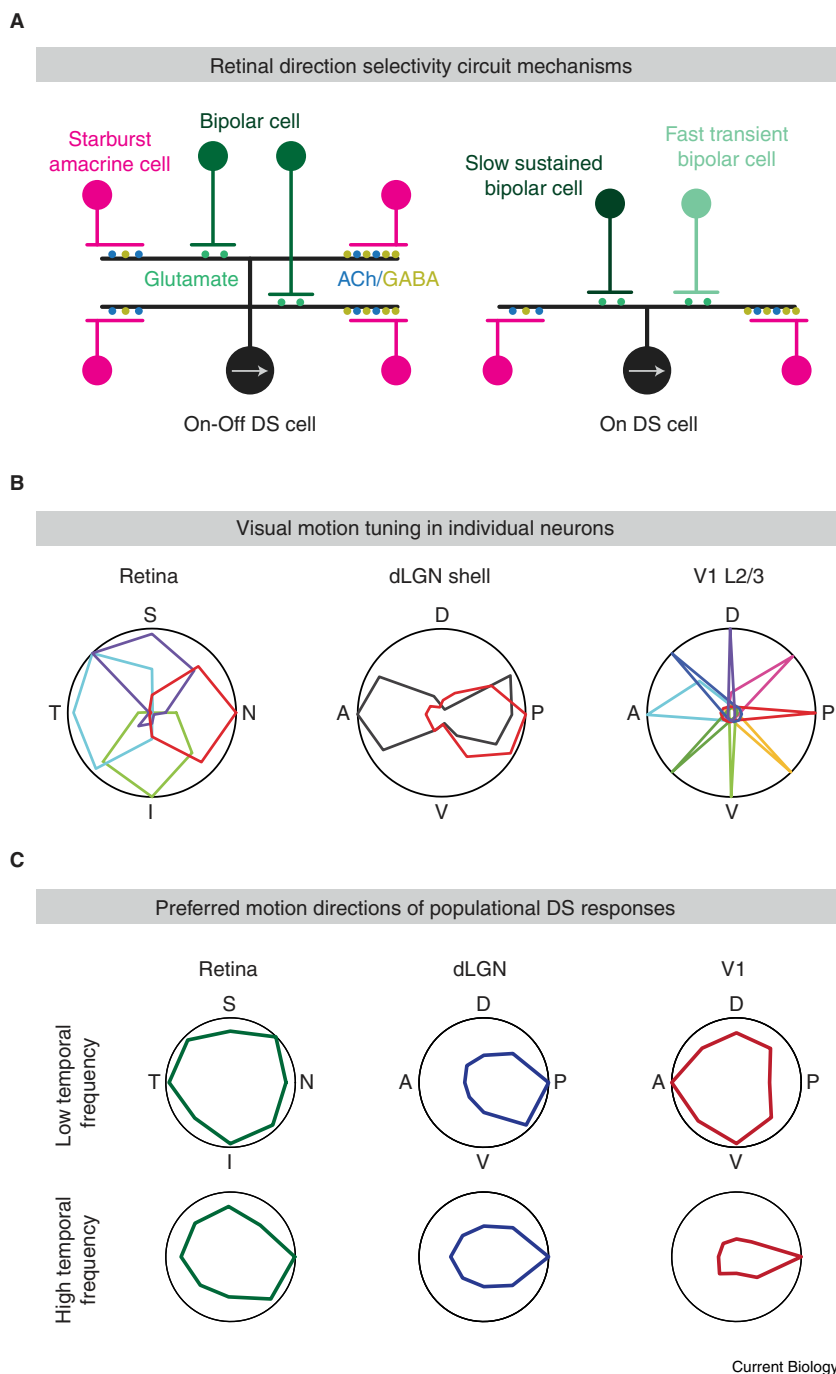
A

B

C

Current Biology

Figure 1. Retinal direction selectivity and motion direction preferences across the visual hierarchy.
(A) Circuitry underlying direction selectivity in On-Off and On DS cells in the retina. On-Off DS cells receive glutamatergic inputs from On and Off bipolar cells, and cholinergic and GABAergic inputs from On and Off starburst amacrine cells. GABAergic input in the null direction is stronger than that in the preferred direction (indicated by the arrow), yielding larger spiking activity in the preferred direction in both On-Off and On DS cells [21–23]. On DS cells have an additional circuit mechanism, consisting of glutamatergic excitation mediated by different bipolar cell types with distinct temporal dynamics: roughly speaking, slow sustained and fast transient groups [10]. Slow sustained and fast transient types are biased to the preferred and null side, respectively. In the preferred direction, the synaptic delays between the two types are offset by the preceding activation of the slow sustained type, yielding temporal summation of the excitatory inputs. In the null direction, such temporal summation is less efficient. (B) Examples of motion tuning in individual retinal, dLGN, and V1 neurons. In the retina, On-Off DS cells include four subtypes, each of which prefers motion in one cardinal direction (anterior [A], posterior [P], superior [S], and inferior [I]). In the shell region of the dLGN, a high proportion of neurons are DS or axis-selective, with a preference for horizontal motion (dorsal [D], and ventral [V]). In layer 2/3 (L2/3) of V1, DS cells are tuned to a rich repertoire of motion directions. Data are modified from [12,29,36]. (C) Preferred motion direction distributions for retinal On-Off, dLGN, and V1 DS cell populations as a function of temporal frequency of the visual stimulus. At high temporal frequencies, DS cells across the retina, dLGN, and V1 are preferentially tuned to posterior-moving motion. Data are modified from [31].

in the opposite direction (null direction), inhibition is maximal [8,9,20]. This directionally tuned inhibition is necessary for establishing DS responses in On-Off and On DS cells [8,9,20]. Spatially asymmetric inhibitory connectivity [21–23] and centrifugal direction selectivity within the processes of starburst amacrine cells [9,20] are the key mechanisms underlying the tuned inhibition.

Retinal DS Cells Contribute to Motion Signaling in the dLGN

The mouse dLGN can be subdivided into a shell and a core region [24]. Genetic labeling of retinal cell subtypes has demonstrated that horizontally tuned On-Off DS cells exclusively innervate the shell [14–16,25], whereas vertically tuned On-Off and non-DS cells predominantly innervate the core, or both regions indiscriminately [16,26,27] (Figure 2). Interestingly, recordings from the dLGN have shown that the shell is enriched in DS and axis-selective cells [28,29] (Figure 1B). Several lines of evidence, described below, support an idea that dLGN DS responses, at least in part, could emerge from similarly tuned retinal DS

are the most numerous retinal DS cells in mice, comprising 15% of retinal ganglion cells [16]. On-Off DS cells include four subtypes, each preferring motion in one cardinal direction: anterior, posterior, superior, or inferior [9,19] (Figure 1B). In the retina, On-Off DS cells receive glutamatergic excitation from bipolar cells, as well as GABAergic inhibition and cholinergic excitation from starburst amacrine cells [8,9,20] (Figure 1A). Importantly, the inhibition from starburst amacrine cells is directionally tuned: during motion in the preferred direction, inhibition is minimal, while during motion
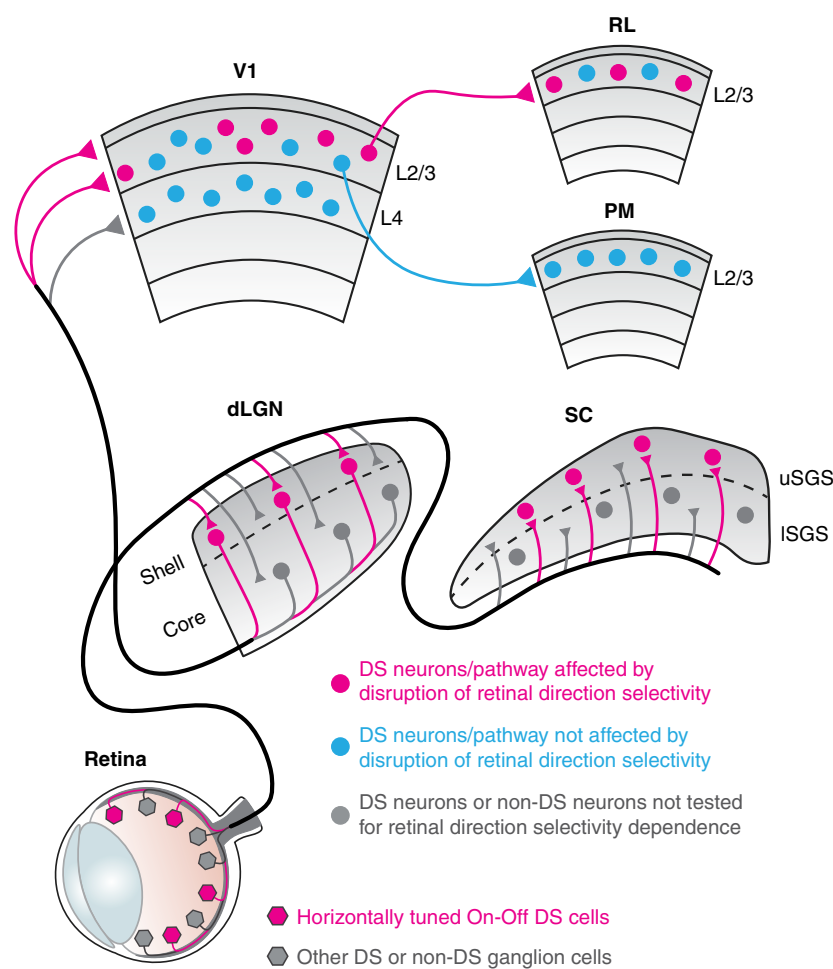
Current Biology
Minireview

Figure 2. Circuit linking horizontally tuned On-Off DS cells to central visual areas.
Schematic diagram of the neuronal circuit linking horizontal motion tuned On-Off DS cells to DS cells in the central visual areas. Horizontally tuned On-Off DS cells (magenta hexagons) innervate the dLGN shell and the most superficial layers of the SC (upper stratum griseum superficialis [uSGS]) [14–16,25], where the activity of postsynaptic DS cells (magenta circles) are affected by the disruption of retinal direction selectivity [31,40]. Other DS or non-DS retinal ganglion cells (gray hexagons) send projections to the dLGN core and shell, as well as to uSGS and lower SGS (lSGS) [16,26,27]. dLGN shell DS cells that receive input from On-Off DS cells target the superficial layers of V1 [25], where On-Off DS cell-originating signaling supports the activity of a subset of DS cells in layer 2/3 (L2/3), preferring high temporal frequencies and posterior motion [31,36] (magenta circles). It is yet unknown if the dLGN DS cells that target layer 4 (L4) of V1 [34] are dependent on intact retinal DS cell signaling (gray circles and pathway). In contrast, DS cells in L4 and a subset of DS cells in L2/3 are not affected by the disruption of retinal direction selectivity [31] (blue circles). Within L2/3 of V1, a segregated circuitry ensures that signaling originating from On-Off DS cells is preferentially streamed into area RL, but not to area PM [31].

attempts to dissect the specific contributions of retinal DS cell-dependent and -independent mechanisms for establishing direction selectivity in the dLGN.

Retinal DS Cells Contribute to a Distinct Form of Direction Selectivity in the Visual Cortex

Work using transsynaptic rabies tracing identified a disynaptic connection between retinal DS cells and layer 1 of V1 that connects via the dLGN shell [25]. Additionally, the authors found a disynaptic connection between non-DS retinal ganglion cells and layer 4 of V1 via the dLGN core; demonstrating two distinct parallel pathways for conveying information from the retina to V1. Intriguingly, a notable fraction of neurons that project from the dLGN into superficial layers of V1 were DS, suggesting a circuit motif for how signaling from On-Off DS cells reach V1 (Figure 2) [25,31,34,35]. A central question is thus whether On-Off DS cells causally contribute to motion computations in the visual cortex. Cortical direction selectivity has been thought to be generated by thalamocortical or cortical mechanisms [3,4]. Indeed, recent work showed that direction selectivity in layer 4 of V1 is created from the combination of untuned thalamic inputs with distinct spatiotemporal response properties [5]. However, two studies have demonstrated retina-dependent and -independent forms of cortical direction selectivity [31,36].

The first study was performed in layer 2/3 of mouse V1 [36]. Using two genetic approaches for disrupting retinal direction selectivity, the authors found a form of cortical direction selectivity that relied on retinal direction selectivity and was characterized by preferences for higher temporal frequencies, and for

inputs, while axis-selective responses could arise from oppositely tuned retinal DS inputs [30].

One seminal study in mice demonstrated a fine-scale and functional logic to the convergence of retinal ganglion cell inputs to the dLGN shell [30]. The authors found a spatial clustering of retinal DS cell boutons preferring similar or near-opposite motion directions; an arrangement that could contribute to creating direction- or axis tuning in target dLGN neurons. Additionally, recent work employing a genetic mouse model demonstrated that when horizontal direction selectivity is lost in the retina, DS thalamic boutons in superficial V1 lose their normal preference to posterior motion (Figure 1C) and instead become preferentially tuned to vertical motion [31]. However, notably, the horizontal direction selectivity in the dLGN was not completely abolished by the disruption of retinal horizontal direction selectivity [31], likely suggesting the existence of a form of dLGN direction selectivity that is independent of retinal motion computations. Such a retinal motion computation-independent form of direction selectivity could potentially be computed *de novo* in the dLGN, or mediated by inputs from other visual areas, such as layer 6 of V1 [32] or superficial layers of the SC [33], and might ultimately be delivered to layer 4 of V1 [34]. In the future, it will be exciting to see experimental

motion in the posterior direction — the dominant optic flow direction when animals locomote forward. V1 is only the first stage of cortical visual processing, and the mouse visual cortex includes up to 16 higher visual areas, each specialized for a set of visual features [37]. Yet, it was unknown whether On-Off DS cells contribute to motion processing in higher visual areas. This was recently addressed in yet another study, similar to the aforementioned [36], employing two genetic approaches for disrupting retinal direction selectivity [31]. This showed that the population of DS cells in the rostrolateral (RL) visual area, in which the anterior area was possibly included, which prefers higher temporal frequencies, and changes direction tuning toward posterior directions as the temporal frequency of a stimulus increases, is selectively reduced in mice with impaired retinal direction selectivity [31]. The temporal frequency-dependent posterior motion bias in cortical DS cells may, at least partially, be explained by the temporal frequency-dependent posterior bias of On-Off DS cells [31] (Figure 1C). Interestingly, RL-projecting layer 2/3 DS cells in V1 were likewise affected by this retinal direction selectivity impairment. In contrast, posteromedial (PM) area DS cells, PM-projecting layer 2/3 V1 DS cells, and L4 V1 DS cells were not significantly affected by the retinal disruption [31]. These studies show that On-Off DS cells make area- and layer-specific contributions to visual motion computations in the mouse visual cortex. This is achieved by a segregated circuitry that routes signaling from On-Off DS cells preferentially into area RL (Figure 2). Such a pathway would be important for establishing specialized response properties of neurons in higher visual areas. The behavioral role of retina-dependent motion computations in the visual cortex has yet to be determined, as well as if retinal DS cells make contributions to any of the other 14 higher visual areas. Finally, our knowledge regarding retina-dependent and -independent forms of cortical direction selectivity is still in its infancy, and further research is needed to understand the differences between these two, both in terms of connectivity and functionality. From the current literature, one hypothesis may be that cortical direction selectivity in response to slow-moving motion is computed *de novo* within the cortex, likely in layer 4, whereas in response to fast-moving motion, a fraction of cortical direction selectivity in layer 2/3 is computed based on signaling from retinal DS cells. These two mechanisms seem to overlap in a subpopulation of cortical layer 2/3 neurons [31], but exciting questions about the underlying synaptic basis for such computations, as well as the specific presynaptic network motifs, remain.

SC Neurons Inherit Direction Selectivity from Retinal DS Cells

The SC is a midbrain structure involved in transforming multimodal sensory stimuli into ethologically relevant behaviors such as escape, defense, and orienting movements [38]. In mice, approximately 85% of retinal ganglion cells project to the SC [39], making it a prominent retinorecipient structure in this species. On-Off DS cells selectively target the superficial half of the retinorecipient SC, whereas the deeper portion of SC is mainly innervated by non-DS retinal ganglion cells [14–16,27] (Figure 2). Neurons in the superficial SC display diverse response properties, and direction selectivity has been observed in all mammalian species studied [40–42]. Interestingly, SC DS cells

are concentrated in the most superficial lamina [43] and DS cells sharing similar direction preferences are spatially proximal [42,43]. With this notable anatomical and functional correspondence between On-Off DS cell innervation and concentration of SC DS cells in superficial SC, a pressing question is whether On-Off DS cells make causal contributions to SC motion processing.

It has been estimated that each SC neuron receives input from, on average, six retinal ganglion cells [44], but only recently was it determined what types of ganglion cells provide such inputs [41]. By combining transsynaptic rabies tracing and functional recordings, this work demonstrated that specific types of retinal ganglion cells, including On-Off DS cells, preferentially target a population of superficial SC neurons which project to the parabigeminal nucleus, compared to a separate pulvinar-projecting population. This preferential On-Off DS cell innervation was accompanied by a high percentage of DS cells in the parabigeminal nucleus, in contrast to the sparseness of DS cells in the pulvinar. The parabigeminal nucleus is thought to contribute to visually guided avoidance behaviors by detecting quickly approaching aversive threats, and On-Off DS cells may play an important role in this function. In the future, this could be elucidated experimentally by combining manipulation of On-Off DS cells with ethologically relevant behavioral assays, such as looming visual stimulus-triggered freezing or escaping [38]. This could even be combined with simultaneous activity recordings of the SC neurons that send projections to the parabigeminal nucleus employing head-mounted miniature microscopes to relate neuronal activity to behavior.

Importantly, one study provided strong evidence for a causal role of On-Off DS cells for SC direction selectivity [40] (Figure 2). By combining *in vivo* electrophysiology, optical imaging with optogenetics, and a genetic model for disrupting retinal direction selectivity, the authors made several significant findings. First, isolating the retinal inputs arriving in superficial SC DS cells showed that these cells receive directionally tuned excitation from the retina, and this excitation predicts the preferred direction of the SC neuron. Second, significantly reducing the selectivity of On-Off DS cells caused a drastic reduction in the number of DS cells in superficial SC. This suggests that direction selectivity in superficial SC is inherited from On-Off DS cell inputs. The behavioral relevance of this retina-originating SC direction selectivity has yet to be identified, but given the central role of SC for innate behaviors, such as escaping and freezing, we propose that such behaviors could serve as a starting point for beginning to dissect the role of retinal DS signaling for SC-mediated behaviors in freely moving animals.

Role of Retinal DS Cells in Visually Guided Behaviors

Although the behavioral functions of On-Off DS cells have yet to be fully resolved, studies have begun to address this topic. In one study mice were trained to report the perceived motion direction of random dot kinematograms; a task that required V1 activity and that elicited DS responses from layer 2/3 neurons in V1 [45]. Interestingly, the same stimulus evoked DS responses in On-Off DS cells, suggesting that these cells may be involved in establishing motion perceptions. We propose that future experiments, wherein mice are trained to perform such visually guided behaviors, presumably requiring conscious motion perceptions,
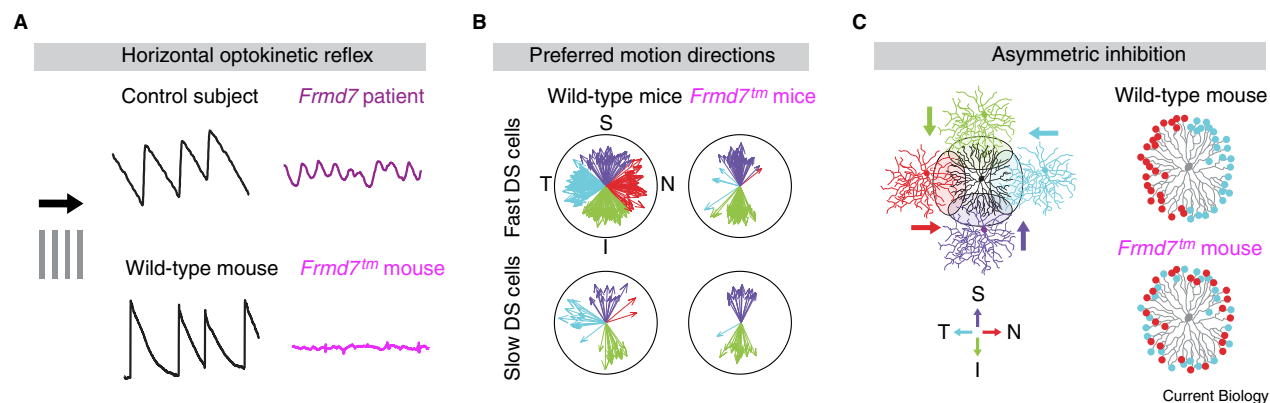
Current Biology
Minireview

Figure 3. Clinical and physiological consequences of retinal horizontal direction selectivity disruption.
(A) Top: example traces show optokinetic reflex eye movements in a control human subject and a subject with a mutation in the *Frmd7* gene, a gene enriched in starburst amacrine cells, in response to motion in the nasal direction on the retina. Bottom: example traces showing optokinetic reflex eye movements produced in a wild-type mouse and an Frmd7 mutant (*Frmd7^{tm}*) mouse in response to motion in the nasal direction on the retina. Notice the lack of horizontal optokinetic reflex in both the human subject and mouse with a mutated *Frmd7* gene. Notably, horizontal eye oscillation observed in a human patient is not observed in an *Frmd7^{tm}* mouse. (B) Polar plots showing the preferred motion directions (indicated by arrow direction) of individual retinal DS cells, tuned to fast (top) or slow (bottom) motion speeds, from wild-type mice and *Frmd7^{tm}* mice. Notice the complete lack of retinal DS cells tuned to horizontal motion in *Frmd7^{tm}* mice. (C) Left: schematic showing the spatial organization of the synaptic connectivity between a starburst amacrine cell (center, black) and four types of retinal DS cells, color-coded according to their preferred motion direction in the cardinal directions (anterior [A], posterior [P], superior [S], and inferior [I]). Right: schematic showing the horizontal asymmetric inhibitory outputs of a starburst amacrine cell from a wild-type and an *Frmd7^{tm}* mouse. Output inhibitory synapses are color-coded according to the preferred directions of the postsynaptic DS cell partner. Notice the complete lack of asymmetric inhibitory connectivity, the dominating circuit mechanisms for creating direction selectivity in the retina, in *Frmd7^{tm}* mice. All data in the figure are modified from [12].

are combined with specific manipulation of retinal DS cells [12,31,36,40] to test this hypothesis causally. Another study tested the effect of disrupting retinal horizontal direction selectivity on whole-brain activity during visual stimulation that evoked the optokinetic reflex [46]. In mice with impaired retinal horizontal direction selectivity, responses to horizontal motion, but not to vertical, were notably decreased in several visual areas including the dLGN, SC, and visual cortex, compared to wild-type mice. These areas receive signaling from On-Off DS cells, but not from On DS cells, suggesting that On-Off DS cells affect wide-spread neural activity in central visual areas during visuomotor behaviors. The causal role of On-Off DS cells specifically in this visuomotor behavior remains open to investigation.

Lastly, several lines of evidence point to an intriguing hypothesis: On-Off DS cells contribute to the representation of self-movement in the posterior parietal cortex (PPC) by analyzing optic flow patterns during locomotion. First, a pioneering study found that the motion preference axes of On-Off DS cells are aligned with gravitational and body axes, making these cells ideal for encoding translational optic flow [19]. Second, area RL was identified as a higher visual area that relied on signaling from On-Off DS cells for establishing its preference to posterior motion moving at higher temporal frequencies [31]. In mice, area RL is considered part of the PPC [47]. Third, areas of the PPC in monkeys respond robustly to optic flow [48]. Taken together these findings suggest that the representation of self-movement in PPC may at least partially depend on signaling from On-Off DS cells, although, and somewhat critically, at this time retinal DS cells have not been identified in primates. However, non-visual cues such as locomotion and vestibular inputs [49,50] likely also contribute to neural activity representing self-movement in the PPC. To resolve this, we propose performing PPC imaging using miniature microscopes while mice are freely

locomoting, to relate self-movement to neuronal activity. This could be combined with the manipulation of On-Off DS cells [12,31,36,40], permitting causality to be tested. As a complement, two-photon PPC imaging of head-fixed mice navigating a virtual environment on a treadmill could be employed [47]. This paradigm allows precise control of the visual stimuli and locomotion; these can even be decoupled to test the contribution of each modality, and two-photon imaging provides better cellular resolution.

Clinical Relevance of Retinal DS Cells
The potential clinical implications of retinal DS cells in vision-related diseases were provided by a recent study [12]. A neurological disease in which impairment of retinal direction selectivity is suggested is idiopathic congenital nystagmus. In 70% of detected cases of this disease, mutations in the *Frmd7* gene have been reported, and subjects with a mutated *Frmd7* gene show two major symptoms: oscillating eye movements along the horizontal plane, and the lack of the horizontal optokinetic reflex (Figure 3A). Importantly, the latter phenotype of patients can be recreated in *Frmd7* mutant mice (Figure 3A) [12,46]. *Ex vivo* recordings in retinas from *Frmd7* mutant mice showed that these mice are characterized by a complete lack of horizontal direction selectivity in On-Off and On DS cells (Figure 3B) [12]. This effect is caused by a transition from asymmetric to symmetric inhibitory connections from starburst amacrine cells (Figure 3C). Importantly, the expression of *Frmd7* was enriched in starburst amacrine cells in the retina of both mice and non-human primates [12]. The missing horizontal optokinetic reflex in mice is likely, at least in part, caused by the incapability of On DS cells to sense the direction of horizontal motion. The strikingly similar phenotype between human patients and gene-mutated mice seems to support the intriguing hypothesis that the retinal circuit

mechanism responsible for computing motion direction for mediating the optokinetic reflex is conserved between mice and humans. In the future, it will be important to establish whether retinas from humans or non-human primates contain On DS cells and if direction selectivity in these is disturbed in idiopathic congenital nystagmus. Furthermore, future experimental efforts should be allocated to searching for other potentially affected visual functions in idiopathic congenital nystagmus, encouraged by the observations that *Frmd7* mutant mice show impaired motion responses in a variety of visual areas including V1, PPC, SC, and thalamic nuclei [31,36,46]. Such efforts may be clinically relevant, however, only if On-Off DS cells exist in the retinas of humans, which remains to be determined.

Conclusion

This minireview has presented a range of examples of how retinal DS cells are involved in visual processing in central visual areas. Collectively, they demonstrate that retinal DS cells make unexpected and causal contributions to thalamic, cortical, and collicular motion computations in mice. Furthermore, emerging literature is illuminating how retinal direction selectivity may support visually guided behaviors, thus beginning to bridge the knowledge gap between cell types and behavior. This surge in studies on how retinal direction selectivity impacts central visual processing has been made possible due to the development of genetic models for manipulating retinal cell types. Now that the tools are available, we expect to continue to see the role of retinal DS cells in visual processing and behavior being tested and uncovered within the next decade. So far, most of our knowledge for the contributions of retinal direction selectivity to central visual processing concerns On-Off and On DS cells; in the future, it will be exciting to attempt investigations of the role of other retinal DS cell types, such as Jam-B retinal ganglion cells [18]. Finally, it will be important to determine whether DS cells exist in the retina of primates and, if so, if these are involved in higher-order visual motion analysis, or if primates developed alternative mechanisms for performing these computations.

REFERENCES

1. Hubel, D.H. (1959). Single unit activity in striate cortex of unrestrained cats. J. Physiol. *147*, 226–238.

2. Salzman, C.D., Britten, K.H., and Newsome, W.T. (1990). Cortical microstimulation influences perceptual judgements of motion direction. Nature *346*, 174–177.

3. Hubel, D.H., and Wiesel, T.N. (1962). Receptive fields, binocular interaction and functional architecture in the cat's visual cortex. J. Physiol. *160*, 106–154.

4. Stanley, G.B., Jin, J., Wang, Y., Desbordes, G., Wang, Q., Black, M.J., and Alonso, J.-M. (2012). Visual orientation and directional selectivity through thalamic synchrony. J. Neurosci. *32*, 9073–9088.

5. Lien, A.D., and Scanziani, M. (2018). Cortical direction selectivity emerges at convergence of thalamic synapses. Nature *558*, 80–86.

6. Barlow, H.B., and Hill, R.M. (1963). Selective sensitivity to direction of movement in ganglion cells of the rabbit retina. Science *139*, 412–412.

7. Weng, S., Sun, W., and He, S. (2005). Identification of ON-OFF direction-selective ganglion cells in the mouse retina. J. Physiol. *562*, 915–923.

8. Wei, W. (2018). Neural mechanisms of motion processing in the mammalian retina. Annu. Rev. Vis. Sci. *4*, 165–192.

9. Vaney, D.I., Sivyer, B., and Taylor, W.R. (2012). Direction selectivity in the retina: symmetry and asymmetry in structure and function. Nat. Rev. Neurosci. *13*, 194–208.

10. Matsumoto, A., Briggman, K.L., and Yonehara, K. (2019). Spatiotemporally asymmetric excitation supports mammalian retinal motion sensitivity. Curr. Biol. *29*, 3277–3288.

11. Sanes, J.R., and Masland, R.H. (2015). The types of retinal ganglion cells: current status and implications for neuronal classification. Annu. Rev. Neurosci. *38*, 221–246.

12. Yonehara, K., Fiscella, M., Drinnenberg, A., Esposti, F., Trenholm, S., Krol, J., Franke, F., Scherf, B.G., Kusnyerik, A., Müller, J., *et al*. (2016). Congenital nystagmus gene FRMD7 is necessary for establishing a neuronal circuit asymmetry for direction selectivity. Neuron *89*, 177–193.

13. Yonehara, K., Ishikane, H., Sakuta, H., Shintani, T., Nakamura-Yonehara, K., Kamiji, N.L., Usui, S., and Noda, M. (2009). Identification of retinal ganglion cells and their projections involved in central transmission of information about upward and downward image motion. PLoS One *4*, e4320.

14. Huberman, A.D., Wei, W., Elstrott, J., Stafford, B.K., Feller, M.B., and Barres, B.A. (2009). Genetic identification of an On-Off direction- selective retinal ganglion cell subtype reveals a layer-specific subcortical map of posterior motion. Neuron *62*, 327–334.

15. Rivlin-Etzion, M., Zhou, K., Wei, W., Elstrott, J., Nguyen, P.L., Barres, B.A., Huberman, A.D., and Feller, M.B. (2011). Transgenic mice reveal unexpected diversity of On-Off direction-selective retinal ganglion cell subtypes and brain structures involved in motion processing. J. Neurosci. *31*, 8760–8769.

16. Kay, J.N., De la Huerta, I., Kim, I.-J., Zhang, Y., Yamagata, M., Chu, M.W., Meister, M., and Sanes, J.R. (2011). Retinal ganglion cells with distinct directional preferences differ in molecular identity, structure, and central projections. J. Neurosci. *31*, 7753–7762.

17. Baden, T., Berens, P., Franke, K., Román Rosón, M., Bethge, M., and Euler, T. (2016). The functional diversity of retinal ganglion cells in the mouse. Nature *529*, 345–350.

18. Kim, I.-J., Zhang, Y., Yamagata, M., Meister, M., and Sanes, J.R. (2008). Molecular identification of a retinal cell type that responds to upward motion. Nature *452*, 478–482.

19. Sabbah, S., Gemmer, J.A., Bhatia-Lin, A., Manoff, G., Castro, G., Siegel, J.K., Jeffery, N., and Berson, D.M. (2017). A retinal code for motion along the gravitational and body axes. Nature *546*, 492–497.

20. Borst, A., and Euler, T. (2011). Seeing things in motion: models, circuits, and mechanisms. Neuron *71*, 974–994.

21. Briggman, K.L., Helmstaedter, M., and Denk, W. (2011). Wiring specificity in the direction-selectivity circuit of the retina. Nature *471*, 183–190.

22. Wei, W., Hamby, A.M., Zhou, K., and Feller, M.B. (2011). Development of asymmetric inhibition underlying direction selectivity in the retina. Nature *469*, 402–406.

23. Yonehara, K., Balint, K., Noda, M., Nagel, G., Bamberg, E., and Roska, B. (2011). Spatially asymmetric reorganization of inhibition establishes a motion-sensitive circuit. Nature *469*, 407–410.

24. Kerschensteiner, D., and Guido, W. (2017). Organization of the dorsal lateral geniculate nucleus in the mouse. Vis. Neurosci. *34*, E008.

25. Cruz-Martín, A., El-Danaf, R.N., Osakada, F., Sriram, B., Dhande, O.S., Nguyen, P.L., Callaway, E.M., Ghosh, A., and Huberman, A.D. (2014). A dedicated circuit links direction-selective retinal ganglion cells to the primary visual cortex. Nature *507*, 358–361.

Current Biology
Minireview

26. Huberman, A.D., Manu, M., Koch, S.M., Susman, M.W., Lutz, A.B., Ullian, E.M., Baccus, S.A., and Barres, B.A. (2008). Architecture and activity-mediated refinement of axonal projections from a mosaic of genetically identified retinal ganglion cells. Neuron 59, 425–438.

27. Kim, I.-J., Zhang, Y., Meister, M., and Sanes, J.R. (2010). Laminar restriction of retinal ganglion cell dendrites and axons: subtype-specific developmental patterns revealed with transgenic markers. J. Neurosci. 30, 1452–1462.

28. Piscopo, D.M., El-Danaf, R.N., Huberman, A.D., and Niell, C.M. (2013). Diverse visual features encoded in mouse lateral geniculate nucleus. J. Neurosci. 33, 4642–4656.

29. Marshel, J.H., Kaye, A.P., Nauhaus, I., and Callaway, E.M. (2012). Anterior-posterior direction opponency in the superficial mouse lateral geniculate nucleus. Neuron 76, 713–720.

30. Liang, L., Fratzl, A., Goldey, G., Ramesh, R.N., Sugden, A.U., Morgan, J.L., Chen, C., and Andermann, M.L. (2018). A fine-scale functional logic to convergence from retina to thalamus. Cell 173, 1343–1355.

31. Rasmussen, R., Matsumoto, A., Dahlstrup Sietam, M., and Yonehara, K. (2020). A segregated cortical stream for retinal direction selectivity. Nat. Commun. 11, 831.

32. Olsen, S.R., Bortone, D.S., Adesnik, H., and Scanziani, M. (2012). Gain control by layer six in cortical circuits of vision. Nature 483, 47–52.

33. Gale, S.D., and Murphy, G.J. (2018). Distinct cell types in the superficial superior colliculus project to the dorsal lateral geniculate and lateral posterior thalamic nuclei. J. Neurophysiol. 120, 1286–1292.

34. Sun, W., Tan, Z., Mensh, B.D., and Ji, N. (2016). Thalamus provides layer 4 of primary visual cortex with orientation- and direction-tuned inputs. Nat. Neurosci. 19, 308–315.

35. Kondo, S., and Ohki, K. (2015). Laminar differences in the orientation selectivity of geniculate afferents in mouse primary visual cortex. Nat. Neurosci. 19, 316–319.

36. Hillier, D., Fiscella, M., Drinnenberg, A., Trenholm, S., Rompani, S.B., Raics, Z., Katona, G., Juettner, J., Hierlemann, A., Rozsa, B., et al. (2017). Causal evidence for retina-dependent and -independent visual motion computations in mouse cortex. Nat. Neurosci. 20, 960–968.

37. Glickfeld, L.L., and Olsen, S.R. (2017). Higher-order areas of the mouse visual cortex. Annu. Rev. Vis. Sci. 3, 251–273.

38. Oliveira, A.F., and Yonehara, K. (2018). The mouse superior colliculus as a model system for investigating cell type-based mechanisms of visual motor transformation. Front. Neural Circuits 12, 59.

39. Ellis, E.M., Gauvain, G., Sivyer, B., and Murphy, G.J. (2016). Shared and distinct retinal input to the mouse superior colliculus and dorsal lateral geniculate nucleus. J. Neurophysiol. 116, 602–610.

40. Shi, X., Barchini, J., Ledesma, H.A., Koren, D., Jin, Y., Liu, X., Wei, W., and Cang, J. (2017). Retinal origin of direction selectivity in the superior colliculus. Nat. Neurosci. 20, 550–558.

41. Reinhard, K., Li, C., Do, Q., Burke, E.G., Heynderickx, S., and Farrow, K. (2019). A projection specific logic to sampling visual inputs in mouse superior colliculus. eLife 8, e50697.

42. de Malmazet, D., Kühn, N.K., and Farrow, K. (2018). Retinotopic separation of nasal and temporal motion selectivity in the mouse superior colliculus. Curr. Biol. 28, 2961–2969.e4.

43. Inayat, S., Barchini, J., Chen, H., Feng, L., Liu, X., and Cang, J. (2015). Neurons in the most superficial lamina of the mouse superior colliculus are highly selective for stimulus direction. J. Neurosci. 35, 7992–8003.

44. Chandrasekaran, A.R., Shah, R.D., and Crair, M.C. (2007). Developmental homeostasis of mouse retinocollicular synapses. J. Neurosci. 27, 1746–1755.

45. Marques, T., Summers, M.T., Fioreze, G., Fridman, M., Dias, R.F., Feller, M.B., and Petreanu, L. (2018). A role for mouse primary visual cortex in motion perception. Curr. Biol. 28, 1703–1713.

46. Macé, É., Montaldo, G., Trenholm, S., Cowan, C., Brignall, A., Urban, A., and Roska, B. (2018). Whole-brain functional ultrasound imaging reveals brain modules for visuomotor integration. Neuron 100, 1241–1251.

47. Minderer, M., Brown, K.D., and Harvey, C.D. (2019). The spatial structure of neural encoding in mouse posterior cortex during navigation. Neuron 102, 232–248.

48. Sunkara, A., DeAngelis, G.C., and Angelaki, D.E. (2016). Joint representation of translational and rotational components of optic flow in parietal cortex. Proc. Natl. Acad. Sci. USA 113, 5077–5082.

49. Keller, G.B., Bonhoeffer, T., and Hübener, M. (2012). Sensorimotor mismatch signals in primary visual cortex of the behaving mouse. Neuron 74, 809–815.

50. Vélez-Fort, M., Bracey, E.F., Keshavarzi, S., Rousseau, C.V., Cossell, L., Lenzi, S.C., Strom, M., and Margrie, T.W. (2018). A circuit for integration of head- and visual-motion signals in layer 6 of mouse primary visual cortex. Neuron 98, 179–191.

5 Retinal motion information contributes to optic flow processing by the cortex

In this chapter, I present the final research project that I conducted during my PhD studies. After writing the review article presented in Chapter 4, we were intrigued about testing the hypothesis that retinal direction selectivity is involved in cortical optic flow processing. Inspired by work done in the zebrafish, I, together with Zoltan Raics (Software engineer, SENS Software Ltd), established a visual stimulus paradigm which allowed us to experimentally test this hypothesis in awake mice. The results from this study were recently accepted for publication in *Current Biology* with myself as shared co-first author and are publicly accessible in our preprint (Rasmussen et al., 2020b).

5.1 Brief introduction

The movement of animals through an environment generates global patterns of visual motion on the retina, known as optic flow. Different locomotor behaviors trigger distinct patterns of optic flow, which provide visual feedback about self-motion relative to the environment: forward and backward movements cause translational optic flow, while turning causes rotational optic flow. Yet, how such optic flow patterns are encoded by the activity of neurons in the mouse cortex remains unknown.

As put forward in Chapter 4, ON-OFF DS cell ensembles may contribute to self-motion representations in the PPC by analyzing optic flow patterns experienced during locomotion (Rasmussen and Yonehara, 2020; Sabbah et al., 2017), however, this hypothesis has thus far not been tested. In this work, we addressed two main questions: Does the mouse visual cortex contain neurons encoding translational and rotational optic flow? and, does signaling from retinal DS cells contribute to such cortical optic flow representations?

5.2 Brief methods

For this project we employed a number of experimental techniques, which I will here briefly summarize. For binocular animals to reliably detect and distinguish optic flow patterns, the brain must integrate motion signals from each eye. Thus, and central to this study, we adopted a stimulus protocol that allowed us to test the full horizontal motion repertoire (Kubo et al., 2014). This protocol consisted of eight conditions, in which moving gratings were first presented to one eye at a time, and then presented to both eyes, simulating the rotational and translational optic flow that the mouse would

experience during natural locomotion. To test the contribution of retinal horizontal direction selectivity, we again used the $Frmd7^{tm}$ mice (Yonehara et al., 2016) (Chapter 2, Figure 6). To identify visual cortical areas we used intrinsic signal optical imaging (Juavinett et al., 2016), and to monitor the responses of individual neurons, we transfected the visual cortex with GCaMP6 and recorded changes in fluorescence intensity using two-photon imaging in awake mice. We mapped the activity of thousands of layer 2/3 neurons in areas V1, RL, A, PM, and AM, which allowed us to investigate optic flow-related response differences between wild-type mice and mice with disrupted retinal direction selectivity.

5.3 Main findings

This study offers four main findings concerning how distinct optic flow patterns are encoded by neurons in the visual cortex. First, we found neurons with response selectivity to translational or rotational optic flow in all imaged areas, but areas RL and A were especially enriched with these neurons. Second, neurons suppressed by binocular motion, yet responsive to monocular motion, were found in all areas, but were particularly abundant in V1. Third, the proportions of translation-selective neurons in V1, and translation-selective and rotation-selective neurons in areas RL and A, but not in areas AM and PM, were decreased in $Frmd7^{tm}$ mice. Furthermore, binocular-suppressed neurons were not decreased in $Frmd7^{tm}$ mice in any of the sampled areas. Fourth, in wild-type mice, cortical areas were functionally segregated based on their neuronal representations, and areas RL and A exhibited specialization for binocular optic flow. This functional segregation was notably affected in $Frmd7^{tm}$ mice, and optic flow representations in areas RL and A became reminiscent of those in V1.

5.4 Reflections and significance

The findings of this work provide several contributions and conceptual advances to the field. One prominent hypothesis proposes that retinal DS cell ensembles are specialized for detecting optic flow during self-motion (Sabbah et al., 2017). By establishing a causal role of retinal horizontal direction selectivity for cortical optic flow processing, our work provides the first *in vivo* support for this hypothesis. This result may provide clues about the behavioral role of retinal direction selectivity. Thus, our findings suggest that a key function of retinal direction selectivity may be to sense distinct patterns of optic flow during locomotion, permitting the brain to readily encode the associated self-motion. Additionally, our results suggest that retinal direction selectivity contributes to the establishment of functional segregation, and areal specialization between visual cortical

areas. It is intriguing to speculate whether optic flow-related signaling from ON-OFF DS cells may be preferentially conveyed to areas RL and A via a specialized subnetwork similar to what we described in Chapter 3 (Rasmussen et al., 2020a). In parallel, our findings point to areas RL and A as key nodes for the processing of self-motion-induced visual information in mice. Interestingly, these areas are extensively interconnected with somatosensory and motor cortical areas (Gămănuţ et al., 2018), and area RL processes multi-sensory information (Olcese et al., 2013). This may spark the hypothesis that visual self-motion information converges with other complementary sensory modalities, such as vibro-tactile information, in the PPC, and the output is conveyed to motor areas to inform and update movement programs during exploratory locomotion.
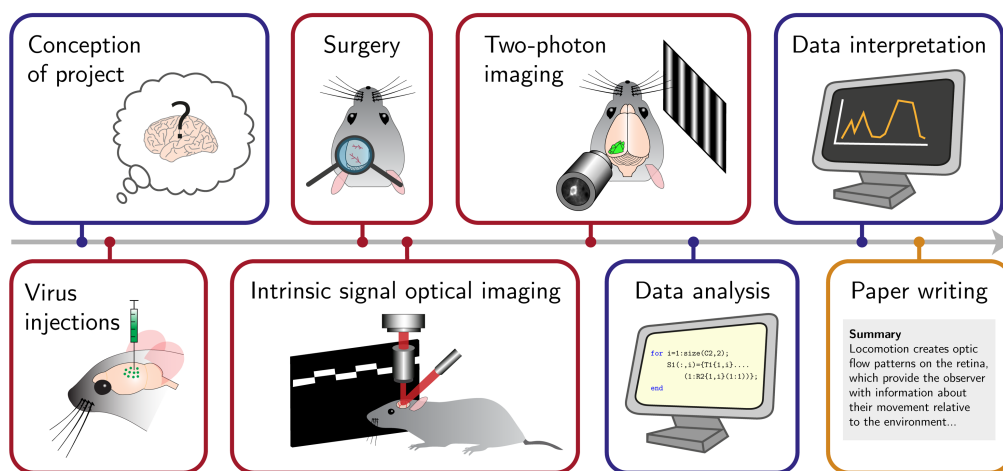
5.5 Author contributions

Figure 9 | Author contributions. *Box colors denote the relative author contribution; blue: shared the work; orange: did the majority of the work; red: did essentially all of the work.*

Supplementary material

The supplementary information accompanying the paper is found in Appendix B.

Binocular integration of retinal motion information underlies optic flow processing by the cortex

Rune N. Rasmussen[1,2], Akihiro Matsumoto[1,2], Simon Arvin[1] and Keisuke Yonehara[1]*

[1]Danish Research Institute of Translational Neuroscience – DANDRITE, Nordic-EMBL Partnership for Molecular Medicine, Department of Biomedicine, Aarhus University, Ole Worms Allé 8, 8000 Aarhus C, Denmark

[2]Authors contributed equally

*Correspondence to K.Y. (keisuke.yonehara@dandrite.au.dk)

Abstract

Locomotion creates various patterns of optic flow on the retina, which provide the observer with information about their movement relative to the environment. However, it is unclear how these optic flow patterns are encoded by the cortex. Here we use two-photon calcium imaging in awake mice to systematically map monocular and binocular responses to horizontal motion in four areas of the visual cortex. We find that neurons selective to translational or rotational optic flow are abundant in higher visual areas, whereas neurons suppressed by binocular motion are more common in the primary visual cortex. Disruption of retinal direction selectivity in *Frmd7* mutant mice reduces the number of translation-selective neurons in the primary visual cortex, and translation- and rotation-selective neurons as well as binocular direction-selective neurons in the rostrolateral and anterior visual cortex, blurring the functional distinction between primary and higher visual areas. Thus, optic flow representations in specific areas of the visual cortex rely on binocular integration of motion information from the retina.

Introduction

The action of moving through an environment produces patterns of visual motion, known as optic flow, on the retina, which animals rely on to guide their behavior. Animal locomotion is largely described by a combination of forward-backward movements and left-right turning. Forward and backward movements induce translational optic flow (nasal-to-temporal or temporal-to-nasal motion in both eyes, respectively) whereas turning induces rotational optic flow (nasal-to-temporal motion in one eye and temporal-to-nasal in the other) (Fig. 1a). However, despite the increasing use of mice to study vision, it is unknown how these distinct optic flow patterns are encoded by the rodent cortex.

An extensive body of research has shown that neurons residing in brain areas involved in optic flow processing have complex receptive fields, often receive binocular inputs, and respond to both translational and rotational optic flow stimuli. Examples include the fly lobula plate (involved in course control)[1,2], the zebrafish pretectal nuclei[3,4], the avian and mammalian accessory optic system (involved in gaze stabilization)[5,6], and both the dorsomedial region of the medial superior temporal area and posterior parietal cortex (PPC) of monkeys (involved in spatial navigation)[7–9]. The mouse visual cortex contains a primary visual cortex (V1) and more than a dozen distinct higher visual areas (HVAs), each with unique sensitivities to visual features[10,11]. The V1 receives retinal inputs via the lateral geniculate nucleus and distributes functionally specialized signals to different HVAs[12–14]. Based on their anatomy, multi-sensory processing, and roles in spatial navigation, the rostrolateral (RL), anterior (A), and anteromedial (AM) HVAs are considered part of the PPC in mice[15–18], raising the possibility that they contain neurons sensitive to binocular optic flow.

In rodents, visual motion computations are not exclusive to the cortex, and start in the retina. The retina contains mosaic arrangements of direction-selective (DS) cells that preferentially respond to motion in one of the four cardinal directions (nasal, temporal, dorsal, and ventral)[19–21]. These cells fall into two canonical classes: ON DS cells (which project to the nuclei of the accessory optic system and mediate the optokinetic reflex) and ON-OFF DS cells (which project to the lateral geniculate nucleus and the superior colliculus)[19,21–23]. Interestingly, disruption of horizontal direction selectivity in the retina impairs monocular motion responses in layer 2/3 of V1 and the RL area, but not in the posteromedial (PM) area nor layer 4 of V1, suggestive of a segregated cortical pathway for processing signals originating from retinal ON-OFF DS cells[12,13,24,25]. An intriguing hypothesis is that information from ON-OFF DS cells in the left and right eyes is systematically integrated in the cortex to create areas with distinct sensitivity to translational and rotational optic flow patterns[21,26]. However, this has yet to be experimentally tested, and the cortical areas that might combine optic flow information from the left and right eyes remain unknown.

Here we systematically map the responses of individual neurons across the visual cortex using two-photon calcium imaging during monocular and binocular optic flow stimulation in awake mice. We test the contribution of retinal DS cells using *Frmd7* mutant (*Frmd7tm*) mice, in which retinal horizontal direction selectivity is disrupted[13,24,27]. Our data demonstrate that the mouse visual cortex contains an abundance of neurons that encode translational or rotational optic flow. Furthermore, our results suggest that information from retinal DS cells in each eye is integrated in the cortex as early as in V1, where it establishes response selectivity to backward translational optic flow, but that binocular retinal DS signaling for establishing selectivity to rotational optic flow is first integrated in the higher areas RL and A. Conversely, our finding that neurons suppressed by binocular motion and robustly activated by monocular motion are not impaired by disruption of retinal direction selectivity, supports the hypothesis that retinal ON-OFF DS cell mosaics are specialized for detecting translational and rotational optic flow rather than local motion[26].
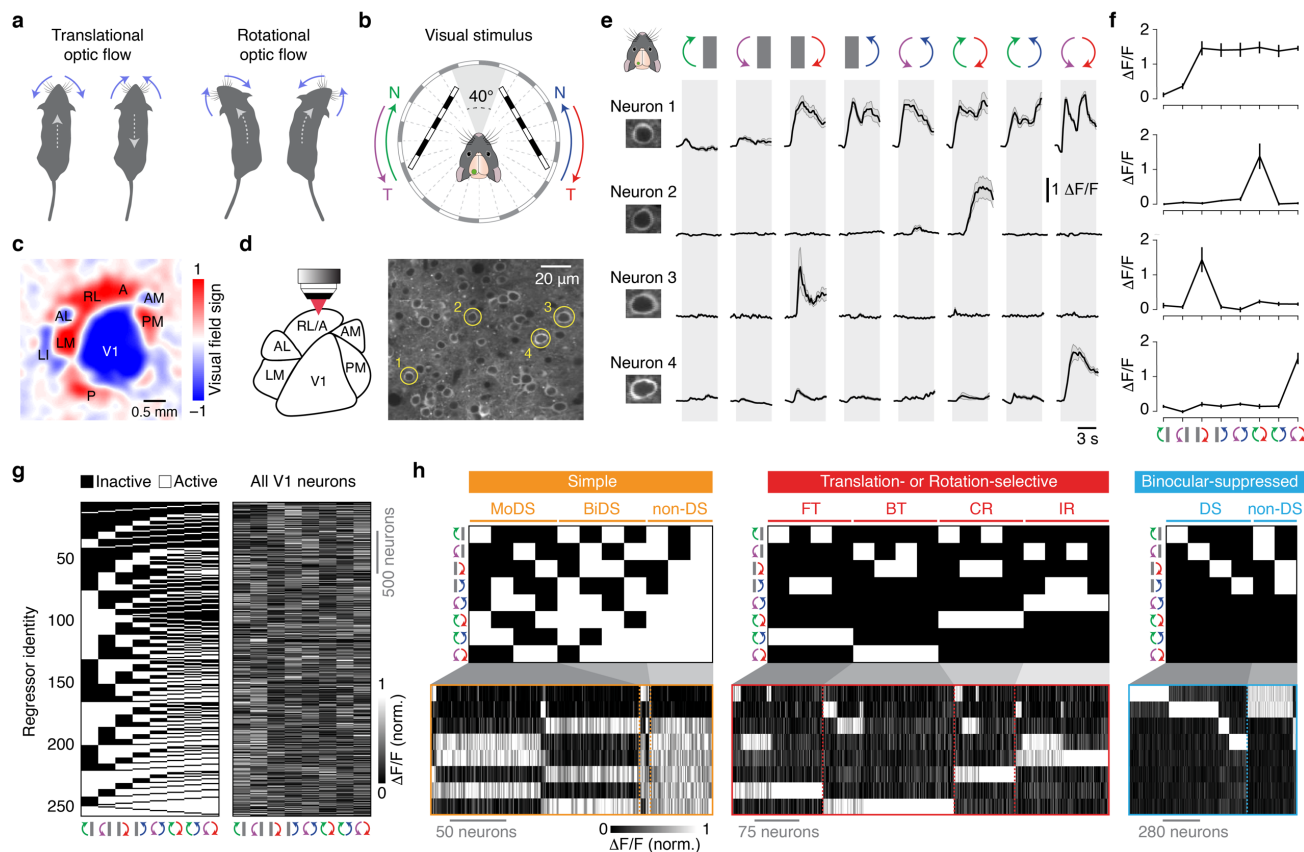
Fig. 1 | Discrete neuronal responses to motion stimuli can be imaged in the visual cortex of awake mice. a, Diagram illustrating optic flow patterns induced by self-motion. Forward and backward movements induce translational optic flow (left), and leftward and rightward turns induce rotational optic flow (right). Blue arrows indicate the dominant apparent motions in the visual space surrounding the mouse; gray dotted arrows indicate direction of locomotion. **b**, Diagram of the visual stimulus setup. Spherically-corrected gratings moved in either nasal (N) or temporal (T) directions (10 or 40 °/s with 0.03 cycles/°). The stimulus was not displayed in the binocular visual field (frontal 40°) to ensure stimulation of only the monocular visual fields. Imaging was performed in the visual cortex of the left hemisphere. **c**, Visual field sign map obtained with intrinsic signal optical imaging showing the location of visual cortical areas. **d**, Left: two-photon imaging was performed from identified visual cortical areas. Right: example image of GCaMP6f-expressing neurons in layer 2/3 of V1. **e**, Example trial-averaged fluorescence intensity (ΔF/F) time courses for the neurons highlighted in (**d**) in response to monocular and binocular motion. Error bars are mean ± s.e.m. **f**, Tuning curves of the neurons in (**e**). Error bars are mean ± s.e.m. **g**, Left: map of all 256 regressors. Right: response matrix of the tuning curves for all consistently-responsive V1 neurons. **h**, Regressor profiles and tuning curves for V1 neurons assigned to functional groups within the simple, translation- or rotation-selective, and binocular-suppressed response classes. MoDS, monocular DS; BiDS, binocular DS; FT, forward translational; BT, backward translational; CR, contraversive rotational; IR, ipsiversive rotational.

Results

Discrete neuronal responses to monocular and binocular motion stimuli can be imaged in the visual cortex of awake mice. To identify individual areas of mouse visual cortex, we used intrinsic signal optical imaging[13,28]. We first generated visual field sign maps from retinotopic maps, allowing us to identify V1 as well as the higher areas RL, A, AM, and PM (Fig. 1c and Extended Data Fig. 1). We chose to combine areas RL and A (RL/A), as these areas could not be not clearly distinguished from each other in our dataset[10,29]. For binocular animals to reliably detect different optic flow patterns, the brain must integrate motion signals from each eye. We therefore investigated the neuronal responses underlying binocular optic flow processing by presenting moving gratings to mice using a stimulus protocol that tests the repertoire of horizontal motions[3]. The eight stimulus conditions in the protocol were generated by presenting gratings moving in a nasal or temporal direction to one eye at a time, and then to both eyes to simulate the rotational (ipsiversive and contraversive) or translational

(forward and backward) optic flow that the mouse would experience during locomotion (Fig. 1a,b; see Methods). To unambiguously probe the interaction of left and right retinal information in the cortex, the stimuli were presented only to the monocular visual fields and not to the frontal binocular visual field (Fig. 1b). Our stimulus protocol did not trigger the optokinetic reflex (Extended Data Fig. 2), likely due to the use of a low spatial frequency[30].

The tuning properties of individual layer 2/3 neurons were characterized in awake mice by transfecting cortical neurons with the genetically encoded calcium sensor GCaMP6f and measuring changes in two-photon fluorescence during stimulus presentation (Fig. 1d,e). A typical field of view contained ~100–150 neurons, and somatic calcium responses showed diverse, but consistent, patterns, depending on the eye being stimulated and the direction of motion (Fig. 1e). Tuning curves for individual neurons were generated by plotting trial-averaged fluorescence changes as a function of stimulus conditions (Fig. 1f). We systematically classified neurons into distinct types according to their tuning curves
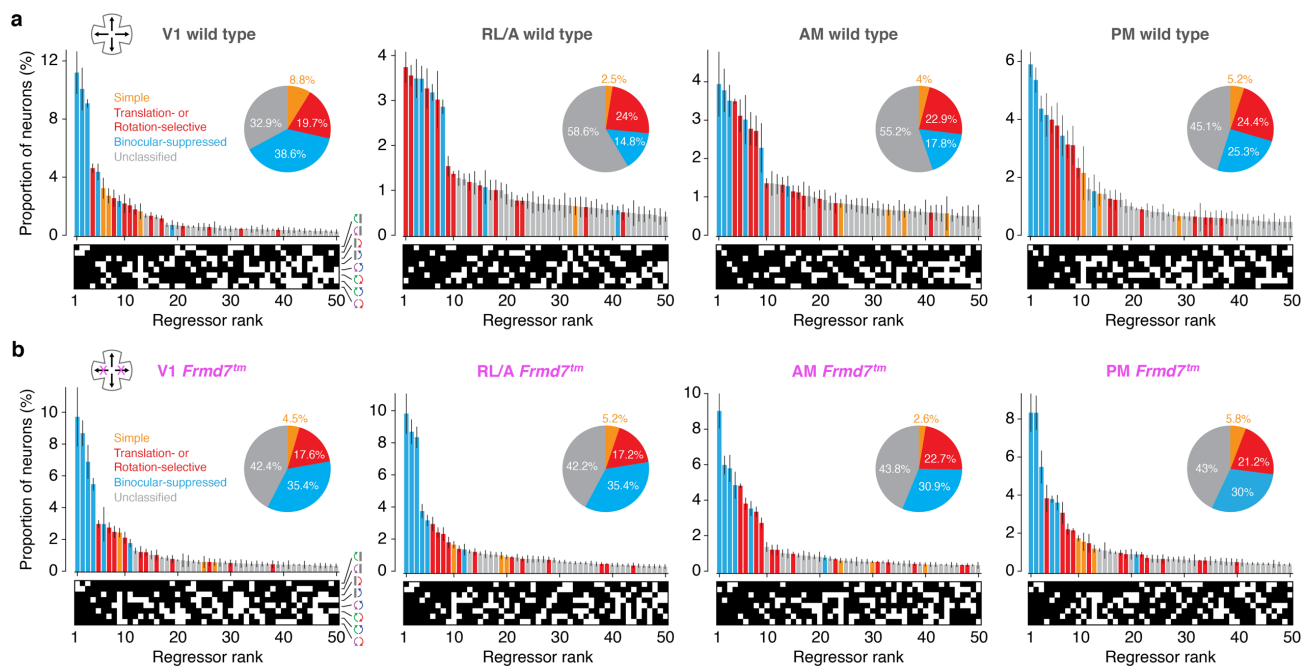
Fig. 2 l The RL/A area of the visual cortex is enriched with optic flow-selective neurons in wild-type mice. a,**b**, Ranked distribution of the 50 most abundant regressor profiles and response classes in the V1, RL/A, AM, and PM areas of wild-type mice (**a**) and *Frmd7tm* mice with disrupted retinal direction selectivity along the horizontal axis (**b**). Error bars are mean ± s.e.m. Inset: proportion of all neurons in the response classes.

using regressor-correlation analysis[3]. First, we generated a regressor map consisting of all possible all-or-none response combinations to the eight stimulus conditions, which resulted in 256 profiles (Fig. 1g; see Methods). Next, the tuning curve for each neuron was assigned to the regressor with the highest correlation (Extended Data Fig. 3). All tuning curves had high correlations with their assigned regressor (mean correlation coefficient, 0.91 ± 0.05, *n* = 26712 neurons from 17 mice). These data confirm that we can reliably elicit responses to monocular and binocular motion stimuli in the visual cortex of awake mice and also robustly classify neurons into discrete response types.

The RL/A area of the visual cortex is enriched with optic flow-selective neurons. We sought to investigate the response specificity of visual cortex neurons by sampling thousands of consistently-responsive neurons in multiple areas of the visual cortex of nine mice (3010 in V1, 4165 in RL/A, 4006 in AM, and 3059 in PM; Supplementary Table 1) and assigning them to regressors (Fig. 1g and Extended Data Fig. 4). To characterize the monocular and binocular optic flow coding properties of these neurons, we initially focused on three response classes: simple, translation- or rotation-selective[3], and binocular-suppressed. The simple class comprised three groups that were characterized by their direction selectivity: monocular DS, binocular DS, and non-DS neurons (Fig. 1h). Translation- and rotation-selective neurons comprised four groups that were characterized by their response selectivity to either forward translational, backward translational, contraversive rotational, or ipsiversive rotational optic flow (Fig. 1a,h). Binocular-suppressed neurons were characterized by a suppressed response during binocular motion stimulation and were further divided according to their DS or non-DS responses to monocular motion (Fig. 1h; see Methods).

For all visual cortical areas, we counted neurons assigned to each regressor and ranked regressors according to their frequency (Fig. 2a and Extended Data Fig. 3). Interestingly, in contrast to previous work in zebrafish[3], the most abundant neurons in V1 were binocular-suppressed neurons, which have been described in the primate V1[31]. These neurons constituted as much as 38.6% of V1 neurons and 50% of the 10 most frequent regressors (Fig. 2a). In contrast, simple and translation- or rotation-selective neurons constituted only 8.8% and 19.7% of all responsive neurons, respectively (Fig. 2a). Neurons that could not be assigned to these three classes were considered unclassified and not investigated further.

The abundance of neuronal classes was different in the HVAs (Fig. 2a). Translation- or rotation-selective neurons were the most abundant response class in the RL/A area (24% of neurons, corresponding to 50% of the 10 most frequent regressors), whereas simple and binocular-suppressed neurons comprised only 2.5% and 14.8% of neurons, respectively. In area AM, translation- or rotation-selective neurons were again abundant and simple neurons sparse (22.9% and 4%, respectively), but there was a higher proportion of binocular-suppressed neurons than in the RL/A area (17.8%). The PM area was characterized by an equal proportion of translation- or rotation-selective and binocular-suppressed neurons, constituting 24.4% and 25.3% of neurons, respectively (Fig. 2a).

These data establish that different areas of mouse visual cortex contain distinct distributions of monocular and binocular optic flow-encoding neurons. In particular, the RL/A area is enriched with neurons encoding translational and rotational optic flow, whereas V1 is enriched with neurons activated by monocular motion but suppressed by binocular motion.
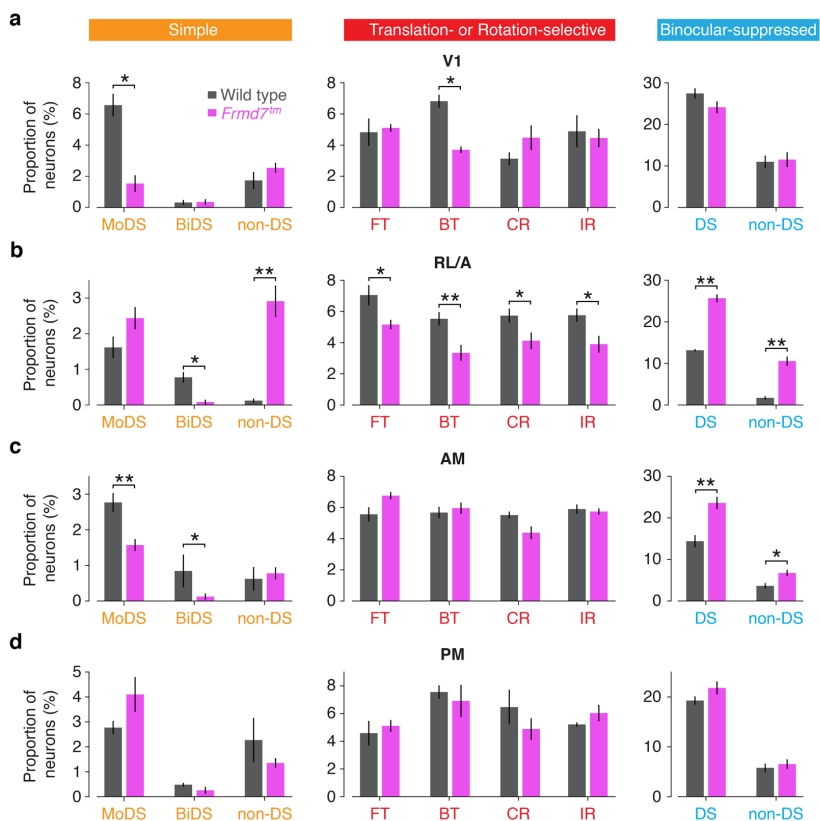
Fig. 3 | Retinal direction selectivity contributes to optic flow-selective responses in an area-specific manner. a,b,c,d Proportion of V1 (**a**), RL/A (**b**), AM (**c**), and PM (**d**) neurons in simple, translation- or rotation-selective, and binocular-suppressed functional groups for wild-type and *Frmd7tm* mice (*$P < 0.05$, **$P < 0.01$, two-way ANOVA with two-sided Mann-Whitney U tests for post hoc comparisons, $n = 4$ mice for V1 and PM and $n = 5$ mice for RL/A and AM). Error bars are mean ± s.e.m.

Retinal direction selectivity contributes to binocular optic flow processing in V1 and RL/A. To determine whether retinal direction selectivity contributes to the processing of optic flow in the visual cortex, we repeated our neuronal mapping in *Frmd7tm* mice, which lack horizontal direction selectivity in the retina[13,24,25,27]. Consistently-responsive neurons were sampled in different areas of the visual cortex of eight mice (2925 in V1, 3125 in RL/A, 3375 in AM, and 3047 in PM; Supplementary Table 1). This revealed a difference in the overall distribution of response classes in certain areas of *Frmd7tm* mice compared to wild-type mice (Fig. 2a,b), which prompted us to examine the effects of direction selectivity on the proportions of monocular- and binocular-responsive neurons in each response class (Fig. 3a–d). In V1, the proportions of monocular DS and backward translation-selective neurons were reduced in *Frmd7tm* mice (Fig. 3a). More strikingly, all groups of translation- or rotation-selective neurons, as well as binocular DS neurons, were reduced in the RL/A area of *Frmd7tm* mice (Fig. 3b). In the AM area, only monocular and binocular DS neurons were reduced (Fig. 3c). The proportion of DS and non-DS binocular-suppressed neurons was increased in both RL/A and AM areas of *Frmd7tm* mice (Fig. 3b,c). Finally, none of the nine functional groups were significantly altered in the PM area of *Frmd7tm* mice (Fig. 3d), underscoring previous work showing that motion processing in the PM area is independent of retinal DS signaling[13].

Together, these data show that simple and translation- or rotation-selective responses, but not binocular-suppressed

responses, are impaired by disrupting retinal direction selectivity. Furthermore, we conclude that retinal direction selectivity contributes to binocular optic flow responses in the V1 and RL/A areas of the visual cortex.

Retinal direction selectivity establishes functional segregation between V1 and RL/A. Individual HVAs form distinct subnetworks, each of which represents a different information stream[10,32,33]. We sought to find out how visual cortical areas are functionally organized with respect to their composition of optic flow-sensitive neurons, and if retinal direction selectivity is involved in creating such an organization. To probe this, we used the mean proportion of neurons in our nine functional groups to create an optic flow fingerprint for each visual area in wild-type and *Frmd7tm* mice, then performed hierarchical clustering (Fig. 4a) and correlation analyses (Fig. 4b; see Methods).

Hierarchical segregation (Fig. 4a) and a weak correlation between optic flow representations (mean correlation coefficient, 0.89 ± 0.03; Fig. 4b) were evident between the cortical areas of wild-type mice. In particular, V1 was separated from the RL/A, AM, and PM areas, suggesting functional specialization between V1 and the HVAs[10]. In addition, the PPC areas (RL/A and AM) branched early from V1 and PM, indicating that the PPC has a distinct role in optic flow processing (Fig. 4a). In contrast, there was little
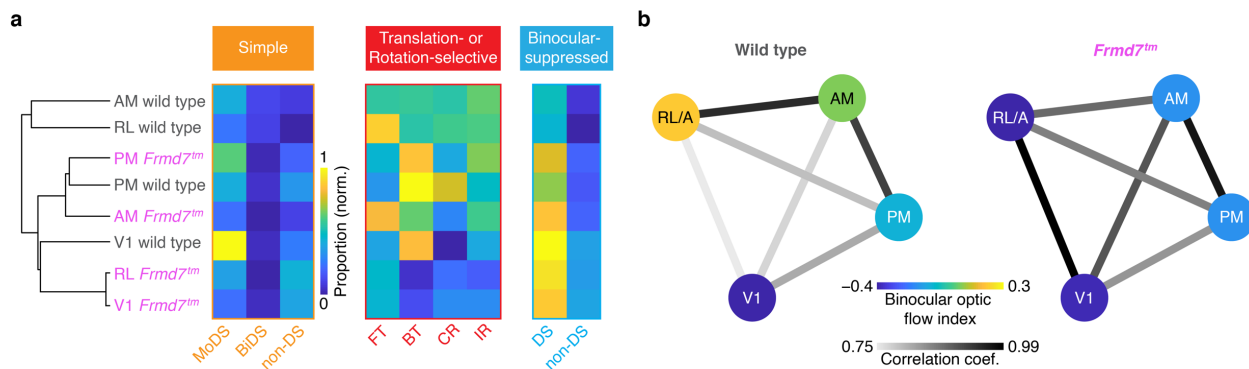
a

b

Fig. 4 | Retinal direction selectivity establishes functional segregation between V1 and RL/A. a, Left: Hierarchy showing similarity in proportion of functional groups between visual areas in wild-type and *Frmd7tm* mice. Right: mean proportion of neurons in simple, translation- or rotation-selective, and binocular-suppressed functional groups between visual areas in wild-type and *Frmd7tm* mice, sorted according to the similarity hierarchy (left). **b**, Diagram of the binocular optic flow index for each visual area, and the correlation in functional group proportions between areas, in wild-type and *Frmd7tm* mice.

hierarchical segregation, and more correlated optic flow representations, between visual areas in *Frmd7tm* mice (mean correlation coefficient, 0.96 ± 0.007; Fig. 4a,b). Notably, optic flow responses in area RL/A were remarkably similar to those in V1 in *Frmd7tm* mice (correlation coefficient, 0.75 and 0.99, for wild-type and *Frmd7tm* mice, respectively; *P* < 0.01, Fischer's transformation, *n* = 9 proportion values; Fig. 4b), abolishing any functional segregation between these areas. In contrast, the PM area of both wild-type and *Frmd7tm* mice appeared on the same branch (Fig. 4a), supporting the notion that motion processing in this area is independent of retinal direction selectivity.

To further investigate area specialization, we assessed the proportion of monocular- versus binocular-driven functional groups within each visual area and quantified the relationship with a selectivity index (Fig. 4b; see Methods). In wild-type mice, the bias towards monocular or binocular motion differed between visual areas to the extent that RL/A emerged as a specialized area for binocular optic flow processing (binocular optic flow index, –0.39 for V1, 0.21 for RL/A, 0.059 for AM, and –0.11 for PM; Fig. 4b). In contrast, this functional diversity was absent in *Frmd7tm* mice, and monocular-driven neurons were overrepresented across the visual areas (binocular optic flow index, –0.38 for V1, –0.44 for RL/A, –0.18 for AM, and –0.19 for PM; Fig. 4b).

From these data we conclude that retinal direction selectivity contributes to functional segregation and response specialization between the different areas of the visual cortex in wild-type mice. The most striking effect of retinal direction selectivity disruption in *Frmd7tm* mice is the transformation of optic flow responses in the RL/A area into V1-like responses, indicating a specific role for the RL/A area in binocular integration of motion information originating from retinal DS cells.

Discussion

Our study provides four major insights into the functional organization of optic flow processing in the visual system of mice. First, translation- and rotation-selective neurons are abundant in areas RL/A, AM, and PM, whereas neurons suppressed by binocular motion are common in V1. Second, translation-selective neurons in V1, and translation- and rotation-selective neurons in the RL/A

but not AM and PM areas, rely on direction selectivity that is computed in the retina. Third, binocular-suppressed neurons, which would be efficiently activated by monocularly-restricted "local" motion but suppressed by self-motion-induced optic flow, do not rely on retinal direction selectivity. Fourth, retinal direction selectivity contributes to the functional segregation of optic flow responses between V1 and RL/A. Our results, therefore, demonstrate a causal link between retinal motion computations and optic flow representations in specific areas of the visual cortex. Furthermore, they establish a critical role for retinal direction selectivity in the cortical processing of whole-field optic flow, rather than local motion, thereby answering a previously proposed hypothesis[26].

The altered optic flow representations in *Frmd7tm* mice imply potential functional circuits to link retinal horizontal DS cells and cortical layer 2/3 neurons with distinct optic flow response preferences (Fig. 5). Our results suggest that information from retinal DS cells, tuned to motion in either the nasal or temporal direction, is propagated to layer 2/3 of the contralateral V1, where it contributes to establishing monocular DS responses tuned to horizontal motion. In turn, a fraction of backward translation-selective responses in V1 are likely synthesized from these monocular DS inputs, converging from V1 in both hemispheres via interhemispherically-projecting neurons[34]. In addition, a fraction of rotation-selective responses in area RL/A are likely synthesized from monocular nasal- and temporal-motion-preferring DS inputs converging from V1 in the same and opposite hemisphere, respectively. These hypotheses could be tested by functionally characterizing the presynaptic network of individual translation- or rotation-selective neurons using rabies virus-based trans-synaptic tracing[35,36]. Our data also suggest that translation- and rotation-selective neurons in V1 and RL/A are suppressed by visual motion in non-preferred directions on either retina (Fig. 5). Such response suppression could be mediated by inhibitory monocular DS neurons or inhibitory interneurons activated by excitatory monocular DS neurons. Future studies could clarify this by genetically assigning imaged neurons into excitatory and inhibitory cell types.

Our results also offer insights into the cortical pathways that process visual motion independently of direction selectivity computed in the retina. Our analyses reveal that neuronal responses
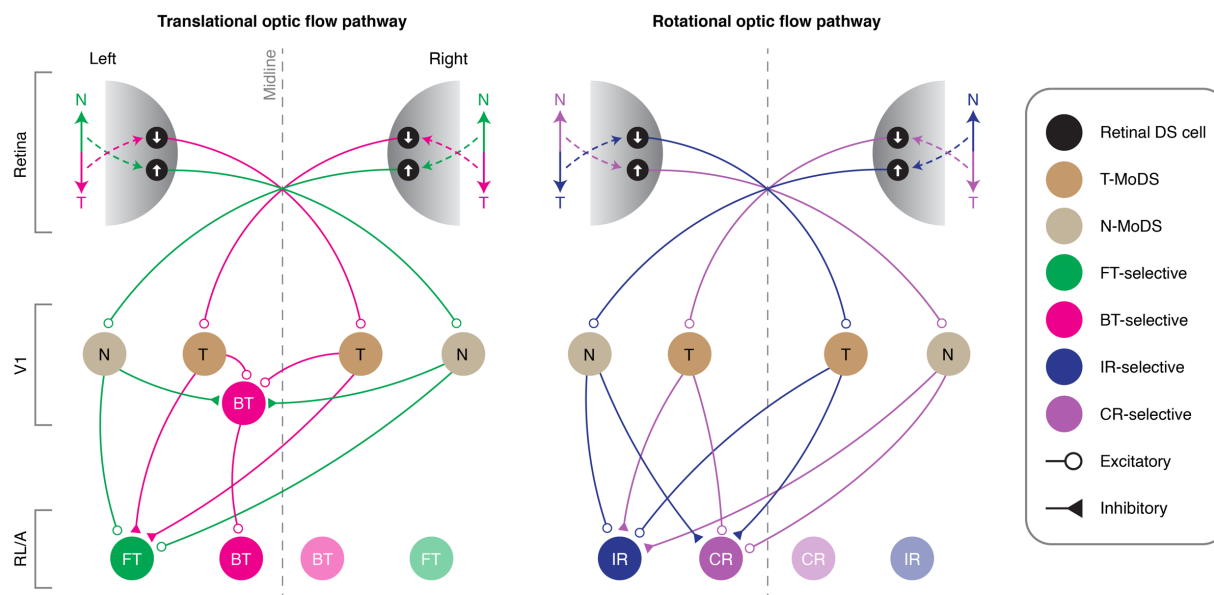
Fig 5 | Proposed circuit model for translational and rotational optic flow processing. Left: FT optic flow activates nasal motion-preferring DS cells in the left and right retinas, mediating activity in nasal (N) motion-preferring MoDS (N-MoDS) neurons in V1 of both hemispheres, and subsequently their combination in FT-selective neurons in area RL/A. Activity in N-MoDS neurons also inhibits BT-selective neurons. BT optic flow activates temporal (T) motion-preferring DS cells in the left and right retinas, mediating activity in temporal motion-preferring MoDS (T-MoDS) neurons in V1 of both hemispheres, and subsequently their combination in BT-selective neurons in V1 and RL/A. Activity in T-MoDS neurons also inhibits FT-selective neurons. Right: IR optic flow activates temporal and nasal motion-preferring DS cells in the left and right retinas, respectively, mediating activity in N- and T-MoDS neurons in V1 of the left and right hemispheres, respectively. The signals from these V1 neurons, in turn, combine at IR-selective neurons in RL/A of the left hemisphere, and their activity inhibits CR-selective neurons in the left hemisphere. CR optic flow activates nasal and temporal motion-preferring DS cells in the left and right retinas, respectively, mediating activity in T- and N-MoDS neurons in V1 of the left and right hemispheres, respectively. The signals from these V1 neurons, in turn, combine at CR-selective neurons in RL/A of the left hemisphere, and their activity inhibits IR-selective neurons of the left hemisphere. The wiring diagram is expected to be mirror-symmetric in relation to the midline.

suppressed by binocular motion are common in V1 and HVAs, and that these do not rely on retinal direction selectivity. This suggests that the V1 circuitry associated with binocular-suppressed neurons is functionally segregated from the circuitry processing retinal direction selectivity[12,13,24,25]. Interestingly, the majority of binocular-suppressed neurons in V1 had a preference for motion in the ipsilateral eye (Fig. 1h), suggesting that these neurons may combine the following two distinct types of input: 1) DS or non-DS excitatory inputs originating from non-DS cells in the ipsilateral eye, via interhemispherically-projecting neurons in the contralateral V1; and 2) non-DS inhibitory inputs driven by the activity of the contralateral eye. Our analyses also detected retinal DS cell-independent binocular optic flow responses in layer 2/3 of the visual cortex (Fig. 3b). Prior work in monkeys showed that binocular-suppressed and binocular-facilitated responses of monocular V1 neurons can be observed in the main visual input layer (layer 4)[31]. In mice, one form of *de novo* direction selectivity emerges in layer 4[37]. Hence, it is plausible that retinal direction selectivity-independent forms of binocular-suppressed and binocular-facilitated DS responses may arise in layer 4 from binocular interactions of DS signals originating from cortically-computed direction selectivity. This idea is consonant with a previous study in mice demonstrating that layer 4 neurons in V1 generate directionally-tuned responses independent of inputs from retinal DS cells[13].

Accumulating evidence suggests that areas RL and A are part of the PPC in mice[15-18] – a key nexus of sensorimotor integration that is involved in decision-making during spatial navigation[38], the encoding of body posture[39], global motion analysis[40,41], and representations of spatial information[42]. Intriguingly, more than 50% of neurons in the RL area are multi-sensory in mice; integrating both tactile and visual sensory inputs[43]. To advance our understanding of the behavioral function of area RL/A, it will thus be important to determine whether translation- and rotation-selective neurons display multi-sensory representations of self-motion (for example, whether they encode the direction of whisker deflections). Moreover, identifying the specific projection targets of these neurons might provide insight into how sensory self-motion information feeds into, for example, neuronal circuits for movement control. We speculate that area RL/A, as defined in our experiments, may be the functional correlate of the ventral intraparietal area of the PPC in monkeys, where multi-sensory representation of self-motion is utilized for goal-directed movements[44]. Thus, an intriguing question that emerges from our results is whether responses to binocular optic flow in the PPC of monkeys rely on retinal direction selectivity, as they do in the RL/A area in mice. A first step towards addressing this would be to determine whether retinal DS cells exist in non-human primates; making it possible to define common principles of visual motion processing as well as the modifications that have occurred throughout the course of evolution.

Acknowledgements

Author contributions

R.N.R. and K.Y. conceived the project and designed all experiments. R.N.R. performed all viral injections and surgeries. R.N.R. performed all intrinsic signal optical imaging and two-photon calcium imaging experiments. R.N.R. and S.A. performed eye movement recording experiments. R.N.R., S.A. and A.M. analyzed the data. K.Y. provided input on all aspects of the project. R.N.R., A.M. and K.Y. wrote the manuscript.

Competing interests

The authors declare no competing interests.

References

1. Krapp, H. G., Hengstenberg, R. & Egelhaaf, M. Binocular Contributions to Optic Flow Processing in the Fly Visual System. *J. Neurophysiol.* **85**, 724–734 (2001).

2. Farrow, K., Haag, J. & Borst, A. Nonlinear, binocular interactions underlying flow field selectivity of a motion-sensitive neuron. *Nat. Neurosci.* **9**, 1312–1320 (2006).

3. Kubo, F. *et al.* Functional Architecture of an Optic Flow-Responsive Area that Drives Horizontal Eye Movements in Zebrafish. *Neuron* **81**, 1344–1359 (2014).

4. Naumann, E. A. *et al.* From Whole-Brain Data to Functional Circuit Models: The Zebrafish Optomotor Response. *Cell* **167**, 947-960.e20 (2016).

5. Wylie, D. R. W., Bischof, W. F. & Frost, B. J. Common reference frame for neural coding of translational and rotational optic flow. *Nature* **392**, 278–282 (1998).

6. Simpson, J. I., Leonard, C. S. & Soodak, R. E. The accessory optic system of rabbit. II. Spatial organization of direction selectivity. *J. Neurophysiol.* **60**, 2055–2072 (1988).

7. Sunkara, A., DeAngelis, G. C. & Angelaki, D. E. Joint representation of translational and rotational components of optic flow in parietal cortex. *Proc. Natl. Acad. Sci. U. S. A.* **113**, 5077–82 (2016).

8. Duffy, C. J. & Wurtz, R. H. Sensitivity of MST neurons to optic flow stimuli. I. A continuum of response selectivity to large-field stimuli. *J. Neurophysiol.* **65**, 1329–1345 (1991).

9. Tanaka, K. & Saito, H. A. Analysis of motion of the visual field by direction, expansion/contraction, and rotation cells clustered in the dorsal part of the medial superior temporal area of the macaque monkey. *J. Neurophysiol.* **62**, 626–641 (1989).

10. Marshel, J. H., Garrett, M. E., Nauhaus, I. & Callaway, E. M. Functional specialization of seven mouse visual cortical areas. *Neuron* **72**, 1040–1054 (2011).

11. Zhuang, J. *et al.* An extended retinotopic map of mouse cortex. *Elife* **6**, (2017).

12. Cruz-Martín, A. *et al.* A dedicated circuit links direction-selective retinal ganglion cells to the primary visual cortex. *Nature* **507**, 358–61 (2014).

13. Rasmussen, R., Matsumoto, A., Dahlstrup Sietam, M. & Yonehara, K. A segregated cortical stream for retinal direction selectivity. *Nat. Commun.* **11**, 831 (2020).

14. Glickfeld, L. L., Andermann, M. L., Bonin, V. & Reid, R. C. Cortico-cortical projections in mouse visual cortex are functionally target specific. *Nat. Neurosci.* **16**, 219–26 (2013).

15. Lyamzin, D. & Benucci, A. The mouse posterior parietal cortex: Anatomy and functions. *Neurosci. Res.* **140**, 14–22 (2019).

16. Hovde, K., Gianatti, M., Witter, M. P. & Whitlock, J. R. Architecture and organization of mouse posterior parietal cortex relative to extrastriate areas. *Eur. J. Neurosci.* **49**, 1313–1329 (2019).

17. Minderer, M., Brown, K. D. & Harvey, C. D. The Spatial Structure of Neural Encoding in Mouse Posterior Cortex during Navigation. *Neuron* **102**, 232-248.e11 (2019).

18. Gilissen, S. R. J., Farrow, K., Bonin, V. & Arckens, L. Reconsidering the border between the visual and posterior parietal cortex of mice. *bioRxiv* 2020.03.24.005462 (2020) doi:10.1101/2020.03.24.005462.

19. Dhande, O. S. & Huberman, A. D. Retinal ganglion cell maps in the brain: implications for visual processing. *Curr. Opin. Neurobiol.* **24**, 133–142 (2014).

20. Borst, A. & Euler, T. Seeing Things in Motion: Models, Circuits, and Mechanisms. *Neuron* **71**, 974–994 (2011).

21. Rasmussen, R. & Yonehara, K. Contributions of Retinal Direction Selectivity to Central Visual Processing. *Curr. Biol.* **30**, R897–R903 (2020).

22. Wei, W. & Feller, M. B. Organization and development of direction-selective circuits in the retina. *Trends in Neurosciences* vol. 34 638–645 (2011).

23. Yonehara, K. *et al.* Identification of Retinal Ganglion Cells and Their Projections Involved in Central Transmission of Information about Upward and Downward Image Motion. *PLoS One* **4**, e4320 (2009).

24. Hillier, D. *et al.* Causal evidence for retina-dependent and -independent visual motion computations in mouse cortex. *Nat. Neurosci.* **20**, 960–968 (2017).

25. Macé, É. *et al.* Whole-Brain Functional Ultrasound Imaging Reveals Brain Modules for Visuomotor Integration. *Neuron* **100**, 1241-1251.e7 (2018).

26. Sabbah, S. *et al.* A retinal code for motion along the gravitational and body axes. *Nature* **546**, 492–497 (2017).

27. Yonehara, K. *et al.* Congenital Nystagmus Gene FRMD7 Is Necessary for Establishing a Neuronal Circuit Asymmetry for Direction Selectivity. *Neuron* **89**, 177–193 (2016).

28. Juavinett, A. L., Nauhaus, I., Garrett, M. E., Zhuang, J. & Callaway, E. M. Automated identification of mouse visual areas with intrinsic signal imaging. *Nat. Protoc.* **12**, 32–43 (2016).

29. Andermann, M. L., Kerlin, A. M., Roumis, D. K., Glickfeld, L. L. & Reid, R. C. Functional Specialization of Mouse Higher Visual Cortical Areas. *Neuron* **72**, 1025–1039 (2011).

30. Kretschmer, F., Tariq, M., Chatila, W., Wu, B. & Badea, T. C. Comparison of optomotor and optokinetic reflexes in mice. *J. Neurophysiol.* **118**, 300–316 (2017).

31. Dougherty, K., Cox, M. A., Westerberg, J. A. & Maier, A. Binocular Modulation of Monocular V1 Neurons. *Curr. Biol.* **29**, 381–391 (2019).

32. Wang, Q., Sporns, O. & Burkhalter, A. Network analysis of corticocortical connections reveals ventral and dorsal processing streams in mouse visual cortex. *J. Neurosci.* **32**, 4386–99 (2012).

33. Smith, I. T., Townsend, L. B., Huh, R., Zhu, H. & Smith, S. L. Stream-

dependent development of higher visual cortical areas. *Nat. Neurosci.* **20**, 200–208 (2017).

34. Ramachandra, V., Pawlak, V., Wallace, D. J. & Kerr, J. N. D. Impact of visual callosal pathway is dependent upon ipsilateral thalamus. *Nat. Commun.* **11**, (2020).

35. Wertz, A. *et al.* Single-cell-initiated monosynaptic tracing reveals layer-specific cortical network modules. *Science (80-.).* **349**, 70–74 (2015).

36. Yonehara, K. *et al.* The First Stage of Cardinal Direction Selectivity Is Localized to the Dendrites of Retinal Ganglion Cells. *Neuron* **79**, 1078–1085 (2013).

37. Lien, A. D. & Scanziani, M. Cortical direction selectivity emerges at convergence of thalamic synapses. *Nature* **558**, 80–86 (2018).

38. Gold, J. I. & Shadlen, M. N. The neural basis of decision making. *Annual Review of Neuroscience* vol. 30 535–574 (2007).

39. Mimica, B., Dunn, B. A., Tombaz, T., Srikanth Bojja, V. P. T. N. & Whitlock, J. R. Efficient cortical coding of 3D posture in freely behaving rats. *Science (80-.).* **362**, 584–589 (2018).

40. Juavinett, A. L. & Callaway, E. M. Pattern and Component Motion Responses in Mouse Visual Cortical Areas. *Curr. Biol.* **25**, 1–6 (2015).

41. Rasmussen, R. & Yonehara, K. Circuit Mechanisms Governing Local vs. Global Motion Processing in Mouse Visual Cortex. *Front. Neural Circuits* **11**, (2017).

42. Save, E. & Poucet, B. Role of the parietal cortex in long-term representation of spatial information in the rat. *Neurobiol. Learn. Mem.* **91**, 172–178 (2009).

43. Olcese, U., Iurilli, G. & Medini, P. Cellular and synaptic architecture of multisensory integration in the mouse neocortex. *Neuron* **79**, 579–593 (2013).

44. Bremmer, F. Navigation in space - The role of the macaque ventral intraparietal area. *J. Physiol.* **566**, 29–35 (2005).

Methods

Mice. All experimental procedures were approved by the Danish National Animal Experiment Committee (2020-15-0201-00452) and were performed in compliance with the Guide for the Care and Use of Laboratory Animals. Wild-type mice (C57BL/6J) were obtained from Janvier Labs. *Frmd7tm* mice were homozygous female or hemizygous male *Frmd7tm1b(KOMP)Wtsi* mice, obtained as *Frmd7tm1a(KOMP)Wtsi* from the Knockout Mouse Project (KOMP) Repository[24,27]: Exon 4 and the neo cassette flanked by loxP sequences were removed by crossing with female Cre-deleter *Edil3Tg(Sox2-cre)1Amc/J* mice (The Jackson Laboratory: stock 4783), as confirmed by PCR of genome DNA, and maintained in a C57BL/6J background. Experiments were performed on 9 male and female wild-type mice, and 8 female and male *Frmd7tm* mice. All mice were 12–18 weeks old during imaging experiments. Mice were kept on a reversed 12 h dark/light cycle and housed in groups of up to four littermates per cage.

Chronic cranial windows. Mice were anaesthetized with an intraperitoneal injection of a Fentanyl (0.05 mg/kg body weight; Hameln), Midazolam (5.0 mg/kg body weight; Hameln), and Medetomidine (0.5 mg/kg body weight; Domitor, Orion) mixture. To prevent neural edema during or after surgery, dexamethasone (0.2 mg/kg body weight; Dexium, Bimeda) was injected subcutaneously. Body temperature was maintained using a feedback-controlled heating pad (ATC2000, World Precision Instruments) and eyes were protected from dehydration with eye ointment (Viscotears, Novartis). The scalp overlying the skull was removed, and a custom head-fixing imaging head-plate, with a circular 8 mm diameter opening, was mounted using a mixture of cyanoacrylate-based glue (Super Glue Precision, Loctite) and dental cement (Jet Denture Repair Powder). The center of the head-plate was positioned above V1 (stereotaxic coordinates: 2.5 mm lateral, 1 mm anterior of lambda). A 5 mm craniotomy was made in the center of the head-plate. After removing the skull flap, the cortical surface was kept moist with Ringer's solution (in mM): 110 NaCl, 2.5 KCl, 1 $CaCl_2$, 1.6 $MgCl_2$, 10 glucose, and 22 $NaHCO_3$. A 5 mm glass coverslip (0.15 mm thickness, Warner Instruments) was placed onto the brain to shield and gently compress the underlying cortex. The cranial window was sealed using a cyanoacrylate-based glue (Super Glue Precision, Loctite) mixed with black dental cement (Jet Denture Repair Powder mixed with iron oxide powdered pigment), to prevent light contamination from the visual display. In addition, a black O-ring was mounted on top of the head-plate to further prevent any light contamination during imaging. Mice were administered subcutaneous analgesia (0.1 mg/kg body weight; Temgesic, Indivior) and returned to their home cage after anesthesia was reversed with an intraperitoneal injection of a Flumazenil (0.5 mg/kg body weight; Hameln) and Atipamezole (2.5 mg/kg body weight; Antisedan, Orion Pharma) mixture.

Virus injections. Mice were anesthetized with an intraperitoneal injection of a Fentanyl (0.05 mg/kg body weight; Hameln), Midazolam (5.0 mg/kg body weight; Hameln), and Medetomidine (0.5 mg/kg body weight; Domitor, Orion) mixture. To prevent neural edema during or after the surgery, dexamethasone (0.2 mg/kg body weight; Dexium, Bimeda) was injected subcutaneously. Three small 0.4 mm diameter craniotomies were made and ~100−150 nL AAV2/1-Syn-GCaMP6f-WPRE (2.13 × 10^{13} vg/ml, Penn Vector Core #AV-1-PV2822) slowly injected (5 min/injection) at a depth of ~275 µm below the dura. Injections were made using a borosilicate glass micropipette (30 µm tip diameter) and a pressure injection system (Picospritzer III, Parker). The micropipette was advanced at a 20° angle relative to vertical to minimize compression of the brain. To prevent backflow during withdrawal, the micropipette was kept at the injection site for 10 min before it was slowly retracted. The skin was sutured shut and postoperative analgesia was administered subcutaneously (0.1 mg/kg body weight; Temgesic, Indivior). Mice were returned to their home cage after anesthesia was reversed with an intraperitoneal injection of a Flumazenil (0.5 mg/kg body weight; Hameln) and Atipamezole (2.5 mg/kg body weight; Antisedan, Orion Pharma) mixture.

Intrinsic signal retinotopic mapping. Before two-photon calcium imaging, cortical visual areas of each mouse were identified by intrinsic signal optical imaging as previously described[13]. Mice were anesthetized with isoflurane (2−3% induction) and head-fixed in a custom holder. Chlorprothexine was administered intraperitoneally (2.5 mg/kg body weight; Sigma) as a sedative[33], and isoflurane reduced to

0.5–1% during visual stimulation. Core body temperature was maintained at 37–38 °C using a feedback-controlled heating pad (ATC2000, World Precision Instruments). The stimulated contralateral eye was kept lubricated by a thin layer of silicone oil. A 2× air-objective (Olympus, 0.08 NA) was mounted on our Scientifica VivoScope, equipped with a CMOS camera (HD1-D-D1312-160-CL-12, PhotonFocus). The camera was connected to a Matrox Solios (eCL/XCL-B) frame-grabber via Camera Link. The microscope was defocused 400–600 μm down from the pial surface, where intrinsic signals were excited using a red LED (KL1600, Schott) delivered through a 610 nm long-pass filter (Chroma). Reflected light was captured through a 700 ± 50 nm band-pass filter (Chroma) positioned in front of the camera, and images were collected at 6 frames per second. The 47.65 × 26.87 cm (width × height) display was angled 30° from the midline of the mouse and the perpendicular bisector was 10 cm from the bottom of the display, centered on the display left to right, and 10 cm from the eye[13,28]. This resulted in a visual field coverage from –41.98° to 60.77° (total 102.75°) in elevation, and from –67.23° to 67.23° (total 134.46°) in azimuth. Retinotopic maps were generated by sweeping a spherically corrected (https://labrigger.com/blog/2012/03/06/mouse-visual-stim/) full-field bar across the display. The bar contained a flickering black-and-white checkerboard pattern on a black background. The width of the bar was 12.5° and the checkerboard square size was 25°. Each square alternated between black and white at 4 Hz. In each trial, the bar was drifted ten times in each of the four cardinal directions, moving at 8–9 °/s. Usually, two to four trials resulted in well-defined retinotopic maps. From the raw image data, we used the response time course for each pixel and computed the phase and magnitude of the Fourier transform at the visual stimulus frequency[45]. The phase maps were then converted into retinotopic coordinates from the geometry of our setup. From this, we identified visual area borders based on the visual field sign maps and superimposed those borders with the anatomical blood-vessel images to accurately localize visual cortical areas.

Two-photon calcium imaging. Imaging was initiated two weeks after virus injections. Mice were awake during all imaging sessions as previously described[13]. To habituate mice to handling and the experimental conditions, one week after cranial window implantation, each mouse was head-fixed onto the imaging stage with its body restrained in a cylindrical cover, reducing struggling and overt body movements[13]. The habituation procedure was repeated for at least three days for each mouse at durations of 15, 30, and 60 min on days one, two, and three, respectively. At the end of each session, mice were rewarded with chocolate paste. Imaging session lasted 1–2 hours. The area targeted for two-photon imaging was localized by previous intrinsic signal optical imaging. Imaging was performed from layer 2/3, 120–275 μm below the dura, using a Scientifica VivoScope with a 7.9 kHz resonant scanner running SciScan, and with dispersion-compensated 940 nm excitation provided by a mode-locked Ti:Sapphire laser (MaiTai DeepSee, Spectra-Physics) through an Olympus 25× (1.05 NA) objective. The emitted fluorescence photons were reflected off a dichroic mirror (525/50 nm) and collected using a GaAsP photomultiplier tube (Scientifica). Clear ultrasound gel (NeurGel, Spes Medica) was used as immersion medium. To prevent light leakage from the visual stimulation, the objective was shielded with black tape, in addition to the O-ring mounted on top of the head-plate, and black cloth covered the microscope. Average excitation laser power varied from 40 to 65 mW. Images had 512 × 512 pixels, at 0.2 μm per pixel, and were acquired at 30.9 Hz using bidirectional scanning. We observed no sign of GCaMP6f bleaching during experiments. Each mouse was imaged repeatedly over the course of 2–3 weeks.

Visual stimulus for two-photon calcium imaging. For visual stimulation during two-photon calcium imaging experiments, two 47.65 × 26.87 cm (width × height) displays were angled 30° from the midline of the mouse on the left and right side; each display subtending 115.61° in azimuth and 80.95° in elevation (Fig. 1b). The visual stimulus protocol employed was adapted from a previous study[3]. Full-field vertical sinusoidal gratings (100% contrast; spatial frequency of 0.03 cycles/°) with a spherical correction to simulate projection onto a virtual sphere moved horizontally at speeds of 10 or 40 °/s. The horizontal transition consisted of eight separate conditions (6 s each, interspersed with 4 s of gray screen between conditions): 1) left nasal, 2) left temporal, 3) right nasal, 4) right temporal, 5) contraversive, 6) ipsiversive, 7) forward, 8) backward. Conditions 1–4 and were thus monocular, and conditions 5–8 binocular, simulating the rotational and translational optic flow experienced during turning and straight movements, respectively. The sequence of eight conditions was repeated in six trials. The mouse's binocular visual field (central 40°) did not contain the visual stimulus, to ensure only stimulation of the monocular visual field[46].

Eye movement tracking. In a subset of experiments, we tracked eye movements in awake mice during presentation of our visual stimulus protocol (Extended Data Fig. 2). We employed an eye-tracking system developed in our laboratory and recently described in detail[47]. Briefly, a small 45° hot mirror was aligned above a CCD camera (Guppy Pro F-031, AlliedVision) lateral to the position of the mouse. The camera was positioned below the visual field. Behind the visual stimulus display, a near-infrared light source (SLS-02082-B, Mightex Systems) was angled at 45° to illuminate the recorded eye. The camera was connected to a PC via a dedicated frame grabber (FIW62, ADLINK) and images were collected at ~65 frames per second. Using the eye-tracking software, EyeLoop, images were processed, and pupil and corneal reflection coordinates were computed[47]. From these, the angular eye coordinates (x and y) were calculated[47]. Horizontal eye speed was obtained by taking the first derivative of the horizontal eye coordinates (Vx and Vy), and low pass filtering Vx and Vy with a 1 s moving average filter[25]. Saccades were identified as events with a speed > 20 °/s. Stimulus-triggered horizontal eye speed and saccade rate traces were obtained by averaging over all trials.

Preprocessing of two-photon calcium imaging data. Imaging data were excluded from analysis if motion along the z-axis was detected. Raw two-photon imaging movies were corrected for in-plane motion using a piecewise non-rigid motion correction algorithm implemented in MATLAB (Mathworks)[48]. To detect regions of interest (ROIs) we used the MATLAB implementation of Suite2p[49]. ROIs were automatically detected using the motion-corrected frames and afterwards manually curated using the Suite2p graphical user interface.

From the motion-corrected movies and detected ROIs, we extracted the fluorescence time courses within each ROI. To correct the calcium traces for contamination from the surrounding neuropil, we also extracted the fluorescence of the surrounding neuropil for each ROI. The time series of the neuropil decontaminated calcium trace, $F_d(t)$, was described by:

$$F_d(t) = F(t) - \alpha \times N(t)$$

where $F(t)$ is the somata calcium trace, $N(t)$ is the neuropil trace, and α is the contamination factor. The contamination factor was determined for each ROI as previously[49]. Briefly, F and N traces were first low pass filtered using the 8th percentile in a 180 s moving window, yielding F_s and N_s, respectively. These were then used to establish $F_f(t) = F(t) - F_s(t)$ and $N_f(t) = N(t) - N_s(t)$. F_f and N_f were then used to determine α as previously described[49,50]. Using the neuropil decontaminated calcium trace, baseline calcium fluorescence, was computed for each stimulus condition as the mean during the pre-stimulus period [10]. Fluorescence values were then converted to relative change compared to baseline according to: $\Delta F/F = (F_d - F)/F$, where F_d is the instantaneous neuropil decontaminated calcium trace and F is the baseline calcium fluorescence. The mean neuronal responses were computed as the average response during the visual stimulus, and the mean and standard deviation across trials for each stimulus condition was computed for each neuron. To identify neurons for further in-depth analysis we used three inclusion criteria: 1) Neurons were defined as visually responsive if their mean $\Delta F/F$ to the preferred stimulus condition exceeded 10%; 2) A response reliability index, δ, was computed for each neuron as:

$$\delta = \frac{\mu_{pref} - \mu_{blank}}{\sigma_{pref} + \sigma_{blank}}$$

where μ_{max} and σ_{max} are the mean and standard deviations of the response to the preferred stimulus condition respectively, and μ_{blank} and σ_{blank} are the mean and standard deviations of the response to a blank stimulus respectively[10]. Neurons with δ exceeding 0.6 were defined as reliable; and 3) A signal-to-noise ratio (SNR) was computed for each neuron as:

$$SNR = \frac{\mu_{pref}}{\mu_{SD}}$$

where μ_{pref} is the mean of the response to the preferred stimulus condition and μ_{SD} is the mean of the standard deviation of the fluorescence trace during the baseline period (0.5 s before stimulus onset) for each trial[51]. Neurons with SNR exceeding 0.5 were defined as robustly responding. Only neurons that fulfilled all inclusion criteria at both stimulus speeds were included for further analysis procedures.

Response profile classification. In order to classify the response of individual neurons into separate functional groups, representing distinct response profiles, we employed regression analysis similar to previously described[3]. First, we summarized the response of each neuron by a tuning curve, including the mean $\Delta F/F$ for each of the eight stimulus conditions. We compiled this tuning curve for both stimulus speeds, and we determined the speed in which the highest mean $\Delta F/F$ was evoked; noted as the preferred speed of the neuron. By considering the response selectivity of a neuron to the eight stimulus conditions, we assumed that the response profile regressors could be described by an indicator function, *R*, as follows:

$$R(x) := \begin{cases} 1 & \text{if responsive to } x \\ 0 & \text{if not responsive to } x \end{cases}$$

where x is the stimulus condition, and 2^8 (i.e. 256) possible regressors exist for *R* (Fig. 1g). These 256 regressors correspond to the possible response combinations from the monocular and binocular stimulations in the nasal and temporal directions. For each neuron we then computed the linear Pearson's correlation for its tuning curve at the preferred speed against each of the 256 regressors and determined the regressor with the highest correlation. All neuronal tuning curves had high correlation with its assigned response regressor (mean correlation coefficient, 0.91 ± 0.05, *n* = 26712 neurons from 17 mice). The response regressors were functionally described using a MATLAB implementation of the Quine and McCluskey algorithm (https://www.mathworks.com/matlabcentral/fileexchange/37118-mintruthtable-tt-flags), in which the Boolean functions were minimized to find the logical function for each response profile that use only a small number of logical operations[3]. Here, we focused on the simple (MoDS: regressors IDs, 75, 43, 61, 56; BiDS: 194, 206, 193, 211; and non-DS: 234, 247, 256), binocular-suppressed (DS: 6, 7, 8, 9; and non-DS: 24, 37), and translation-selective or rotation-selective (FT: 32, 17, 80, 3; BT: 25, 20, 68, 2; CR: 33, 22, 85, 4; and IR: 28, 19, 67, 5) response classes (Fig. 1h and Extended Data Fig. 4). The simple and translation- or rotation-selective response classes are responsive to both monocular and binocular motion stimulation, and these were identified and described in detail previously[3]. In this work, we identified the binocular-suppressed response class, characterized by only responding to monocular motion stimulation, in a DS or non-DS manner. The binocular-suppressed functional groups (regressor IDs) were described by the following Boolean logical operations:

$$\#6 = (\neg NL \cap NR) \cap (\neg TR \cap NR)$$
$$\#7 = (\neg TL \cap TR) \cap (TR \cap \neg NR)$$

$$\#8 = (TL \cap \neg TR) \cap (TL \cap \neg NL)$$
$$\#9 = (NL \cap \neg NR) \cap (\neg TL \cap NL)$$
$$\#24 = (NL \cap TL) \cap (\neg NR \cap TR)$$
$$\#37 = (\neg NL \cap \neg TL) \cap (NR \cap TR)$$

where # is the identity of the regressors, and N and T are nasal and temporal motion directions, respectively, and L and R are stimulation of the left and right eyes, respectively, and $\neg$ is a logical "NOT" gate operator.

Comparison of response classes and functional groups among visual cortical areas. To examine similarities and disparities in response class distributions across visual areas in wild-type and *Frmd7tm* mice, we performed a hierarchical clustering analysis. For this, we used the mean proportion of the nine functional groups (simple: MoDS, BiDS, and non-DS; binocular-suppressed: DS and non-DS; and translation- or rotation-selective: FT, BT, IR, and CR) to create a monocular and binocular motion flow "fingerprint" for each visual area in wild-type and *Frmd7tm* mice. To create a hierarchical cluster tree, we used the *linkage* function in MATLAB, and visualized the result in a dendrogram (Fig. 4a). For quantifying similarities and disparities across visual areas within wild-type and *Frmd7tm* mice (Fig. 4b), we computed Pearson's correlation coefficients using the motion flow fingerprint of each visual area. To quantify the proportions of monocular versus binocular functional groups within each visual cortical area, we computed a binocular optic flow index (BOFI). For this, we determined the proportion of monocular driven (simple MoDS and non-DS, and binocular-suppressed DS and non-DS) and binocular driven (simple BiDS, and FT, BT, CR, and IR) functional groups, and computed the BOFI as:

$$\text{BOFI} = \frac{\% \text{ binocular} - \% \text{ monocular}}{\% \text{ binocular} + \% \text{ monocular}}$$

with a BOFI of 1 indicating that only binocular driven functional groups are represented, while a BOFI of –1 indicates only monocular driven groups are represented.

Quantification and statistical analysis. To statistically evaluate populational differences in functional groups between wild-type and *Frmd7tm* mice, we performed a two-way ANOVA test followed by post hoc comparisons using the two-sided Mann-Whitney *U* test. To compare Pearson's correlation coefficients obtained from two independent samples, i.e. wild-type and *Frmd7tm* mice, we used the Fischer's *r*-to-*z* transformation and obtained the corresponding two-sided *P* value. Center and spread values are reported as mean ± s.e.m. We used no statistical methods to plan sample sizes but used sample sizes similar to those frequently used in the field[10,13,17]. Exact *n* (i.e. number of animals and neurons) is included in the Result section and Supplementary Table 1. *P* < 0.05 was considered statistically significant, where **P* < 0.05 and ***P* < 0.01. Statistical analyses were carried out in MATLAB.

6 Final remarks

6.1 Conclusion

The aim of the work presented in this PhD dissertation was to provide answers to the questions of how direction selectivity computed in the retina contributes to motion processing in primary and higher-order areas of the visual cortex of mice. The first paper demonstrates that retinal direction selectivity contributes to the construction of specialized neuronal responses in the cortical area RL and identifies a cortical processing stream preferentially conveying signaling from retinal DS cells to this area. The second paper synthesizes the current literature to form a renewed perspective on the role of retinal direction selectivity in visual processing by central brain areas. Furthermore, this review formulates and proposes a concrete hypothesis for how retinal direction selectivity might be involved in optic flow processing in the PPC. The third paper tests this hypothesis and establishes that direction selectivity computed in the retina contributes to the development of area-specific optic flow representations in the visual cortex. Collectively, the work presented in this dissertation provides novel insights into how retinal motion computations are causally involved in the establishment of specialized neuronal responses and motion representations in distinct areas of the visual cortex of mice. The findings derived from these lines of investigation provide us a mechanistic understanding of how the brain builds complex visual representations, and underscores the critical role of processing occurring in the peripheral end of sensory systems.

6.2 Considerations and future directions

This PhD project is only a first step toward a comprehensive description of the role retinal direction selectivity in visual cortical processing, and much work still remains.

One limitation of the experiments presented in this dissertation is that they were carried out in stationary mice that were passively exposed to visual stimulation. Neurons along the visual hierarchy, including in the cortex and thalamus, are not only sensitive to visual inputs, but their activity is also notably modulated by the ongoing internal brain state and locomotor activity (Keller et al., 2012; Niell and Stryker, 2010; Polack et al., 2013; Rasmussen et al., 2019; Roth et al., 2015). With the recent discovery that the activity of RGCs is likewise state-dependent (Liang et al., 2020; Schröder et al., 2020), it is intriguing to speculate that the influence of retinal DS cells on motion processing in downstream brain areas may be modulated by state and behavioral context. Perhaps the signaling of optic flow-sensing retinal DS cells is elevated during high-arousal states of

locomotion, in which such visual information seems more salient, in comparison with periods of low arousal and quiescence. In the future, it will be interesting to investigate the contextual modulations of the contribution of retinal direction selectivity to cortical motion processing. Along the same lines, these PhD studies did not directly test the behavioral role of retina-originating direction selectivity. Based on the results of this dissertation, I suggest that future work should aim to test the contribution of retinal direction selectivity to natural behaviors that involve optic flow analysis, such as goal-directed navigation (Gibson, 1950; Srinivasan et al., 2000; Warren et al., 2001). With the tools for manipulating retinal DS cells now being readily available (Hillier et al., 2017; Pei et al., 2015; Shi et al., 2017; Yonehara et al., 2016; Yoshida et al., 2001), in combination with sophisticated experimental setups which allow the activity of cortical neurons to be tracked while animals navigate in virtual environments (Harvey et al., 2012; Keller et al., 2012), this endeavor now seems more tractable than ever.

All recordings of neuronal activity presented in this dissertation relied on two-photon imaging of genetically encoded calcium indicators. While this technique offers significant advantages, such as the ability to record repeatedly from hundreds to thousands of neurons simultaneously, it also has limitations. One of these being that it predominantly reports changes in neuronal spiking activity and cannot accurately detect subthreshold membrane potential dynamics (Lin and Schnitzer, 2016), precluding the investigation of synaptic computations in individual neurons. In the future, it would be truly exciting to explore the membrane potential properties and synaptic inputs that give rise to translation- and rotation-selective responses in the visual cortex, and how retinal direction selectivity influences these computations. These questions could be investigated using *in vivo* whole-cell electrophysiological recordings of neuronal membrane potentials or synaptic currents, which are now feasible to obtain from awake mice (Petersen, 2017).

The work involved in this PhD project studied only the contribution of retinal DS signaling within the anatomical confines of the visual cortex. In the future, it will be important to identify where in the brain this retina-originating motion information is propagated downstream of the visual cortex. One might speculate that, for example, the optic flow-related signaling of translation- and rotation-selective neurons may be directed to motor areas in order to update motor programs based on visual feedback concerning the direction and speed of self-motion. Alternatively, or in parallel, optic flow-related signaling may be directed to the SC where this self-motion information could be subtracted in order to robustly detect salient object motions (such as a predator or prey) during explorative locomotion.

The collected works presented in this dissertation primarily focused on how signaling from ON-OFF DS cells is conveyed via the retino-geniculate pathway to V1 and HVAs. However, in the mouse, roughly 85% of RGCs project to the SC of the retino-collicular

pathway (Ellis et al., 2016), including ON-OFF DS cells (Huberman et al., 2009; Kay et al., 2011; Kim et al., 2010; Rivlin-Etzion et al., 2011). Because the SC connects to V1 and HVAs via the thalamic nucleus LP, it is indeed possible that the altered motion processing in the cortex of mice with disrupted retinal direction selectivity could, at least in part, originate from the retino-collicular pathway. Therefore, to begin dissecting the role of distinct pathways for cortical motion processing, it would be decidedly interesting to record the activity of SC neurons, and/or cortical axonal boutons originating from LP, in mice in which retinal direction selectivity is disrupted.

Finally, it remains unresolved whether retinal DS cells exist in primates. However, several lines of work compellingly indicate that they may indeed be present. Most notably, human patients and mice with a mutated form of the *Frmd7* gene show a strikingly similar phenotype, expressed by a lack of the horizontal optokinetic reflex (Yonehara et al., 2016). The same work documented that this phenotype, in mice, is linked to a lack of retinal direction selectivity along the horizontal axis. Importantly, in both non-human primates and mice, the *Frmd7* gene is overexpressed in SACs (Yonehara et al., 2016); the cell type dominantly responsible for creating DS responses in the retina of mice (Borst and Euler, 2011; Vaney et al., 2012). Furthermore, a type of RGC found in the primate retina, the recursive bistratified ganglion cell, shares morphological features with ON-OFF DS cells found in mice in that it possesses dendrites which innervate both the ON and OFF sublamina of the inner plexiform layer, and co-stratify with cholinergic SACs (Moritoh et al., 2013). In addition, preliminary work has shown that the recursive bistratified ganglion cell of macaque monkey retinas exhibit ON-OFF DS responses (Detwiler et al., 2019, Conference abstract). Collectively, these data seem to support that the primate retina may contain DS cells. However, in the future, it will be critical to settle this question. Should DS cells turn out to exist in the primate retina, the next fascinating question will be whether these cells contribute to motion processing in primary and higher-order visual cortical areas, or whether primates over the course of evolution developed alternative circuit mechanisms for performing these behaviorally indispensable computations.

References

Adesnik, H. (2017). Synaptic Mechanisms of Feature Coding in the Visual Cortex of Awake Mice. Neuron *95*, 1147–1159.

Adesnik, H., Bruns, W., Taniguchi, H., Huang, Z.J., and Scanziani, M. (2012). A neural circuit for spatial summation in visual cortex. Nature *490*, 226–230.

Albright, T.D., and Stoner, G.R. (1995). Visual motion perception. Proc. Natl. Acad. Sci. U. S. A. *92*, 2433–2440.

Andermann, M.L., Kerlin, A.M., Roumis, D.K., Glickfeld, L.L., and Reid, R.C. (2011). Functional Specialization of Mouse Higher Visual Cortical Areas. Neuron *72*, 1025–1039.

Andersen, R.A. (1997). Neural mechanisms of visual motion perception in primates. Neuron *18*, 865–872.

Baden, T., Berens, P., Franke, K., Román Rosón, M., Bethge, M., and Euler, T. (2016). The functional diversity of retinal ganglion cells in the mouse. Nature *529*, 345–350.

Baden, T., Euler, T., and Berens, P. (2020). Understanding the retinal basis of vision across species. Nat. Rev. Neurosci. *21*, 5–20.

Baker, M. (2013). Through the eyes of a mouse. Nature *502*, 156–158.

Barlow, H.B., and Hill, R.M. (1963). Selective Sensitivity to Direction of Movement in Ganglion Cells of the Rabbit Retina. Science *139*, 412–412.

Barlow, H.B., and Levick, W.R. (1965). The mechanism of directionally selective units in rabbit's retina. J. Physiol. *178*, 477–504.

Barlow, H.B., Hill, R.M., and Levick, W.R. (1964). Retinal ganglion cells responding selectively to direction and speed of image motion in the rabbit. J. Physiol. *173*, 377–407.

Beltramo, R., and Scanziani, M. (2019). A collicular visual cortex: Neocortical space for an ancient midbrain visual structure. Science *363*, 64–69.

Bickford, M.E., Zhou, N., Krahe, T.E., Govindaiah, G., and Guido, W. (2015). Retinal and Tectal "Driver-Like" Inputs Converge in the Shell of the Mouse Dorsal Lateral Geniculate Nucleus. J. Neurosci. *35*, 10523–10534.

Blot, A., Roth, M., Gasler, I., Javadzadeh, M., Imhof, F., and Hofer, S. (2020). Visual intracortical and transthalamic pathways carry distinct information to cortical areas. BioRxiv 2020.07.06.189902.

Borst, A., and Euler, T. (2011). Seeing Things in Motion: Models, Circuits, and Mechanisms. Neuron *71*, 974–994.

Briggman, K.L., Helmstaedter, M., and Denk, W. (2011). Wiring specificity in the direction-selectivity circuit of the retina. Nature *471*, 183–188.

Britten, K.H., Shadlen, M.N., Newsome, W.T., and Movshon, J. a (1992). The analysis of visual motion: a comparison of neuronal and psychophysical performance. J. Neurosci. *12*, 4745–4765.

Chen, T.-W., Wardill, T.J., Sun, Y., Pulver, S.R., Renninger, S.L., Baohan, A., Schreiter, E.R., Kerr, R.A., Orger, M.B., Jayaraman, V., et al. (2013). Ultrasensitive fluorescent proteins for imaging neuronal activity. Nature *499*, 295–300.

Cossell, L., Iacaruso, M.F., Muir, D.R., Houlton, R., Sader, E.N., Ko, H., Hofer, S.B., and Mrsic-Flogel, T.D. (2015). Functional organization of excitatory synaptic strength in primary visual cortex. Nature *518*, 399–403.

Cruz-Martín, A., El-Danaf, R.N., Osakada, F., Sriram, B., Dhande, O.S., Nguyen, P.L., Callaway, E.M., Ghosh, A., and Huberman, A.D. (2014). A dedicated circuit links direction-selective retinal ganglion cells to the primary visual cortex. Nature *507*, 358–361.

Detwiler, P.B., Crook, J., Packer, O., Robinson, F., and Dacey, D.M. (2019). The recursive bistratified ganglion cell type of the macaque monkey retina is ON-OFF direction selective. In Investigative Ophthalmology & Visual Science, p. 3884.

Dhande, O.S., and Huberman, A.D. (2014). Retinal ganglion cell maps in the brain: implications for visual processing. Curr. Opin. Neurobiol. *24*, 133–142.

Dhande, O.S., Stafford, B.K., Lim, J.-H.A., and Huberman, A.D. (2015). Contributions of Retinal Ganglion Cells to Subcortical Visual Processing and Behaviors. Annu. Rev. Vis. Sci. *1*, 291–328.

Dräger, U.C. (1975). Receptive fields of single cells and topography in mouse visual cortex. J. Comp. Neurol. *160*, 269–289.

Ecker, J.L., Dumitrescu, O.N., Wong, K.Y., Alam, N.M., Chen, S.K., LeGates, T., Renna, J.M., Prusky, G.T., Berson, D.M., and Hattar, S. (2010). Melanopsin-expressing retinal ganglion-cell photoreceptors: Cellular diversity and role in pattern vision. Neuron *67*, 49–60.

Ellis, E.M., Gauvain, G., Sivyer, B., and Murphy, G.J. (2016). Shared and distinct retinal input to the mouse superior colliculus and dorsal lateral geniculate nucleus. J. Neurophysiol. *116*, 602–610.

Frenz, H., and Lappe, M. (2005). Absolute travel distance from optic flow. Vision Res. *45*, 1679–1692.

Gămănuţ, R., Kennedy, H., Toroczkai, Z., Ercsey-Ravasz, M., Van Essen, D.C., Knoblauch, K., and Burkhalter, A. (2018). The Mouse Cortical Connectome, Characterized by an Ultra-Dense Cortical Graph, Maintains Specificity by Distinct Connectivity Profiles. Neuron *97*, 698–715.

Gao, E., DeAngelis, G.C., and Burkhalter, A. (2010). Parallel input channels to mouse primary visual cortex. J. Neurosci. *30*, 5912–5926.

Garrett, M.E., Nauhaus, I., Marshel, J.H., and Callaway, E.M. (2014). Topography and areal organization of mouse visual cortex. J. Neurosci. *34*, 12587–12600.

Gibson, J.J. (1950). The perception of the visual world (Oxford, England: Houghton Mifflin).

Gilissen, S.R.J., Farrow, K., Bonin, V., and Arckens, L. (2020). Reconsidering the Border between the Visual and Posterior Parietal Cortex of Mice. Cereb. Cortex bhaa318.

Girman, S. V., Sauvé, Y., and Lund, R.D. (1999). Receptive field properties of single neurons in rat primary visual cortex. J. Neurophysiol. *82*, 301–311.

Glickfeld, L.L., and Olsen, S.R. (2017). Higher-Order Areas of the Mouse Visual Cortex. Annu. Rev. Vis. Sci. *3*, 251–273.

Glickfeld, L.L., Andermann, M.L., Bonin, V., and Reid, R.C. (2013). Cortico-cortical projections in mouse visual cortex are functionally target specific. Nat. Neurosci. *16*, 219–226.

Goldbach, H.C., Akitake, B., Leedy, C.E., and Histed, M.H. (2020). Performance in even a simple perceptual task depends on mouse secondary visual areas. BioRxiv 2020.06.25.171884.

Gottlob, I., and Proudlock, F.A. (2014). Aetiology of infantile nystagmus. Curr. Opin. Neurol. *27*, 83–91.

Hammer, S., Monavarfeshani, A., Lemon, T., Su, J., and Fox, M.A. (2015). Multiple Retinal Axons Converge onto Relay Cells in the Adult Mouse Thalamus. Cell Rep. *12*, 1575–1583.

Harvey, C.D., Coen, P., and Tank, D.W. (2012). Choice-specific sequences in parietal cortex during a virtual-navigation decision task. Nature *484*, 62–68.

Hillier, D., Fiscella, M., Drinnenberg, A., Trenholm, S., Rompani, S.B., Raics, Z., Katona, G., Juettner, J., Hierlemann, A., Rozsa, B., et al. (2017). Causal evidence for retina-dependent and -independent visual motion computations in mouse cortex. Nat. Neurosci. *20*, 960–968.

Hofer, S.B., Ko, H., Pichler, B., Vogelstein, J., Ros, H., Zeng, H., Lein, E., Lesica, N.A., and Mrsic-Flogel, T.D. (2011). Differential connectivity and response dynamics of excitatory and inhibitory neurons in visual cortex. Nat. Neurosci. *14*, 1045–1052.

Hong, Y.K., Park, S.H., Litvina, E.Y., Morales, J., Sanes, J.R., and Chen, C. (2014). Refinement of the Retinogeniculate Synapse by Bouton Clustering. Neuron *84*, 332–339.

Van Hooser, S.D., Heimel, J.A.F., Chung, S., Nelson, S.B., and Toth, L.J. (2005). Orientation selectivity without orientation maps in visual cortex of a highly visual mammal. J. Neurosci. *25*, 19–28.

Hovde, K., Gianatti, M., Witter, M.P., and Whitlock, J.R. (2019). Architecture and organization of mouse posterior parietal cortex relative to extrastriate areas. Eur. J. Neurosci. *49*, 1313–1329.

Hubel, D.H., and Wiesel, T.N. (1959). Receptive fields of single neurones in the cat's striate cortex. J. Physiol. *148*, 574–591.

Hubel, D.H., and Wiesel, T.N. (1968). Receptive fields and functional architecture of monkey striate cortex. J. Physiol. *195*, 215–243.

Hübener, M. (2003). Mouse visual cortex. Curr. Opin. Neurobiol. *13*, 413–420.

Huberman, A.D., and Niell, C.M. (2011). What can mice tell us about how vision works? Trends Neurosci. *34*, 464–473.

Huberman, A.D., Manu, M., Koch, S.M., Susman, M.W., Lutz, A.B., Ullian, E.M., Baccus, S.A., and Barres, B.A. (2008). Architecture and Activity-Mediated Refinement of Axonal Projections from a Mosaic of Genetically Identified Retinal Ganglion Cells. Neuron *59*, 425–438.

Huberman, A.D., Wei, W., Elstrott, J., Stafford, B.K., Feller, M.B., and Barres, B.A. (2009). Genetic Identification of an On-Off Direction- Selective Retinal Ganglion Cell Subtype Reveals a Layer-Specific Subcortical Map of Posterior Motion. Neuron *62*, 327–334.

Jeon, C.J., Strettoi, E., and Masland, R.H. (1998). The major cell populations of the mouse retina. J. Neurosci. *18*, 8936–8946.

Ji, X.Y., Zingg, B., Mesik, L., Xiao, Z., Zhang, L.I., and Tao, H.W. (2016). Thalamocortical Innervation Pattern in Mouse Auditory and Visual Cortex: Laminar and Cell-Type Specificity. Cereb. Cortex *26*, 2612–2625.

Jin, M., and Glickfeld, L.L. (2020). Mouse Higher Visual Areas Provide Both Distributed and Specialized Contributions to Visually Guided Behaviors. Curr. Biol. *30*, 4682–4692.

Juavinett, A.L., and Callaway, E.M. (2015). Pattern and Component Motion Responses in Mouse Visual Cortical Areas. Curr. Biol. *25*, 1759–1764.

Juavinett, A.L., Nauhaus, I., Garrett, M.E., Zhuang, J., and Callaway, E.M. (2016). Automated identification of mouse visual areas with intrinsic signal imaging. Nat. Protoc. *12*, 32–43.

Kay, J.N., De la Huerta, I., Kim, I.-J., Zhang, Y., Yamagata, M., Chu, M.W., Meister, M., and Sanes, J.R. (2011). Retinal Ganglion Cells with Distinct Directional Preferences Differ in Molecular Identity, Structure, and Central Projections. J. Neurosci. *31*, 7753–7762.

Keller, G.B., Bonhoeffer, T., and Hübener, M. (2012). Sensorimotor Mismatch Signals in Primary Visual Cortex of the Behaving Mouse. Neuron *74*, 809–815.

Kerlin, A.M., Andermann, M.L., Berezovskii, V.K., and Reid, R.C. (2010). Broadly Tuned Response Properties of Diverse Inhibitory Neuron Subtypes in Mouse Visual Cortex. Neuron *67*, 858–871.

Kerschensteiner, D., and Guido, W. (2017). Organization of the dorsal lateral geniculate nucleus in the mouse. Vis. Neurosci. *34*, E008.

Kim, I.-J., Zhang, Y., Yamagata, M., Meister, M., and Sanes, J.R. (2008). Molecular identification of a retinal cell type that responds to upward motion. Nature *452*, 478–482.

Kim, I.-J., Zhang, Y., Meister, M., and Sanes, J.R. (2010). Laminar Restriction of Retinal Ganglion Cell Dendrites and Axons: Subtype-Specific Developmental Patterns Revealed with Transgenic Markers. J. Neurosci. *30*, 1452–1462.

Kim, M.-H., Znamenskiy, P., Iacaruso, M.F., and Mrsic-Flogel, T.D. (2018). Segregated Subnetworks of Intracortical Projection Neurons in Primary Visual Cortex. Neuron *100*, 1313–1321.

Ko, H., Hofer, S.B., Pichler, B., Buchanan, K. a, Sjöström, P.J., and Mrsic-Flogel, T.D. (2011). Functional specificity of local synaptic connections in neocortical networks. Nature *473*, 87–91.

Kondo, S., and Ohki, K. (2015). Laminar differences in the orientation selectivity of geniculate afferents in mouse primary visual cortex. Nat. Neurosci. *19*, 316–319.

Kubo, F., Hablitzel, B., Dal Maschio, M., Driever, W., Baier, H., and Arrenberg, A.B. (2014). Functional Architecture of an Optic Flow-Responsive Area that Drives Horizontal Eye Movements in Zebrafish. Neuron *81*, 1344–1359.

Lappe, M., Bremmer, F., and Van Den Berg, A. V. (1999). Perception of self-motion from visual flow. Trends Cogn. Sci. *3*, 329–336.

Lee, W.-C.A., Bonin, V., Reed, M., Graham, B.J., Hood, G., Glattfelder, K., and Reid, R.C. (2016). Anatomy and function of an excitatory network in the visual cortex. Nature *532*, 370–374.

Li, Y., Lu, H., Cheng, P.L., Ge, S., Xu, H., Shi, S.H., and Dan, Y. (2012). Clonally related visual cortical neurons show similar stimulus feature selectivity. Nature *486*, 118–121.

Liang, L., and Chen, C. (2020). Organization, Function, and Development of the Mouse Retinogeniculate Synapse. Annu. Rev. Vis. Sci. *6*, 261–285.

Liang, L., Fratzl, A., Goldey, G., Ramesh, R.N., Sugden, A.U., Morgan, J.L., Chen, C., and Andermann, M.L. (2018). A Fine-Scale Functional Logic to Convergence from Retina to Thalamus. Cell *173*, 1343–1355.

Liang, L., Fratzl, A., Reggiani, J.D.S., El Mansour, O., Chen, C., and Andermann, M.L. (2020). Retinal Inputs to the Thalamus Are Selectively Gated by Arousal. Curr. Biol. *30*, 3923–3934.

Lien, A.D., and Scanziani, M. (2018). Cortical direction selectivity emerges at convergence of thalamic synapses. Nature *558*, 80–86.

Lin, M.Z., and Schnitzer, M.J. (2016). Genetically encoded indicators of neuronal activity. Nat. Neurosci. *19*, 1142–1153.

Lyamzin, D., and Benucci, A. (2019). The mouse posterior parietal cortex: Anatomy and functions. Neurosci. Res. *140*, 14–22.

Macé, É., Montaldo, G., Trenholm, S., Cowan, C., Brignall, A., Urban, A., and Roska, B. (2018). Whole-Brain Functional Ultrasound Imaging Reveals Brain Modules for Visuomotor Integration. Neuron *100*, 1241–1251.

Marques, T., Summers, M.T., Fioreze, G., Fridman, M., Dias, R.F., Feller, M.B., and Petreanu, L. (2018). A Role for Mouse Primary Visual Cortex in Motion Perception. Curr. Biol. *28*, 1703–1713.

Marshel, J.H., Garrett, M.E., Nauhaus, I., and Callaway, E.M. (2011). Functional specialization of seven mouse visual cortical areas. Neuron *72*, 1040–1054.

Marshel, J.H., Kaye, A.P., Nauhaus, I., and Callaway, E.M. (2012). Anterior-Posterior Direction Opponency in the Superficial Mouse Lateral Geniculate Nucleus. Neuron *76*, 713–720.

Martersteck, E.M., Hirokawa, K.E., Zeng, H., Sanes, J.R., Harris, J.A., Evarts, M., Bernard, A., Duan, X., Li, Y., Ng, L., et al. (2017). Diverse Central Projection Patterns of Retinal Ganglion Cells. Cell Rep. *18*, 2058–2072.

Martin, P.R. (1986). The projection of different retinal ganglion cell classes to the dorsal lateral geniculate nucleus in the hooded rat. Exp. Brain Res. *62*, 77–88.

Masland, R.H. (2001). The fundamental plan of the retina. Nat. Neurosci. *4*, 877–886.

Matsui, T., and Ohki, K. (2013). Target dependence of orientation and direction selectivity of corticocortical projection neurons in the mouse V1. Front. Neural Circuits *7*, 143.

Matsumoto, A., Briggman, K.L., and Yonehara, K. (2019). Spatiotemporally Asymmetric Excitation Supports Mammalian Retinal Motion Sensitivity. Curr. Biol. *29*, 3277–3288.

Maunsell, J.H.R., and Newsome, W.T. (1987). Visual processing in monkey extrastriate cortex. Annu. Rev. Neurosci. *10*, 363–401.

Mauss, A.S., Vlasits, A., Borst, A., and Feller, M. (2017). Visual Circuits for Direction Selectivity. Annu. Rev. Neurosci. *40*, 211–230.

Mcnaughton, B.L., Mizumori, S.J.Y., Barnes, C.A., Leonard, B.J., Marquis, M., and Green, E.J. (1994). Cortical representation of motion during unrestrained spatial navigation in the rat. Cereb. Cortex *4*, 27–39.

Métin, C., Godement, P., and Imbert, M. (1988). The primary visual cortex in the mouse: Receptive field properties and functional organization. Exp. Brain Res. *69*, 594–612.

Minderer, M., Brown, K.D., and Harvey, C.D. (2019). The Spatial Structure of Neural Encoding in Mouse Posterior Cortex during Navigation. Neuron *102*, 232–248.

Morgan, J.L., Berger, D.R., Wetzel, A.W., and Lichtman, J.W. (2016). The Fuzzy Logic of Network Connectivity in Mouse Visual Thalamus. Cell *165*, 192–206.

Morgenstern, N.A., Bourg, J., and Petreanu, L. (2016). Multilaminar networks of cortical neurons integrate common inputs from sensory thalamus. Nat. Neurosci. *19*, 1034–1040.

Moritoh, S., Komatsu, Y., Yamamori, T., and Koizumi, A. (2013). Diversity of Retinal Ganglion Cells Identified by Transient GFP Transfection in Organotypic Tissue Culture of Adult Marmoset Monkey Retina. PLoS One *8*, 54667.

Movshon, J.A., and Newsome, W.T. (1996). Visual response properties of striate cortical neurons projecting to area MT in macaque monkeys. J. Neurosci. *16*, 7733–7741.

Movshon, J. a, Adelson, E.H., Gizzi, M.S., and Newsome, W.T. (1985). The analysis of moving visual patterns. Pattern Recognit. Mech. *54*, 117–151.

Mrsic-Flogel, T.D., Hofer, S.B., Ohki, K., Reid, R.C., Bonhoeffer, T., and Hübener, M. (2007). Homeostatic Regulation of Eye-Specific Responses in Visual Cortex during Ocular Dominance Plasticity. Neuron *54*, 961–972.

Nassi, J.J., and Callaway, E.M. (2009). Parallel processing strategies of the primate visual system. Nat. Rev. Neurosci. *10*, 360–372.

Newsome, W.T., and Paré, E.B. (1988). A selective impairment of motion perception following lesions of the middle temporal visual area (MT). J. Neurosci. *8*, 2201–2211.

Niell, C.M., and Stryker, M.P. (2008). Highly selective receptive fields in mouse visual cortex. J. Neurosci. *28*, 7520–7536.

Niell, C.M., and Stryker, M.P. (2010). Modulation of Visual Responses by Behavioral State in Mouse Visual Cortex. Neuron *65*, 472–479.

O'Connor, D.H., Huber, D., and Svoboda, K. (2009). Reverse engineering the mouse brain. Nature *461*, 923–929.

Odoemene, O., Pisupati, S., Nguyen, H., and Churchland, A.K. (2018). Visual evidence accumulation guides decision-making in unrestrained mice. J. Neurosci. *38*, 10143–10155.

Ohki, K., and Reid, R.C. (2007). Specificity and randomness in the visual cortex. Curr. Opin. Neurobiol. *17*, 401–407.

Ohki, K., Chung, S., Ch'ng, Y.H., Kara, P., and Reid, R.C. (2005). Functional imaging with cellular resolution reveals precise micro-architecture in visual cortex. Nature *433*, 597–603.

Olcese, U., Iurilli, G., and Medini, P. (2013). Cellular and synaptic architecture of multisensory integration in the mouse neocortex. Neuron *79*, 579–593.

Oyster, C.W., and Barlow, H.B. (1967). Direction-Selective Units in Rabbit Retina: Distribution of Preferred Directions. Science *155*, 841–842.

Pei, Z., Chen, Q., Koren, D., Giammarinaro, B., Ledesma, H.A., and Wei, W. (2015). Conditional knock-out of vesicular GABA transporter gene from starburst amacrine cells reveals the contributions of multiple synaptic mechanisms underlying direction selectivity in the retina. J. Neurosci. *35*, 13219–13232.

Petersen, C.C.H. (2017). Whole-Cell Recording of Neuronal Membrane Potential during Behavior. Neuron *95*, 1266–1281.

Piscopo, D.M., El-Danaf, R.N., Huberman, A.D., and Niell, C.M. (2013). Diverse visual features encoded in mouse lateral geniculate nucleus. J. Neurosci. *33*, 4642–4656.

Polack, P.O., Friedman, J., and Golshani, P. (2013). Cellular mechanisms of brain state–dependent gain modulation in visual cortex. Nat. Neurosci. *16*, 1331–1339.

Prokop, T., Schubert, M., and Berger, W. (1997). Visual influence on human locomotion. Modulation to changes in optic flow. Exp. Brain Res. *114*, 63–70.

Rasmussen, R., and Sabbagh, U. (2020). Neural Polyamory: One Cell Forms Meaningful Connections with Hundreds of Partners. Cell Syst. *10*, 381–383.

Rasmussen, R., and Yonehara, K. (2017). Circuit Mechanisms Governing Local vs. Global Motion Processing in Mouse Visual Cortex. Front. Neural Circuits *11*.

Rasmussen, R., and Yonehara, K. (2020). Contributions of Retinal Direction Selectivity to Central Visual Processing. Curr. Biol. *30*, R897–R903.

Rasmussen, R., Nicholas, E., Petersen, N.C., Dietz, A.G., Xu, Q., Sun, Q., and Nedergaard, M. (2019). Cortex-wide Changes in Extracellular Potassium Ions Parallel Brain State Transitions in Awake Behaving Mice. Cell Rep. *28*, 1182–1194.

Rasmussen, R., Matsumoto, A., Dahlstrup Sietam, M., and Yonehara, K. (2020a). A segregated cortical stream for retinal direction selectivity. Nat. Commun. *11*, 831.

Rasmussen, R.N., Matsumoto, A., Arvin, S., and Yonehara, K. (2020b). Binocular integration of retinal motion information underlies optic flow processing by the cortex. BioRxiv 2020.10.16.342402.

Reese, B.E. (1988). "Hidden lamination" in the dorsal lateral geniculate nucleus: the functional organization of this thalamic region in the rat. Brain Res. Rev. *13*, 119–137.

Rivlin-Etzion, M., Zhou, K., Wei, W., Elstrott, J., Nguyen, P.L., Barres, B.A., Huberman, A.D., and Feller, M.B. (2011). Transgenic Mice Reveal Unexpected Diversity of On-Off Direction-Selective Retinal Ganglion Cell Subtypes and Brain Structures Involved in Motion Processing. J. Neurosci. *31*, 8760–8769.

Rodman, H.R., and Albright, T.D. (1989). Single-unit analysis of pattern-motion selective properties in the middle temporal visual area (MT). Exp. Brain Res. *75*, 53–64.

Román Rosón, M., Bauer, Y., Kotkat, A.H., Berens, P., Euler, T., and Busse, L. (2019). Mouse dLGN Receives Functional Input from a Diverse Population of Retinal Ganglion Cells with Limited Convergence. Neuron *102*, 462-476.

Rompani, S.B., Wanner, A., Zhang, C., Roth, C.N., Yonehara, K., and Roska, B. (2017). Different Modes of Visual Integration in the Lateral Geniculate Nucleus Revealed by Single-Cell- Initiated Transsynaptic Tracing. Neuron *93*, 767–776.

Roth, M.M., Helmchen, F., and Kampa, B.M. (2012). Distinct Functional Properties of Primary and Posteromedial Visual Area of Mouse Neocortex. J. Neurosci. *32*, 9716–9726.

Roth, M.M., Dahmen, J.C., Muir, D.R., Imhof, F., Martini, F.J., and Hofer, S.B. (2015). Thalamic nuclei convey diverse contextual information to layer 1 of visual cortex. Nat. Neurosci. *19*, 299–307.

Sabbah, S., Gemmer, J.A., Bhatia-Lin, A., Manoff, G., Castro, G., Siegel, J.K., Jeffery, N., and Berson, D.M. (2017). A retinal code for motion along the gravitational and body axes. Nature *546*, 492–497.

Salzman, C.D., Britten, K.H., and Newsome, W.T. (1990). Cortical microstimulation influences perceptual judgements of motion direction. Nature *346*, 174–177.

Save, E., and Poucet, B. (2009). Role of the parietal cortex in long-term representation of spatial information in the rat. Neurobiol. Learn. Mem. *91*, 172–178.

Scholl, B., Tan, A.Y.Y., Corey, J., and Priebe, N.J. (2013). Emergence of orientation selectivity in the Mammalian visual pathway. J. Neurosci. *33*, 10616–10624.

Scholl, B., Pattadkal, J.J., Rowe, A., and Priebe, N.J. (2017). Functional characterization and spatial clustering of visual cortical neurons in the predatory grasshopper mouse *Onychomys arenicola*. J. Neurophysiol. *117*, 910–918.

Schröder, S., Steinmetz, N.A., Krumin, M., Pachitariu, M., Rizzi, M., Lagnado, L., Harris, K.D., and Carandini, M. (2020). Arousal Modulates Retinal Output. Neuron *107*, 487–495.

Schubert, M., Bohner, C., Berger, W., Sprundel, M. V., and Duysens, J.E.J. (2003). The role of vision in maintaining heading direction: Effects of changing gaze and optic flow on human gait. Exp. Brain Res. *150*, 163–173.

Seabrook, T.A., Burbridge, T.J., Crair, M.C., and Huberman, A.D. (2017). Architecture, Function, and Assembly of the Mouse Visual System. Annu. Rev. Neurosci. *40*, 499–538.

Shi, X., Barchini, J., Ledesma, H.A., Koren, D., Jin, Y., Liu, X., Wei, W., and Cang, J. (2017). Retinal origin of direction selectivity in the superior colliculus. Nat. Neurosci. *20*, 550–558.

Simpson, J.I. (1984). The Accessory Optic System. Annu. Rev. Neurosci. *7*, 13–41.

Smith, I.T., Townsend, L.B., Huh, R., Zhu, H., and Smith, S.L. (2017). Stream-dependent development of higher visual cortical areas. Nat. Neurosci. *20*, 200–208.

Smith, M.A., Majaj, N.J., and Movshon, J.A. (2005). Dynamics of motion signaling by neurons in macaque area MT. Nat. Neurosci. *8*, 220–228.

Solomon, S.S., Tailby, C., Gharaei, S., Camp, A.J., Bourne, J.A., and Solomon, S.G. (2011). Visual motion integration by neurons in the middle temporal area of a New World monkey, the marmoset. J. Physiol. *589*, 5741–5758.

Srinivasan, M. V., Zhang, S., Altwein, M., and Tautz, J. (2000). Honeybee navigation: Nature and calibration of the "odometer." Science *287*, 851–853.

Sun, L.O., Brady, C.M., Cahill, H., Al-Khindi, T., Sakuta, H., Dhande, O.S., Noda, M., Huberman, A.D., Nathans, J., and Kolodkin, A.L. (2015). Functional Assembly of Accessory Optic System Circuitry Critical for Compensatory Eye Movements. Neuron *86*, 971–984.

Sun, W., Tan, Z., Mensh, B.D., and Ji, N. (2016). Thalamus provides layer 4 of primary visual cortex with orientation- and direction-tuned inputs. Nat. Neurosci. *19*, 308–315.

Sunkara, A., DeAngelis, G.C., and Angelaki, D.E. (2016). Joint representation of translational and rotational components of optic flow in parietal cortex. Proc. Natl. Acad. Sci. U. S. A. *113*, 5077–5082.

Tarpey, P., Thomas, S., Sarvananthan, N., Mallya, U., Lisgo, S., Talbot, C.J., Roberts, E.O., Awan, M., Surendran, M., McLean, R.J., et al. (2006). Mutations in FRMD7, a newly identified member of the FERM family, cause X-linked idiopathic congenital nystagmus. Nat. Genet. *38*, 1242–1244.

Tervo, D.G.R., Hwang, B.Y., Viswanathan, S., Gaj, T., Lavzin, M., Ritola, K.D., Lindo, S., Michael, S., Kuleshova, E., Ojala, D., et al. (2016). A Designer AAV Variant Permits Efficient Retrograde Access to Projection Neurons. Neuron *92*, 372–382.

Tohmi, M., Meguro, R., Tsukano, H., Hishida, R., and Shibuki, K. (2014). The extrageniculate visual pathway generates distinct response properties in the higher visual areas of mice. Curr. Biol. *24*, 587–597.

Tong, F. (2003). Cognitive neuroscience: Primary visual cortex and visual awareness. Nat. Rev. Neurosci. *4*, 219–229.

Trenholm, S., Johnson, K., Li, X., Smith, R.G., and Awatramani, G.B. (2011). Parallel mechanisms encode direction in the retina. Neuron *71*, 683–694.

Vaney, D.I., Sivyer, B., and Taylor, W.R. (2012). Direction selectivity in the retina: symmetry and asymmetry in structure and function. Nat. Rev. Neurosci. *13*, 194–208.

Wang, Q., and Burkhalter, A. (2007). Area map of mouse visual cortex. J. Comp. Neurol. *502*, 339–357.

Wang, Q., Gao, E., and Burkhalter, A. (2011). Gateways of Ventral and Dorsal Streams in Mouse Visual Cortex. J. Neurosci. *31*, 1905–1918.

Wang, Q., Sporns, O., and Burkhalter, A. (2012). Network analysis of corticocortical connections reveals ventral and dorsal processing streams in mouse visual cortex. J. Neurosci. *32*, 4386–4399.

Warren, J., Kay, B.A., Zosh, W.D., Duchon, A.P., and Sahuc, S. (2001). Optic flow is used to control human walking. Nat. Neurosci. *4*, 213–216.

Warren, W.H., Morris, M.W., and Kalish, M. (1988). Perception of Translational Heading From Optical Flow. J. Exp. Psychol. Hum. Percept. Perform. *14*, 646–660.

Wei, W. (2018). Neural Mechanisms of Motion Processing in the Mammalian Retina. Annu. Rev. Vis. Sci. *4*, 165–192.

Wei, W., and Feller, M.B. (2011). Organization and development of direction-selective circuits in the retina. Trends Neurosci. *34*, 638–645.

Wei, W., Hamby, A.M., Zhou, K., and Feller, M.B. (2011). Development of asymmetric inhibition underlying direction selectivity in the retina. Nature *469*, 402–406.

Weng, S., Sun, W., and He, S. (2005). Identification of ON-OFF direction-selective ganglion cells in the mouse retina. J. Physiol. *562*, 915–923.

Yonehara, K., Shintani, T., Suzuki, R., Sakuta, H., Takeuchi, Y., Nakamura-Yonehara, K., and Noda, M. (2008). Expression of SPIG1 reveals development of a retinal ganglion cell subtype projecting to the medial terminal nucleus in the mouse. PLoS One *3*, 1533.

Yonehara, K., Ishikane, H., Sakuta, H., Shintani, T., Nakamura-Yonehara, K., Kamiji, N.L., Usui, S., and Noda, M. (2009). Identification of Retinal Ganglion Cells and Their Projections Involved in Central Transmission of Information about Upward and Downward Image Motion. PLoS One *4*, 4320.

Yonehara, K., Balint, K., Noda, M., Nagel, G., Bamberg, E., and Roska, B. (2011). Spatially asymmetric reorganization of inhibition establishes a motion-sensitive circuit. Nature *469*, 407–410.

Yonehara, K., Fiscella, M., Drinnenberg, A., Esposti, F., Trenholm, S., Krol, J., Franke, F., Scherf, B.G., Kusnyerik, A., Müller, J., et al. (2016). Congenital Nystagmus Gene FRMD7 Is Necessary for Establishing a Neuronal Circuit Asymmetry for Direction Selectivity. Neuron *89*, 177–193.

Yoshida, K., Watanabe, D., Ishikane, H., Tachibana, M., Pastan, I., and Nakanishi, S. (2001). A key role of starburst amacrine cells in originating retinal directional selectivity and optokinetic eye movement. Neuron *30*, 771–780.

Zhao, X., Chen, H., Liu, X., and Cang, J. (2013). Orientation-selective responses in the mouse lateral geniculate nucleus. J. Neurosci. *33*, 12751–12763.

Zhuang, J., Ng, L., Williams, D., Valley, M., Li, Y., Garrett, M., and Waters, J. (2017). An extended retinotopic map of mouse cortex. Elife *6*, 18372.

Co-authorship declarations

AARHUS
UNIVERSITY

Declaration of co-authorship concerning <u>article for PhD dissertations</u>

Full name of the PhD student: Rune Nguyen Rasmussen

This declaration concerns the following article/manuscript:

Title:	A segregated cortical stream for retinal direction selectivity
Authors:	Rune Nguyen Rasmussen, Akihiro Matsumoto, Monica Dahlstrup Sietam and Keisuke Yonehara

The article/manuscript is: Published ☒ Accepted ☐ Submitted ☐ In preperation ☐

If published, state full reference: https://doi.org/10.1038/s41467-020-14643-z

If accepted or submitted, state journal: Nature Communications

Has the article/manuscript previously been used in other PhD or doctoral dissertations?

No ☒ Yes ☐ If yes, give details:

Your contribution

Please rate (A-F) your contribution to the elements of this article/manuscript, **and** elaborate on your rating in the free text section below.

- A. Has essentially done all the work (>90%)
- B. Has done most of the work (67-90 %)
- C. Has contributed considerably (34-66 %)
- D. Has contributed (10-33 %)
- E. No or little contribution (<10%)
- F. N/A

Category of contribution	Extent (A-F)
The conception or design of the work:	C
Free text description of PhD student's contribution (mandatory) In close collaboration with Keisuke Yonehara (KY) and Akihiro Matsumoto (AM), Rune Nguyen Rasmussen (RNR) formulated the conceptual as well as experimental design of this work.	
The acquisition, analysis, or interpretation of data:	C
Free text description of PhD student's contribution (mandatory) RNR performed all in vivo experiments including cranial window surgeries, cortical viral injections, intrinsic signal optical imaging, and two-photon calcium imaging. RNR, in close collaboration with AM, performed most of the data analysis and data interpretation.	
Drafting the manuscript:	B
Free text description of PhD student's contribution (mandatory) RNR wrote the manuscript draft and submission cover letter together with KY and with help from AM. RNR made all figures for publication.	

AARHUS UNIVERSITY

Submission process including revisions:	C
*Free text description of PhD student's contribution **(mandatory)***	
For revisions, RNR performed most of the in vivo experiments including cranial window surgeries, cortical viral injections, intrinsic signal optical imaging, and two-photon calcium imaging. RNR, together with KY wrote the rebuttal letter and revised the manuscript.	

Signatures of first- and last author, and main supervisor

Date	Name	Signature
05/12-20	Rune Nguyen Rasmussen	*Rune Rasmussen*
05/12-20	Keisuke Yonehara	*[signature]*

Date: 05/12-20

Rune Rasmussen

_____

Signature of the PhD student

Declaration of co-authorship concerning <u>article for PhD dissertations</u>

Full name of the PhD student: Rune Nguyen Rasmussen

This declaration concerns the following article/manuscript:

Title:	Contributions of retinal dirction selectivity to central visual processing
Authors:	Rune Nguyen Rasmussen and Keisuke Yonehara

The article/manuscript is: Published ☒ Accepted ☐ Submitted ☐ In preperation ☐

If published, state full reference: https://doi.org/10.1016/j.cub.2020.06.002

If accepted or submitted, state journal: Current Biology

Has the article/manuscript previously been used in other PhD or doctoral dissertations?

No ☒ Yes ☐ If yes, give details:

Your contribution

Please rate (A-F) your contribution to the elements of this article/manuscript, **and** elaborate on your rating in the free text section below.

- A. Has essentially done all the work (>90%)
- B. Has done most of the work (67-90 %)
- C. Has contributed considerably (34-66 %)
- D. Has contributed (10-33 %)
- E. No or little contribution (<10%)
- F. N/A

Category of contribution	Extent (A-F)
The conception or design of the work:	C
Free text description of PhD student's contribution (mandatory) In close collaboration with Keisuke Yonehara (KY), Rune Nguyen Rasmussen (RNR) formulated the conceptual ideas and outline of this review article.	
The acquisition, analysis, or interpretation of data:	C
Free text description of PhD student's contribution (mandatory) RNR, together with KY, gathered the litterature and interpreted the published body of work.	
Drafting the manuscript:	B
Free text description of PhD student's contribution (mandatory) RNR wrote the manuscript together with KY. RNR made all the figures for publication.	

AARHUS UNIVERSITY

Submission process including revisions:	C
Free text description of PhD student's contribution **(mandatory)** RNR, together with KY, wrote the rebuttal letter and revised the manuscript.	

Signatures of first- and last author, and main supervisor

Date	Name	Signature
05/12-20	Rune Nguyen Rasmussen	
05/12-20	Keisuke Yonehara	

Date: 05/12-20

_____
Signature of the PhD student

AARHUS UNIVERSITY

Declaration of co-authorship concerning <u>article for PhD dissertations</u>

Full name of the PhD student: Rune Nguyen Rasmussen

This declaration concerns the following article/manuscript:

Title:	Binocular integration of retinal motion information underlies optic flow processing by the cortex
Authors:	Rune Nguyen Rasmussen, Akihiro Matsumoto, Simon Arvin and Keisuke Yonehars

The article/manuscript is: Published ☐ Accepted ☒ Submitted ☐ In preperation ☐

If published, state full reference: N/A

If accepted or submitted, state journal: Accepted in Current Biology

Has the article/manuscript previously been used in other PhD or doctoral dissertations?

No ☒ Yes ☐ If yes, give details:

Your contribution

Please rate (A-F) your contribution to the elements of this article/manuscript, **and** elaborate on your rating in the free text section below.

- A.   Has essentially done all the work (>90%)
- B.   Has done most of the work (67-90 %)
- C.   Has contributed considerably (34-66 %)
- D.   Has contributed (10-33 %)
- E.   No or little contribution (<10%)
- F.   N/A

Category of contribution	Extent (A-F)
The conception or design of the work:	C
Free text description of PhD student's contribution (mandatory) In close collaboration with supervisor Keisuke Yonehara (KY), Rune Nguyen Rasmussen (RNR) formulated the conceptual as well as experimental design of this work.	
The acquisition, analysis, or interpretation of data:	B
Free text description of PhD student's contribution (mandatory) RNR performed all experiments included in this work, including cranial window surgeries, cortical viral injections, intrinsic signal optical imaging, and two-photon calcium imaging. RNR, in close collaboration with postdoc Akihiro Matsumoto (AM), performed most of the data analysis and data interpretation. RNR helped Simon Arvin with eye-tracking recordings.	
Drafting the manuscript:	B
Free text description of PhD student's contribution (mandatory) RNR wrote the manuscript draft and submission cover letter together with Keisuke Yonehara. RNR made all figures for publication.	

AARHUS UNIVERSITY

Submission process including revisions:		C
Free text description of PhD student's contribution **(mandatory)** RNR, together with AM, KY, and Simon Arvin, revised the manuscript and RNR wrote most of the rebuttal letter.		

Signatures of first- and last author, and main supervisor

Date	Name	Signature
15/12-20	Rune Nguyen Rasmussen	*Rune Rasmussen*
15/12-20	Keisuke Yonehara	*(signature)*

Date:

Rune Rasmussen
_____
Signature of the PhD student

Appendix A

Supplemental Information

A segregated cortical stream for retinal direction selectivity

Rasmussen et al.
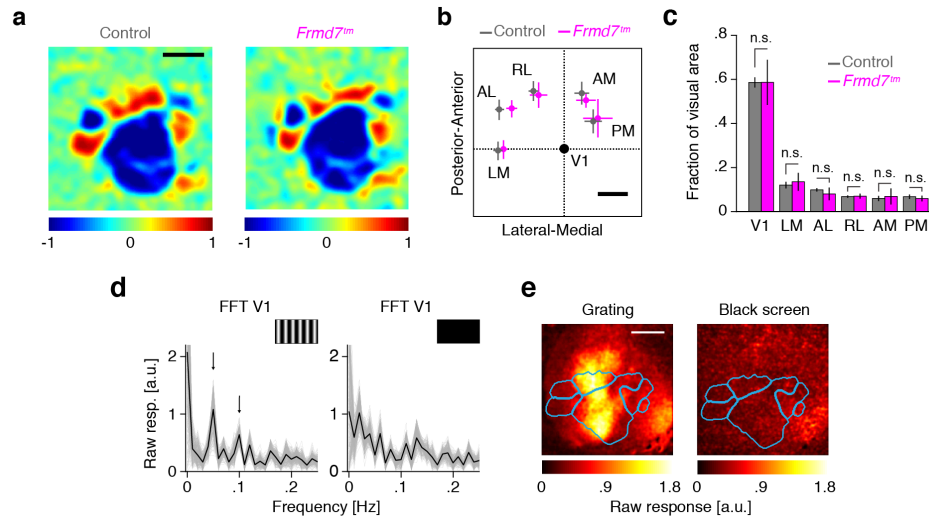
Supplementary Fig. 1: ISOI in control and *Frmd7^tm* mice. (a) Example visual field sign maps from control and *Frmd7^tm* mice generated using ISOI (scale bar, 1 mm). (b) Higher visual area centers relative to the center of V1 along posterior-anterior and lateral-medial axes (5 mice per group). Error bars are mean ± SEM (scale bar, 0.5 mm). (c) Size of each visual area (5 mice per group) as a fraction of the total (n.s., not significant, two-sided Mann-Whitney U test). Error bars are mean ± SEM. (d) Fast-Fourier transform (FFT) of V1 pixels during grating (left) and black screen (right). Individual pixels are gray, mean is black. (e) Example intrinsic signal response maps depicting the raw response signal for each pixel, determined as the peak power of the visually-evoked signal at the visual stimulus frequency (0.05−0.1 Hz), with visual area borders overlaid. Source data are provided as a Source Data file.
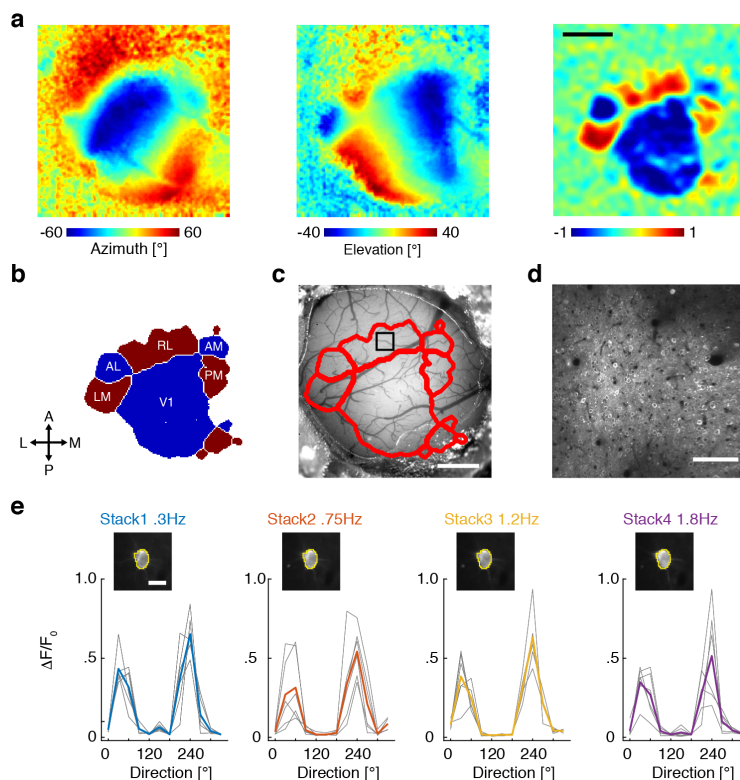
Supplementary Fig. 2: Targeted *in-vivo* two-photon calcium imaging in the visual cortex. (a) Example maps of horizontal (left) and vertical (middle) retinotopy and the corresponding visual field sign (VFS) map from a control mouse (right; scale bar, 1 mm). (b) Thresholded VFS patches computed from the VFS map in (a) showing the location of areas V1, RL and PM, together with the additional three higher visual areas (areas LM, AL, and AM). (c) Visual area borders derived from the VFS patches computed in (b) overlaid on blood vessel map. Black rectangle depicts representative field of view in area RL that was targeted for two-photon calcium imaging (scale bar, 1 mm). (d) Example two-photon mean projection image of RL L2/3 neurons labeled with GCaMP6f in the field of view depicted in (c) (scale bar, 100 μm). (e) Top: Example two-photon mean projection images showing a neuronal somata with overlaid region of interest from the four imaging stacks acquired over a 40 min period (scale bar, 10 μm); one imaging stack per visual temporal frequency condition (0.3, 0.75, 1.2, and 1.8Hz) was acquired. Bottom: Tuning curves at each of the four conditions for the neuron depicted above. Gray lines are individual trials, colored line is the trial-averaged mean.
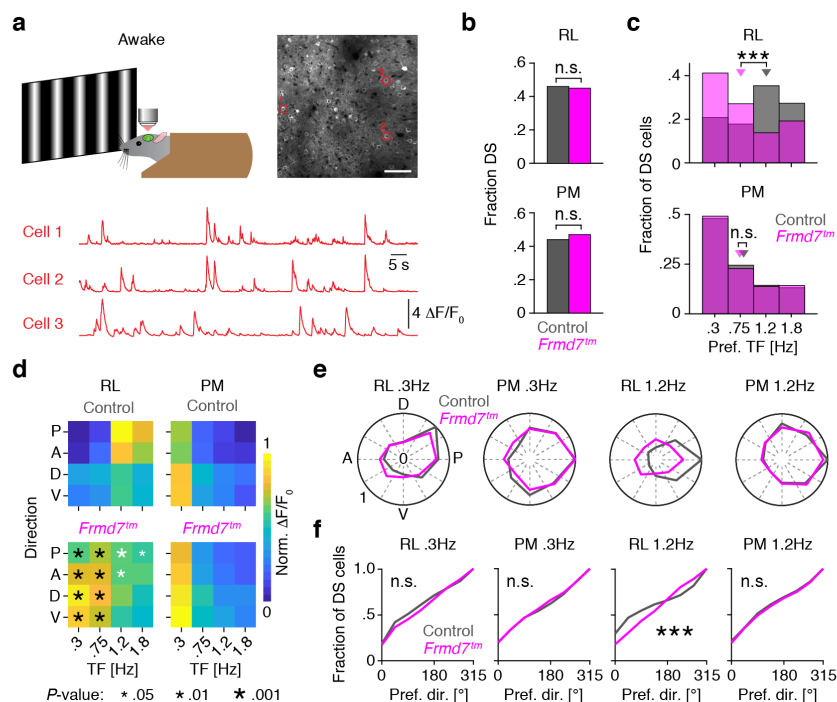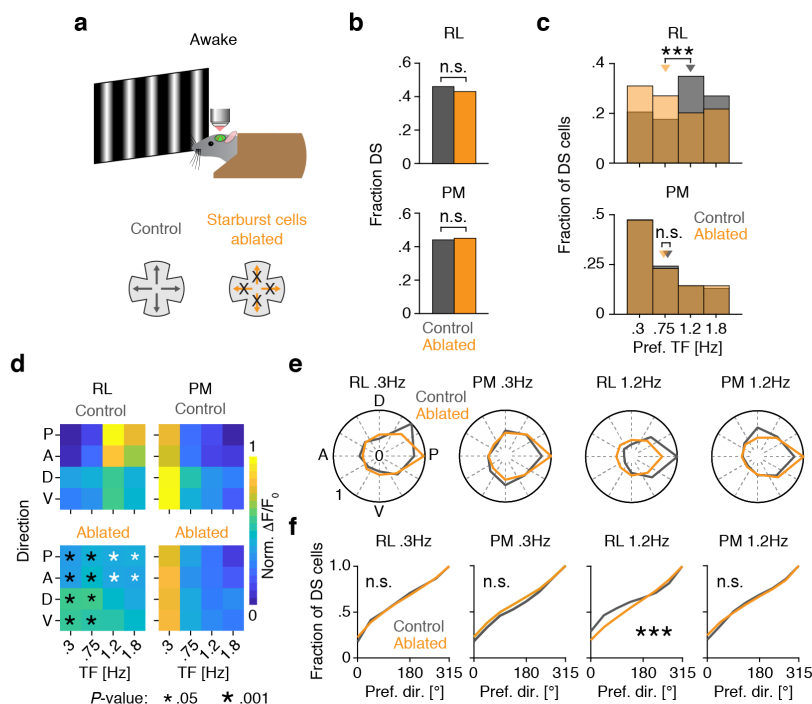
Supplementary Fig. 3: Preference of RL neurons for posterior motion at higher TFs depends on retinal horizontal direction selectivity in awake mice. (a) Two-photon calcium imaging was performed from L2/3 in areas RL and PM of awake control mice (1,652 and 2,018 DS cells, respectively; 4 mice) and *Frmd7^{tm}* mice (2,093 and 4,049 DS cells, respectively; 3 mice). Example image shows two-photon mean projection image of RL neurons expressing GCaMP6f (scale bar, 100 µm). Example traces show activity from three neurons (circled in the image) recorded while the mouse was awake and quietly resting in the cylindrical cover. (b) Fraction of DS cells in RL and PM (two-sided χ^2 test with Yates correction). (c) Preferred TF for DS cells in RL (two-sided Mann-Whitney U test) and PM (two-sided Mann-Whitney U test). Triangles show medians. (d) Response amplitude as a function of motion direction and TF for RL and PM DS cells. White and black asterisks: significantly decreased and increased response amplitude in *Frmd7^{tm}* mice, respectively, two-sided Mann-Whitney U test. (e) Fractional distributions of preferred motion directions for RL and PM DS cells at 0.3 and 1.2Hz; fractions are normalized to the largest fraction across genetic groups. (f) Distributions of preferred direction at 0.3 and 1.2Hz in RL and PM (two-sided Kolmogorov-Smirnov test). *$P < 0.05$, **$P < 0.01$, ***$P < 0.001$, n.s., not significant, in (b), (c) and (f). Source data are provided as a Source Data file.

4
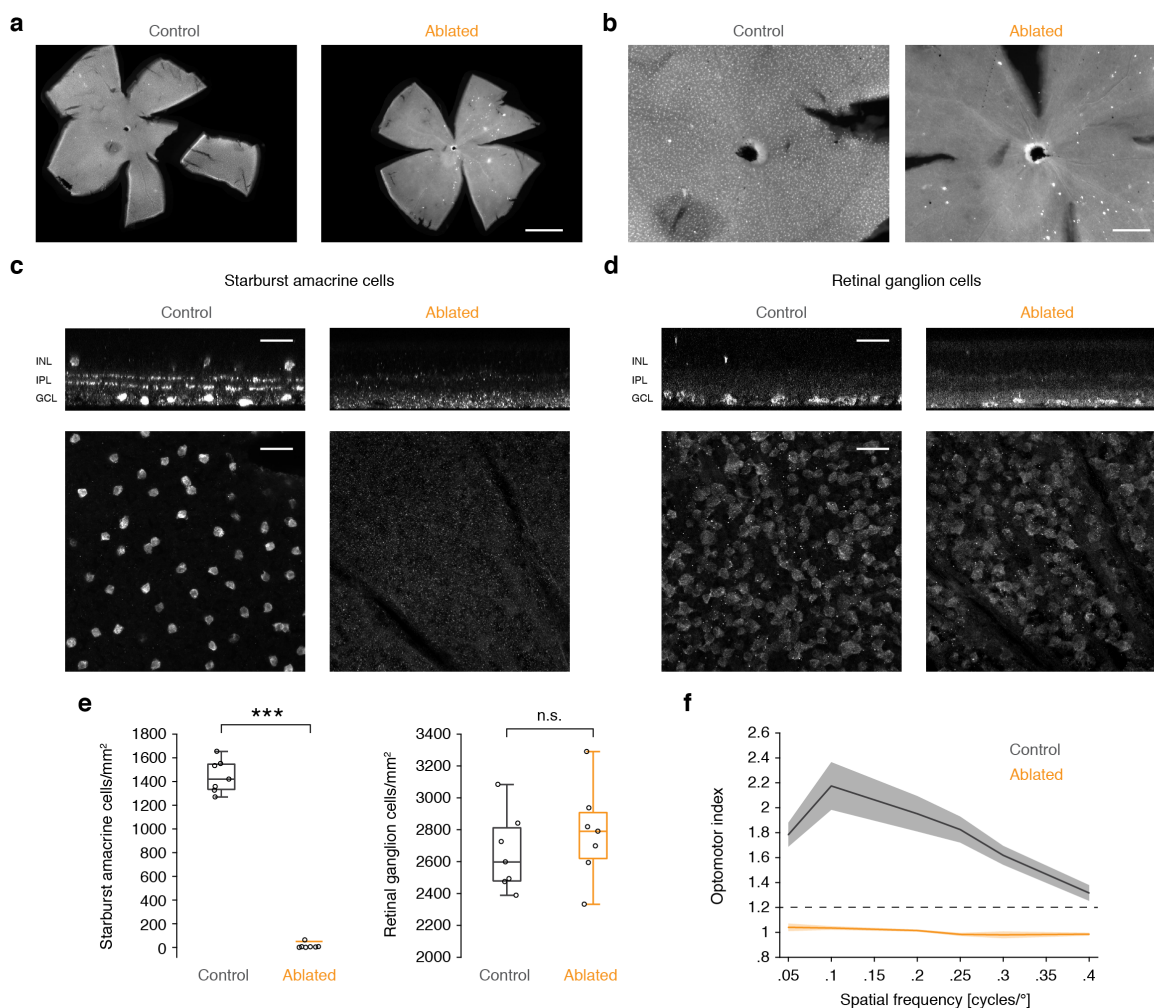
Supplementary Fig. 4: Diphtheria toxin injection selectively ablates starburst amacrine cells in the retina and annihilates optomotor responses. (a) Example whole-mount retinas stained for ChAT to label starburst amacrine cells (white dots show somata) in retinas from control (PBS-injected) and starburst-ablated mice (diphtheria toxin-injected). The white dots in the starburst-ablated retina are fluorescence aggregates, not somata (scale bar, 1 mm). (b) Example higher magnification of the retinas shown in (a) showing the absence of starburst amacrine cells in ablated mice (scale bar, 250 μm). (c) Example side view (top; scale bar, 30 μm) and top view (bottom; scale bar, 30 μm) of retinal z-projection stained for ChAT (starburst amacrine cells) from control (left) and starburst-ablated (right) mice. (d) Example side view (top; scale bar, 30 μm) and top view (bottom; scale bar, 30 μm) of retinal z-projection stained for RBPMS (retinal ganglion cells) from control (left) and starburst-ablated (right) mice. GCL, ganglion cell layer.

INL, inner nuclear layer; IPL, inner plexiform layer. (e) Density quantification of starburst amacrine cells and retinal ganglion cells in control and starburst-ablated mice (7 retinas in each group; ***$P < 0.001$, n.s., not significant, two-sided Mann-Whitney U test). Circles are individual data points, center line is median, box limits are 25th and 75th percentiles, and whiskers show minimum and maximum values. (f) Horizontal optomotor response measured in control (5 mice, 7−8 trials per mouse) and starburst-ablated mice (5 mice, 8 trials per mouse). The dotted horizontal line represents the upper quartile of the OMR index previously collected from 3 blind control mice (*rd1*/*rd1* mutants)[1]. Shading indicates SEM.

Supplementary Fig. 5: Ablating retinal starburst cells impairs posterior motion preference of RL DS cells at higher TFs. (a) Two-photon calcium imaging was performed from L2/3 in areas RL and PM of awake control mice (1,652 and 2,018 DS cells, respectively; 4 mice) and starburst-cell-ablated mice (2,511 and 2,777 DS cells, respectively; 4 mice). (b) Fraction of DS cells in RL and PM (two-sided χ^2 test with Yates correction). (c) Preferred TF for DS cells in RL (two-sided Mann-Whitney U test) and PM (two-sided Mann-Whitney U test). Triangles show medians. (d) Response amplitude as a function of motion direction and TF for RL and PM DS cells. White and black asterisks: significantly decreased and increased response amplitude in starburst-ablated mice, respectively, two-sided Mann-Whitney U test. (e) Fractional distributions of preferred motion directions for RL and PM DS cells at 0.3 and 1.2Hz; fractions are normalized to the largest fraction across genetic groups. (f) Distributions of preferred direction at 0.3 and 1.2Hz in RL and PM (two-sided Kolmogorov-Smirnov test). ***$P < 0.001$, n.s., not significant, in (b), (c) and (f). Source data are provided as a Source Data file.
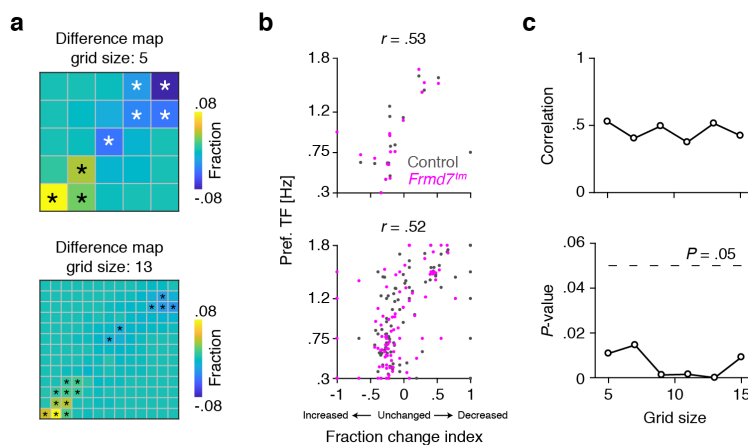
Supplementary Fig. 6: The correlation between the fraction alteration in *Frmd7^tm* mice and TF preference is not affected by the grid size used for segmentation. (a) Fraction difference map between control and *Frmd7^tm* mice using 5 × 5 (top) or 13 × 13 (bottom) grids in the V1 L2/3 DS cell population (see Fig. 4). Black and white asterisks: significantly decreased and increased fractions in *Frmd7^tm* mice, respectively, $P < 0.05$, two-sided χ^2 test with Yates correction. (b) Relationship between fraction changes in *Frmd7^tm* mice and the mean preferred TF of each grid for cells from control and *Frmd7^tm* mice when 5 × 5 (top) or 13 × 13 (bottom) grids were used. Two-sided Pearson's correlation coefficient is noted on each plot. (c) Two-sided Pearson's correlation coefficient between the fraction change index and mean preferred TF as a function of grid size (top). Corresponding *P*-values testing the significance of the correlation between the fraction change index and mean preferred TF as a function of grid size (bottom).
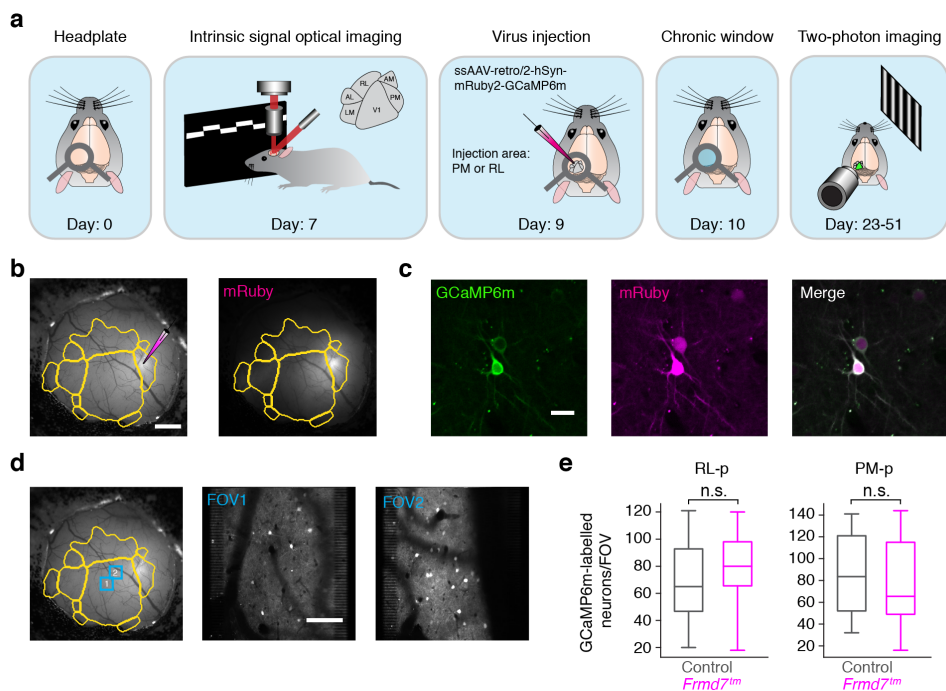
Supplementary Fig. 7: Retrograde viral labeling and GCaMP6 expression in V1 projection neurons.
(a) Experimental pipeline employed for achieving GCaMP6 expression in V1 neurons projecting to either area RL or PM. (b) Left: Example image of a cranial window with visual area borders overlaid showing viral (ssAAV-retro/2-hSyn1-mRuby2-GCaMP6m-WPRE) injection site for retrograde expression from area PM in a control mouse (scale bar, 1 mm). Right: mRuby signal in the same cranial window showing site of injection and retrograde expression outside of PM, including in V1. (c) Example V1 neurons expressing GCaMP6m and mRuby (scale bar, 20 µm). (d) Left: Blue rectangles depict fields of view (FOVs) in V1 targeted for two-photon calcium imaging in the same cranial window as shown in (b). Middle and right: Two-photon mean projection images showing neurons labeled with GCaMP6m in the FOVs depicted on the left (scale bar, 100 µm). (e) Number of GCaMP6m-labelled RL-projecting (RL-p) and PM-projecting (PM-p) V1 neurons per FOV in control (21 and 37 FOVs for RL-p and PM-p, respectively) and *Frmd7^{tm}* mice (21 and 34 FOVs for RL-p and PM-p, respectively; n.s., not significant, two-sided Mann-Whitney U test). Center line is median, box limits are 25th and 75th percentiles, and whiskers show minimum and maximum values. Source data are provided as a Source Data file.
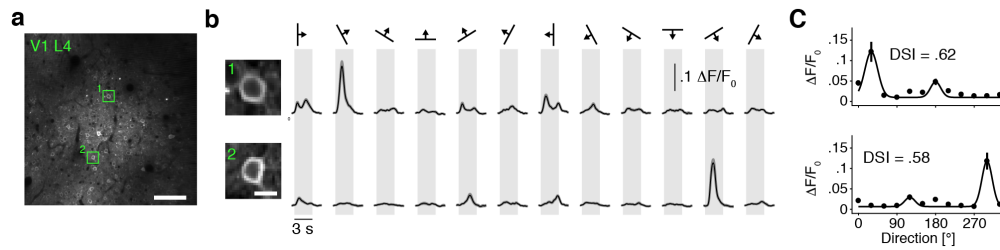
Supplementary Fig. 8: Two-photon calcium imaging from V1 L4 neurons. (a) Example two-photon mean projection image of V1 L4 neurons (395 μm below the dura) labeled with GCaMP6f (scale bar, 100 μm). (b) Example V1 L4 neurons expressing GCaMP6f (scale bar, 10 μm) and trial-averaged fluorescence ($\Delta F/F_0$) time courses for the same neurons. Shading indicates SEM. (c) Tuning curves for the neurons shown in (b). Error bars are SEM; solid line is Gaussian fit.
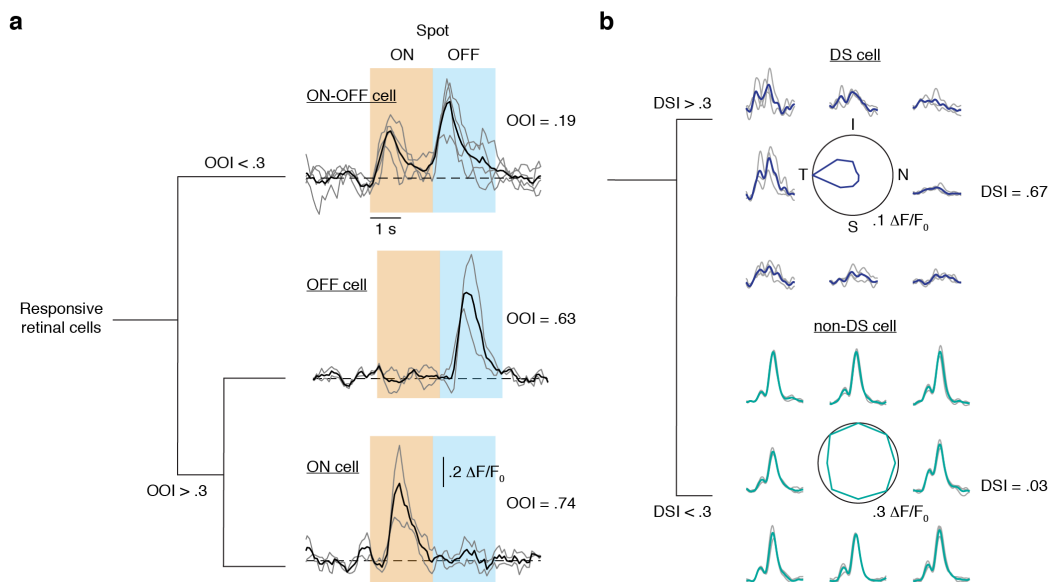
Supplementary Fig. 9: Classification of ON-OFF DS in the retina. (a) To identify ON-OFF DS cells, we first separated the visually responsive retinal cells into two groups: ON-OFF and non-ON-OFF cells, based on an ON-OFF index (OOI, see Methods), denoting the ratio of responses during and after a static flash stimulus (ON phase, orange area; OFF phase, blue area). If cells are responding to both the ON and OFF phase, the OOI value is low: we classified cells with an OOI < 0.3 as ON-OFF cells. Example ON-OFF, OFF, and ON cells are shown. (b) We defined ON-OFF DS cells as ON-OFF cells with a DSI > 0.3. Example ON-OFF DS cells and ON-OFF non-DS cells are shown.

Supplementary references

1. Kretschmer, F., Tariq, M., Chatila, W., Wu, B. & Badea, T. C. Comparison of optomotor and optokinetic reflexes in mice. *J. Neurophysiol.* **118**, 300–316 (2017).

Appendix B
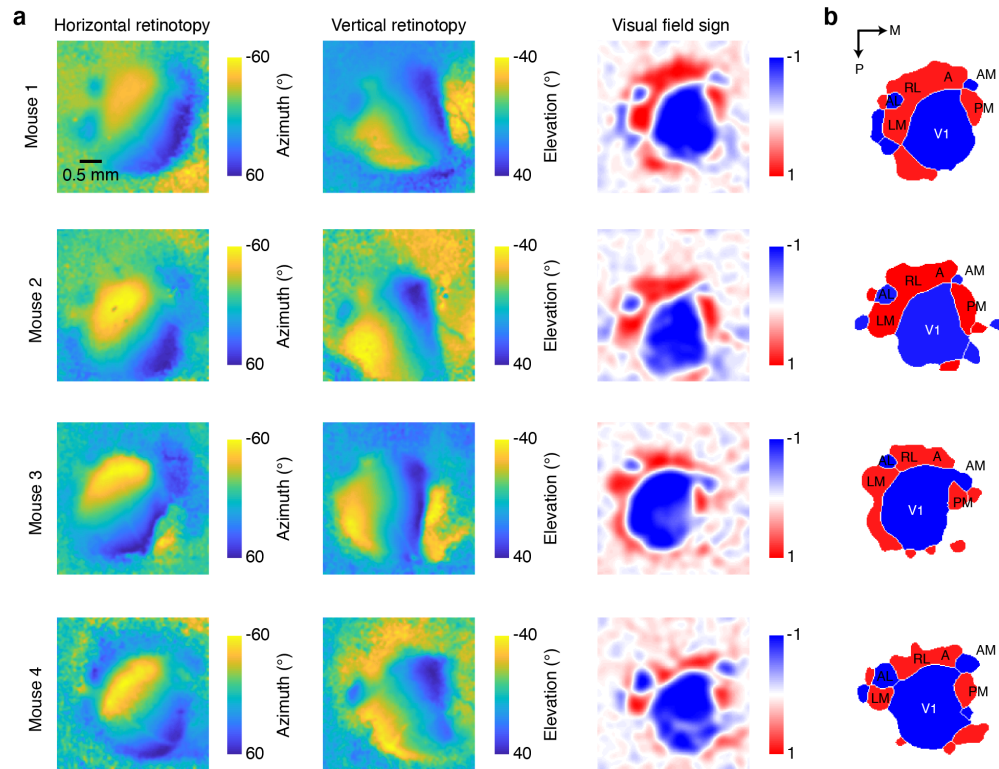
Extended Data Fig. 1 | Identification of visual cortical areas using intrinsic signal optical imaging. a, Maps of horizontal (left) and vertical retinotopy (middle), and the corresponding visual field sign map (right) from four example mice. **b**, Thresholded visual field sign patches showing the location of primary visual cortex (V1), and the higher visual areas: lateromedial (LM), anterolateral (AL), rostrolateral (RL), anterior (A), anteromedial (AM), and posteromedial (PM). Coordinates indicate posterior (P) and medial (M) directions.
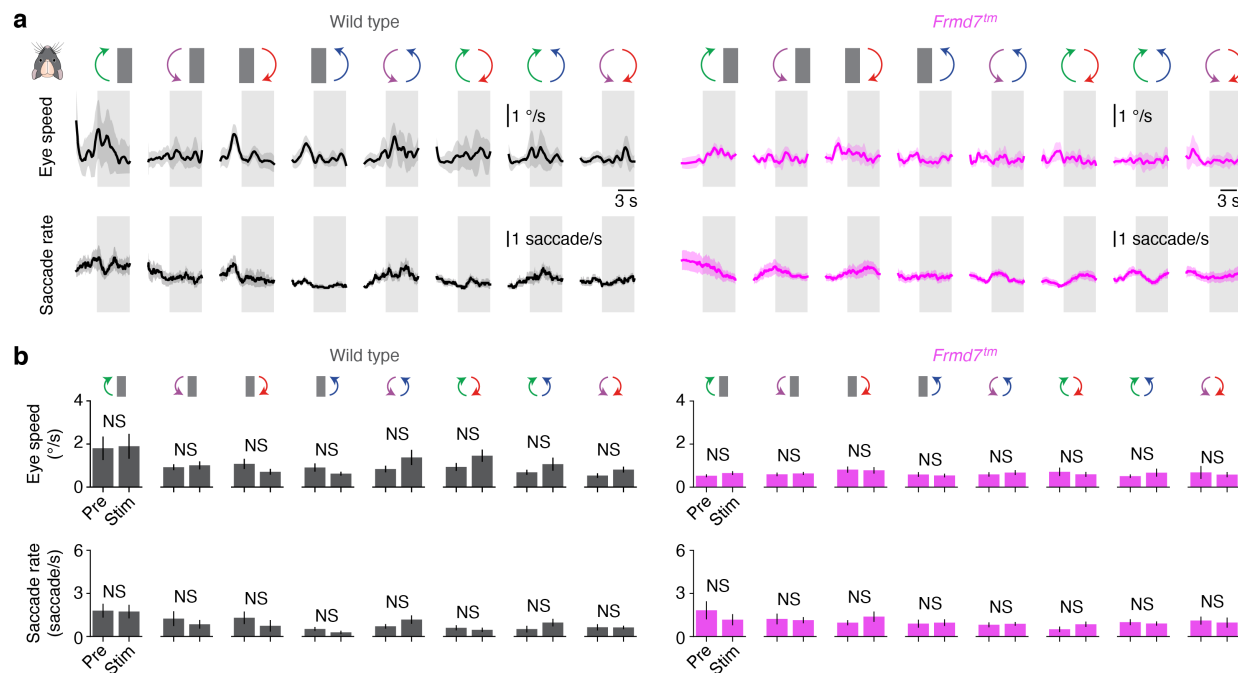
Extended Data Fig. 2 | Eye movements in awake wild-type and *Frmd7tm* mice during visual stimulus protocol. a, Trial-averaged horizontal eye speed and saccade rate time courses recorded in wild-type mice (left; *n* = 9 recordings) and *Frmd7tm* mice (right; *n* = 9 recordings) in response to the monocular and binocular horizontal motion conditions presented at 10 °/s. Error bars are mean ± s.e.m. **b**, Quantification of mean horizontal eye speed (upper) and mean saccade rate (lower) before and during visual stimulation in wild-type (left) and *Frmd7tm* mice (right) (NS, not significant, *P* ≥ 0.05; Wilcoxon signed-rank test; *n* = 9 recordings from 3 wild type mice and 9 recordings from 3 *Frmd7tm* mice). Error bars are mean ± s.e.m.
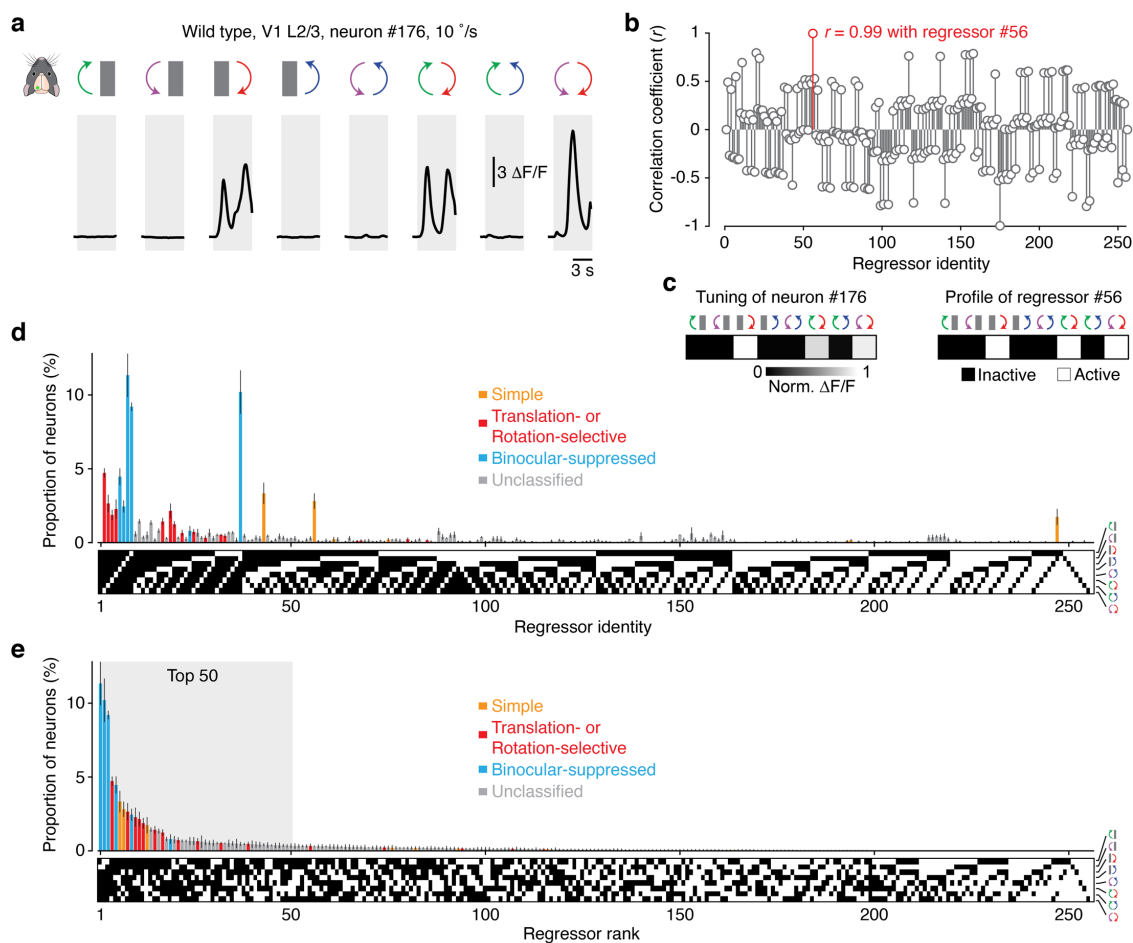
Extended Data Fig. 3 | Regression analysis for classifying individual neurons to discrete response types. a, Trial-averaged fluorescence intensity (ΔF/F) time course for example layer 2/3 V1 neuron (#176) from a wild-type mouse in response to the monocular and binocular motion conditions at 10 °/s. **b**, The tuning curve at the preferred speed was correlated to each of the 256 regressors, yielding a correlation profile. Correlation coefficients were calculated as Pearson's r. Neuron #176 showed the highest correlation with regressor #56 ($r = 0.99$) and was thus assigned to this response type. **c**, Tuning profile of neuron #176 and response profile of regressor #56. **d**, Distribution of all reliably responsive V1 neurons from wild-type mice ($n = 3010$ neurons from 4 mice) grouped according to the 256 regressors and response class (simple, translation- or rotation-selective, binocular-suppressed, and unclassified). Error bars are mean ± s.e.m. **e**, Distribution from (**d**) ranked according to regressor frequency. The shaded region depicts the 50 most abundant regressors (as shown in Fig. 2).

Extended Data Fig. 4 | Tuning of higher visual area neurons assigned to functional groups. a,b,c Regressor profiles and tuning of RL/A (**a**), AM (**b**) and PM (**c**) neurons assigned to functional groups within simple, translation- or rotation-selective, and binocular-suppressed response classes. MoDS: monocular DS; BiDS: binocular DS; FT: forward translational; BT: backward translational; CR: contraversive rotational; IR: ipsiversive rotational.

Area	Total neurons		Consistently responsive		Animals	
	WT: n	$Frmd7^{tm}$: n	WT: n (%)	$Frmd7^{tm}$: n (%)	WT: n	$Frmd7^{tm}$: n
V1	5748	5534	3010 (52%)	2925 (53%)	4	4
RL/A	6563	6746	4165 (63%)	3125 (46%)	5	5
AM	6664	6919	4006 (60%)	3375 (49%)	5	5
PM	5419	5868	3059 (56%)	3047 (52%)	4	4

Supplementary Table 1 | Numbers of neurons sampled by visual cortical area and genetics. Total neurons: total number (n) of neurons recorded in wild-type (WT) and $Frmd7^{tm}$ mice experiments for each visual cortical area. Consistently responsive: number (n) and percent of total of neurons that met the inclusion criteria for responsiveness (ΔF/F > 10%), reliability (δ > 0.5), and signal-to-noise (SNR > 0.5) and were included for regressor correlation analysis. Animals: number (n) of WT and $Frmd7^{tm}$ mice that data were collected from for each area.